Resource Allocation for Broadband Wireless Access Networks with Imperfect CSI

by

Mohamad Awad

A thesis
presented to the University of Waterloo
in fulfillment of the
thesis requirement for the degree of
Doctor of Philosophy
in
Electrical and Computer Engineering

Waterloo, Ontario, Canada, 2009

I hereby declare that I am the sole author of this thesis. This is a true copy of the thesis, including any required final revisions, as accepted by my examiners.

I understand that my thesis may be made electronically available to the public.

Abstract

The high deployment and maintenance costs of last mile wireline networks (i.e., DSL and cable networks) have urged service providers to search for new cost-effective solutions to provide broadband connectivity. Broadband wireless access (BWA) networks, which offer a wide coverage area and high transmission rates in addition to their fast and low-cost deployment, have emerged as an alternative to last mile wireline networks. Therefore, BWA networks are expected to be deployed in areas with different terrain profiles (e.g., urban, suburban, rural) where wireless communication faces different channel impairments. This fact necessitates the adoption of various transmission technologies that combat the channel impairments of each profile. Implementation scenarios of BWA networks considered in this thesis are multicarrier-based direct transmission and single carrier-based cooperative transmission scenarios. The performance of these transmission technologies highly depends on how resources are allocated. In this thesis, we focus on the development of practical resource allocation schemes for the mentioned BWA networks implementation scenarios. In order to develop practical schemes, the imperfection of channel state information (CSI) and computational power limitations are among considered practical implementation issues.

The design of efficient resource allocation schemes at the MAC layer heavily relies on the CSI reported from the PHY layer as a measure of the wireless channel condition. The channel estimation error and feedback delay renders the reported CSI erroneous. The inaccuracy in CSI propagates to higher layers, resulting in performance degradation. Although this effect is intuitive, a quantitative measure of this degradation is necessary for the design of practical resource allocation schemes. An approach to the evaluation of the ergodic mutual information that reflects this degradation is developed for single carrier, multicarrier, direct, and cooperative scenarios with inaccurate CSI. Given the CSI estimates and estimation error statistics, the presented evaluation of ergodic mutual information can be used in resource allocation and in assessing the severity of estimation error on performance degradation.

A point-to-multipoint (PMP) network that employs orthogonal frequency division

multiple access (OFDMA) is considered as one of the most common implementation scenarios of BWA networks. Replacing wireline networks requires not only providing the last mile connectivity to subscribers but also supporting their diverse services with stringent quality of service (QoS) requirements. Therefore, the resource allocation problem (i.e., subcarriers, rate and power allocation) is modeled as a network utility maximization (NUM) one that captures the characteristics of this implementation scenario. A dual decomposition-based resource allocation scheme that takes into consideration the diversity of service requirements and inaccuracy of the CSI estimation is developed. Numerical evaluations and simulations are conducted to validate our theoretical claims that the scheme maximizes resource utilization, coordinates with the call admission controller to guarantee QoS, and accounts for CSI inaccuracy.

Cooperation has recently received great attention from the research community and industry because of its low cost and fast deployment in addition to the performance improvement it brings to BWA networks. In cooperative scenarios, subscribers cooperate to relay each other's signals. For this implementation scenario of BWA networks, a robust and constrained Kalman filter-based power allocation scheme is proposed to minimize power consumption and guarantee bit error probability (BEP) requirements. The proposed scheme is robust to CSI inaccuracy, responsive to changes in BEP requirements, and optimal in allocating resources.

In summary, research results presented in this thesis contribute to the development of practical resource allocation schemes for BWA networks.

Acknowledgements

This thesis would not have been possible without the support of many people. I wish to express my gratitude to my supervisor, Prof. Xuemin (Sherman) Shen who was abundantly helpful and offered endless support and guidance. He is a role model of professionalism, integrity, respect, and work ethic who I admire.

I would like to thank my committee, Prof. Sagar Naik, Prof. Kumaraswamy Ponnambalam, Prof. Liang-Liang Xie and the external examiner, Prof. Xianbin Wang from the University of Western Ontario, for their constructive feedback and valuable comments. I appreciate the time and effort they devoted for reading my thesis.

Gratitude is also due to Prof. Jon W. Mark without whose knowledge and guidance this study would not have been successful. I am also grateful to my colleagues Dr. Mehri Mehrjoo and Dr. Mahinthan Veluppillai who have helped me in developing the approaches and ideas presented in this thesis. I would like to extend my special thanks to all members of the Broadband Communication Research (BBCR) group for their discussions and suggestions in our weekly group meeting. I would also like to convey thanks to my uncles Mohammad Awad, Abbas Farhat and Dr. Ali Farhat for their assistance and support throughout various stages of my education.

I like to express my deepest gratitude to my parents, brothers and sister without whose motivation and endless support completing this work would not have been possible. Special thanks to my brothers Ali and Hadi for assisting me in producing various illustrative images. I am in debt to my wife Rouba for her support, encouragement, patience and endless love throughout my studies. I can't thank enough my son Khattar and daughter Tala for their understanding at times when I was unavailable.

Dedication

To martyrs who sacrificed their lives for us to live in liberty.

To Parents, Khattar Awad & Zeinab Farhat

To my wife, Rouba and my children, Khattar and Tala

To my niece, Zeina

Contents

List of Tables

List of Figures

List of Abbreviations

AMC	Adaptive Modulation and Coding
AMPS	Advanced Mobile Phone Services
AWGN	Additive White Gaussian Noise
BEP	Bit Error Probability
BWA	Broadband Wireless Access
BS	Base Station
CAC	Call Admission Control
CD	Cooperative Diversity
CKF	Constrained Kalman Filtering
CSI	Channel State Information
DF	Decode-and-Forward
DFT	Discrete Fourier Transform
DL	Downlink
DSA	Dynamic Subcarrier Assignment
DSTBC	Distributed Space-Time Block Coding
FDM	Frequency Division Multiplexing
FDMA	Frequency Division Multiple Access
FFT	Fast Fourier Transform
HiperMAN	High Performance Radio Metropolitan Area Network

ICI	Inter-Carrier Interference
IDFT	Inverse Discrete Fourier Transform
ISI	Intersymbol Interference
KF	Kalman Filter
LTV	Linear-Time-Varying
MIMO	Multiple-Input Multiple-Output
MMSE	Minimum Mean Square Error
MRC	Maximal Ratio Combining
NUM	Network Utility Maximization
OFDMA	Orthogonal Frequency Division Multiple Access
OFDM	Orthogonal Frequency Multiplexing Division
PDF	Probability Density Function
PDP	Power Delay Profile
PMP	Point to Multi-point
QoS	Quality of Service
RAU	Resource Allocation Unit
RCKF	Robust and Constrained Kalman filtering
SDF	Selective-Decode-and-Forward
SNR	Signal to Noise Ratio
TDD	Time Division Duplex
TDL	Tapped Delay Line
VAA	Virtual Antenna Array
2I1O	Two Inputs One Output
3GPP	3rd Generation Partnership Project
3GPP-LTE	3rd Generation Partnership Project Long Term Evolution
4G	Fourth-Generation

List of Symbols

$\delta(\cdot)$	Dirac impulse function
φ_p	Multipath phase
N_p	Number of multipath complex-valued amplitude
$f_{D,p}$	Multipath Doppler frequency
τ_p	Multipath arrival excess delay
v	Terminal velocity
c	Speed of light
f_c	Carrier frequency
α_p	Angle of arrival
$\bar{\tau}$	Average delay
τ_{RMS}	RMS delay spread
τ_{max}	Maximum multipath arrival delay
T_s	Symbol duration
B_c	Coherence bandwidth
T_c	Coherence time
$h(\tau, t)$	Time varying channel's impulse response
$h(\tau)$	Temporally stationary discrete-time
$R(\delta f)$	Channel frequency response auto-correlation function
$\overline{H}(f, t)$	Channel frequency response

T	Total number of TDL taps
T_s'	Serial symbols duration
T_g	Guard interval Length
L_g	Sampled Guard interval Length
T_s''	Cycle extended OFDM symbol
$\mathbf{H}$	Channel matrix
H_n^{xy}	Perfect CSI of the nth subcarrier in the link between station x and y
$\hat{H}_n^{xy}$	Estimated CSI of the nth subcarrier in the link between station x and y
$\breve{H}_n^{xy}$	Imperfect CSI estimate of the nth subcarrier in the link between station x and y
R	Threshold for cooperative communication
$(\sigma_\epsilon^{xy})^2$	Estimation error variance on the link between station x and y
$(\sigma_z^{xy})^2$	Additive noise variance on the link between station x and y
N_{sc}	Number of subcarriers available to the cell
$E_i(\cdot)$	Exponential integral function
N_{sc}	Number of subcarriers available to the cell
I_n	nth subcarrier transmission rate
I_n^{xy}	x's subscriber station transmission rate to the y's receiver on the nth subcarrier
p_n	nth subcarrier allocated power
I_n^{AMC}	AMC transmission rate on the nth subcarrier
$\mathbf{I}$	Identity matrix of the appropriate size
$I^{(x)}$	In-phase channel of subscriber x
$Q^{(x)}$	Quadrature channel of subscriber x
$E_b^{I^{(x)}}$	Bit energy spent at the in-phase channel of subscriber x
$E_b^{Q^{(x)}}$	Bit energy spent at the quadrature channel of subscriber x
P_b	Average bit error probability
$\Upsilon^{(x)}\|\varepsilon^{(x)}$	Target SNR of subscriber x that satisfies average BEP $\varepsilon^{(x)}$
$\bar{\gamma}_f^{I^{(x)}}$	Estimated average SNR of the fth frame at the in-phase channel of subscriber x
$\bar{\gamma}_f^{Q^{(x)}}$	Estimated average SNR of the fth frame at the quadrature channel of subscriber x

Notations

$R(\cdot)$	Auto-correlation function
$E\{\cdot\}$	Expectation of random variables
$(\cdot)^*$	Complex conjugate
$(\cdot)^H$	Matrix hermitian
$*$	Convolution
$(\cdot)^{-1}$	Inverse
$\mathcal{O}(\cdot)$	Order of magnitude
$X \sim \mathcal{CN}(m_X, \sigma_X^2)$	Random variable X is a circularly symmetric complex Gaussian with m_X mean and σ_X^2 variance
$Pr\{x\}$	Probability of event x
diag$([\cdot])$	Diagonal matrix of the vector $[\cdot]$
$[\cdot]_{x,y}$	The element of the x-th row and y-th column of matrix $[\cdot]$
$(\cdot)^T$	Matrix transpose

Chapter 1

Introduction

1.1 Research Motivation

Broadband wireless access (BWA) networks are being developed to replace the last mile wireline access networks such as DSL and cable networks. The simple and small receiver structure allows BWA networks to provide service directly to subscribers, without the need for intermediate receivers (i.e., modems), which is the case for wireline networks. In addition, BWA networks are suitable for providing service in countries that lack fiber optics infrastructure, or have low population density or with rough topographies where laying cables is expensive. Because of their fast deployment in comparison to wired networks, they can be used in disaster recovery [2]. Standards that specify the technical aspects of the network under consideration are IEEE 802.16[1], the high performance radio metropolitan area network (HiperMAN), the European telecommunication standard, and the 3rd generation partnership project (3GPP) [3].

In spite of the above-mentioned advantages of BWA networks over wireline networks, wireless networks are challenged by channel impairments. In particular, wireless systems suffer from frequency selective fading and distance dependent fading (i.e.,

[1]WiMAX is a commercialization of IEEE 802.16, and WiMAX certified products do not support all features specified in the IEEE 802.16 standard.

large-scale fading). While small-scale fading results in intersymbol interference (ISI), large-scale fading attenuates the transmitted signal strength below the minimum level that is required for correct decoding. Solutions to overcome the wireless communication challenges are still being developed by both the research community and industry. Generally, multicarrier transmission has been proposed as a replacement for single carrier transmission in scenarios where multipath fading is severe, and relaying has been proposed to overcome the challenge of distance dependent fading. However, as with most engineering designs, there is a trade off between performance and complexity; in addition, in certain implementations these challenges may not always be faced by BWA networks. Therefore, multicarrier and/or relaying technologies may not always be the best solution(s) and the consideration of single carrier or multicarrier transmissions, and direct or relaying transmissions in resource allocation schemes become necessary.

The absence of wireless coverage could be life threatening for service subscribers in emergency situations or for patients who are being wirelessly monitored. However, from the service providers' point of view, extending the service coverage in less populated areas is financially expensive as the expected revenue is less than the infrastructure and operating costs: cabling, land leasing and base station installation costs. The use of wireless relay technologies reduces these costs via wirelessly backhauling the traffic to the wired network. In other words, relay technologies help service providers to reach out subscribers who are beyond the base station (BS) coverage area, without installing a new BS which would also require a wired connection to the backbone. Because of the limited radio frequency spectrum, the frequency bands to be allocated to fourth-generation (4G) technologies are above 3 GHz [4]. Such 4G systems are more vulnerable to no-line-of-sight propagation due to high penetration loss at high frequencies. As a result, signals experience large propagation losses that degrade transmission performance [5]. Wireless relay technologies take advantage of the broadcasting nature of wireless transmissions to retransmit received signals to an intended destination. To further exploit wireless channel capacity, a subscriber station can cooperate with a relay station through a time division duplex (TDD) based decode-and-forward (DF) relaying scheme. In this way, the

destination receives the direct signal from the transmitter in the first frame and receives the same signal but regenerated by the relay station in the second [6]. The transmission between the source and relay limits the performance of DF. Thus, DF can be further improved by selection of a relay to cooperate only if cooperation brings performance improvement in a selection-decode-and-forward (SDF) scheme. The relay technology properties of reducing the propagation loss and deployment cost, in addition to exploiting spatial diversity, have been receiving major attention from various standards working groups.

Since the first mobile communication system (i.e., advanced mobile phone services (AMPS)) became commercially available in the mid-1980s, wireless systems have been challenged to support an increasing demand for high data rates and stringent quality of service (QoS) anywhere, at any time. However, single-carrier signals are limited by the channel coherence bandwidth. As the data rate increases (signal bandwidth increases), the signal becomes subject to ISI in frequency selective channels. This challenge can be overcome if the wide-band signal is transmitted as multiple narrow band signals using the orthogonal frequency division multiple access (OFDMA) PHY and MAC technologies [7, 8]. OFDMA is being considered in current broadband standards because of its essential features of exploiting multiuser diversity in a frequency selective channel and eliminating ISI.

Despite the features these technologies bring to the network, they exacerbate the MAC protocol complexity, and conventional MAC protocols fail to manage such networks. The performance improvement of adopting OFDMA or relaying relies on how intelligently the resources are allocated to subscribers. Hence, the development of practical resource allocation schemes with low complexity for managing the resources of BWA networks becomes necessary, and is the focus of this thesis.

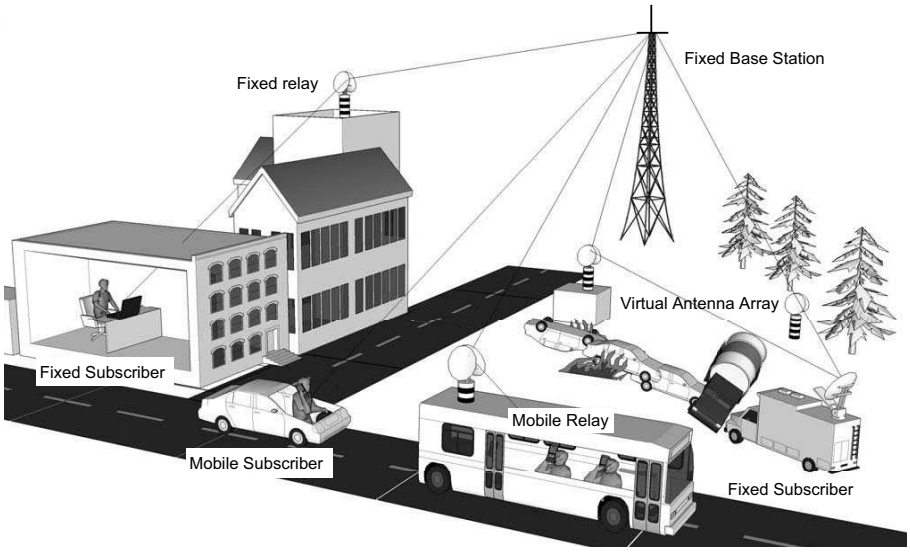

Figure 1.1: Illustration of BWA networks.

1.2 Problem Description

BWA networks are expected to be deployed in any area where subscribers are located. Figure 1.1 illustrates an example of a single cell scenario of BWA networks. As different areas may have different types of terrain profile (e.g. rural, suburban and urban), wireless channels in each of these profiles may not face the same wireless propagation challenges. For instance, in urban areas, where subscribers may be located very close to the base station but in cluttered surroundings, multipath fading effect on the transmitted signal is more pronounced than distance dependant fading. Thus, multicarrier transmission, OFDMA, is necessary to combat ISI, whereas relaying is not. The converse is true for rural areas where the major challenge is distance dependant fading rather than multipath fading because of the large propagation distances and low number of scatterers. In suburban areas, both multipath fading and large scale fading may exist, which requires both OFDMA and relaying. Therefore, BWA networks designers may selectively implement transmission technologies (i.e., multicarrier, single carrier, cooperative, non-cooperative) based on the deployment area and system complexity constraints.

As mentioned previously, OFDMA has proven itself successful in combating ISI. At the PHY layer, OFDMA transmits the wideband signal over multiple narrowband signals that modulate multiple subcarriers; the bandwidth of each narrowband signal is less than the channel coherence bandwidth for the frequency selectivity to be avoided. At the MAC layer, the resource allocation problem is to allocate a subset of the available subcarriers exclusively to subscribers and allocate power on each subcarrier such that the allocated power does not exceed subscribers' power constraints and base station transmission power constraint in the uplink and downlink, respectively. This allocation problem is an optimization problem that is $\mathcal{NP}$-complete, as shown in Appendix A. In addition, the exclusive subcarrier assignment constraint makes the feasible region of the resource allocation problem non-convex, which increases the complexity of the problem. The problem complexity is further increased as QoS constraints are considered.

Relaying effectiveness in reducing distance dependent fading and shadowing effects have made it the focus of many research activities. Among numerous cooperative schemes proposed in the literature, a quadrature signaling cooperative scheme is considered in this thesis. With quadrature signaling, instead of expanding the bandwidth or reducing the effective data rate of the cooperative system, the signal constellation of the modulation scheme is expanded to accommodate the transmissions by the partner. This scheme falls in the class of SDF cooperative schemes. Such schemes require power allocation at the source and relay to preserve each of the subscriber's battery power and guarantee bit error probability (BEP) requirements.

BWA networks support multiple services, which may have different utility functions. These utility functions represent subscribers' satisfaction with the service level granted to them. Some subscribers can have more demanding utility functions than others; resource allocation schemes that purely maximize aggregate utility functions may allocate all network resources to demanding subscribers leaving the rest unsupported. The design of resource allocation schemes that impose fairness among supported services is considered in this thesis.

All the aforementioned salient features of OFDMA and cooperative relaying tech-

nologies hinge on the availability of accurate channel state information (CSI) at the resource allocation unit (RAU), which is not the situation in practical networks and needs to be considered in the design of resource allocation schemes. Schemes that are designed based on the assumption that the CSI is perfectly available at the RAU without feedback delay and/or estimation error fail in practical wireless networks for two reasons. First, channel estimations are subject to noise and error that affect the accuracy of the available CSI. Second, in large cells with multiple relay stations and large number of subscriber stations, reporting the CSI of every subcarrier[2] between all possible pairs (i.e., subscribers and relays, relays and base station, base station and subscribers) could snowball into a huge communication overhead; thus, the zero delay feedback assumption becomes unacceptable. Hence, the development of practical resource allocation schemes requires accounting for the inaccuracy of CSI.

Although commercial optimization tools are available for solving the resource allocation problem (e.g., CPLEX), the time required to obtain a close to optimal solution is long, during which the channel changes make the obtained solution obsolete. In addition, subscribers or the base station do not have the computational power required to run such optimization tools for each resource allocation instant. Therefore, low complexity resource allocation schemes that consider practical network scenarios are desired for BWA networks.

1.3 Research Objectives and Contributions

The major objective of this research is to develop practical resource allocation schemes for various transmission technologies employed by BWA networks. Developed schemes address practical issues such as, inaccuracy of CSI, limited computational power, and the support of multiple services with diverse QoS requirements in BWA networks that employ single carrier, multicarrier (i.e., OFDMA), direct and cooperative (i.e., SDF) transmission technologies. Developed schemes balance between optimality of resource

[2]The total number of subcarriers can be as large as 2048.

utilization and computational complexity, while guaranteeing QoS requirements and satisfying constraints related to employed technologies. This research objective is reached over several stages.

In the first stage, an approach to the evaluation of the ergodic mutual information of BWA networks under a practical assumption, inaccurate CSI, was developed. A general system model was considered such that insights on the effect of CSI inaccuracy in BWA networks that employ various transmission technologies can be obtained. Particularly, the CSI inaccuracy effect on the performance of BWA networks as a function of estimation and delay error statistics was quantified in terms of the ergodic mutual information. With knowledge of error statistics and based on the developed approach, resources can be allocated to achieve a performance that is close to that achieved if an accurate CSI can be available. In addition, the performance degradation is not always severe and this effect is negligible in specific situations.

In the second stage, a dual decomposition-based resource allocation scheme for point to multipoint (PMP) BWA networks that employ OFDMA and support multiple services was developed to allocate subcarriers, power and rate to subscribers. The problem was posed as a network utility maximization (NUM) problem which is solved via decomposing it into a hierarchy of several sub-problems that are easier to solve. The approach developed in the first stage was used in resource allocation to account for CSI inaccuracy. Resources were allocated in coordination with the call admission controller to limit the aggregate rate of each class of service to a partition of the network capacity. Imposing limits on the aggregate rate allocated to each class of service guarantees fairness among classes, a feature that is important for QoS satisfaction.

Power allocation, which has a major effect on the performance of cooperative BWA networks, was considered at the third stage. Resource allocation in these BWA networks with CSI inaccuracy was modeled as an uncertain system. A robust and constrained Kalman filter-based based approach was developed to allocate power for both the source and relay while guaranteeing BEP requirements. The developed scheme enjoys fast responsiveness to changes in BEP requirements and low computational complexity of

Kalman filter.

1.4 Thesis Structure

Wireless channel impairments have the predominant effect on the performance of BWA networks. The type and severity of these impairments relate to the environment in the vicinity of the transmitter and receiver; thus, channel modeling metrics vary from one environment to another. The development of transmission technologies that combat each type of channel impairments has been the focus of many research activities. Because of this tight relation between wireless channel impairments and considered transmission technologies, Chapter 2 presents an overview of the wireless channel characteristics and BWA networks-adopted technologies such as OFDMA and cooperative relaying technologies. A description of the PHY and MAC layers of the considered technologies is also presented. In addition, commonly invoked assumptions related to these technologies in various networks are surveyed. Literature related to each considered research problem and proposed scheme are discussed in each chapter.

The ergodic mutual information of BWA networks that employ single carrier, OFDMA, direct and SDF cooperative technologies is investigated in Chapter 3. After modeling the CSI inaccuracy that results from channel estimation error and feedback delay, the inaccuracy is embedded in the evaluation of the ergodic mutual information of BWA networks. In BWA networks that employ SDF, the relay cooperates with the source only if the source to relay channel can support a specific rate that guarantees performance gain. Otherwise, the source transmits directly to the receiver without the cooperation of the relay. Therefore, SDF consists of cooperative and direct transmissions. The relay may be a subscriber or a dedicated relay; both scenarios are considered in Chapter 3. Performance evaluations are presented over two parts: in the first part, numerical evaluations illustrate the substantial gain achieved when CSI inaccuracy is considered and it highlights the dependency of a SDF network's mutual information on CSI accuracy at the three links (i.e., source to relay, relay to destination and source to destination). In the second part, it is

shown that with the knowledge of estimation error statistics and CSI estimates, channel adaptive schemes can achieve an ergodic mutual information close to that attained with the perfect CSI.

Using the results obtained in Chapter 3, Chapter 4 address the problem of resource allocation (i.e., subcarriers, power and rate) for PMP OFDMA-based multiservice BWA networks with inaccurate CSI. Appendix A shows that this problem is $\mathcal{NP}$-complete. The system model described in Chapter 3 is very general to capture the characteristics of various implementation scenarios. However, in Chapter 4, the focus is on only PMP OFDMA-based networks which requires limiting the system model in this chapter accordingly. Subscribers running different application may have different utility functions that represent their satisfaction with allocated resources. Thus, the resource allocation problem is posed as a NUM problem in which constraints model OFDMA networks specifications. Several decompositions are then carried out in the dual domain to decompose the problem into subproblems that are easier to solve. Throughout resource allocation, the RAU coordinates with the call admission controller to impose fairness among supported services. Power is allocated through inversion of the expected rate equations obtained following an approach similar to the one presented in Chapter 3. Then, complexity analysis is presented to show the proposed scheme's low complexity. Performance evaluations focus on the evaluation of two aspects: first, the gain achieved by considering CSI inaccuracy; second, the schemes's performance in limiting the aggregate rate of each service to a partition of the network capacity specified by the call admission controller in addition its performance in satisfying the exclusive subcarrier assignment and power constraints.

Whereas, in Chapter 4, resource allocation for PMP OFDMA-based BWA networks is considered, cooperative and single carrier BWA networks are considered in Chapter 5. After describing the cooperative scheme under consideration, a quadrature signaling cooperative scheme, power allocation is represented by an uncertain system in which uncertainty models CSI inaccuracy. Then, a robust and constrained Kalman filter-based power allocation scheme is proposed to minimize the allocated power and guarantee

BEP requirements. Unlike the schemes available in the literature, power is allocated such that certain signal to noise ratio (SNR) levels are maintained on both links of the broadcast phase (i.e., source to relay and source to destination), thereby providing a strong guarantee on maintaining the required BEP. Numerical results demonstrating the performance of the proposed scheme in terms of achieving the optimal power allocation, robustness to channel estimation error and adaptive responsiveness to changes in the BEP requirements are then presented.

Chapter 6 discusses contributions of this research towards solving the research allocation problem as well as possible future research directions are discussed.

1.5 Bibliographic Notes

Research presented in the thesis has appeared in [7–16]. The concepts discussed in Chapter 2 can be found [8]. The research results in Chapters 3, 4 and 5, respectively, can be found in [10, 12], [9, 11, 14, 15] and [13, 16]. A complete list of author's publications appears on page **??**.

Chapter 2

Overview of Broadband Access Networks

In this chapter, an overview of the OFDMA transceiver structure along with a detailed explanation of their operations is presented, we discuss the fading channel characteristics and how OFDMA and cooperative relaying improve communication over fading channels. In addition, the required knowledge of PHY and MAC relevant to the resource allocation problem formulation is described. Finally, a literature survey on assumptions related to resource allocation in BWA networks is presented.

2.1 The Radio Channel

The wireless propagation channel constrains the information communication capacity between a transmitter and a receiver. The design of a wireless communication system's coding, modulation, signal processing schemes and multiple access scheme is based on the channel model. The wireless channel is also generally time-varying, space-varying, frequency-varying, polarization-varying, dependent on the particular environment and the transmitter and receiver's location. Each type of variation presents randomness and

unpredictability. Nevertheless, the communication channel modeling has been well established to characterize the channel by various time and frequency metrics.

A channel's impulse response to a Dirac impulse function, $\delta(\tau)$, transmitted at the moment τ, looks like a series of impulses, because of the multipath reflections, represented by a time-variant function [17]

$$h(\tau, t) = \sum_{p=0}^{N_p-1} a_p(t) e^{j(2\pi f_{D,p} t + \varphi_p)} \delta\left(\tau - \tau_p(t)\right). \tag{2.1}$$

a_p, $f_{D,p}$, φ_p and τ_p respectively refer to the pth multipath's complex-valued arrival amplitude, doppler frequency, phase, and arrival excess delay, i.e., the delay measured with respect to the arrival of the first multipath component. N_p symbolizes the number of multipaths whose amplitudes exceed the detection threshold. In practice the number of multipath components that can be distinguished is very large. Therefore, only those multipaths that are temporally resolvable, i.e., their difference in arrival time to the receiver is greater than the inverse of the input signal bandwidth, are considered in detection.

The multipath propagation mechanisms (i.e., reflection, diffraction and scattering) result in delay dispersion which corresponds to frequency selectivity in the spectral domain. Each multipath's power and delay are given by the power delay profile (PDP), denoted by $|h(\tau)|^2$, where $h(\tau)$ denotes the temporally stationary discrete-time channel's impulse response:

$$h(\tau) = \sum_{p=0}^{N_p-1} a_p \delta\left(\tau - \tau_p\right). \tag{2.2}$$

The channel's PDP is a mathematical function whose complete characterization necessitates a long signal. However, the scalar metrics mean delay

$$\bar{\tau} = \frac{\int_0^\infty |h(t)|^2 \, t dt}{\int_0^\infty |h(t)|^2 \, dt} = \frac{\sum_{p=0}^{N_p-1} |a_p|^2 \tau_p}{\sum_{p=0}^{N_p-1} |a_p|^2} \tag{2.3}$$

and RMS delay spread

$$\tau_{RMS} = \frac{\int_0^\infty |h(t)\,(t-\bar{\tau})|^2 \, dt}{\int_0^\infty |h(t)|^2 \, dt} = \frac{\sum_{p=0}^{N_p-1} |a_p\,(\tau_p - \bar{\tau})|^2}{\sum_{p=0}^{N_p-1} |a_p|^2} \tag{2.4}$$

characterize the PDP temporal dispersion [18]. Figure 2.1-(a) shows the graphical representations of the mean delay and RMS delay spread. When the channel delay dispersion is greater than the signal reciprocal bandwidth, i.e., the symbol duration $T_s \ll \tau_{RMS}$, the transmitted train of symbols overlaps at the receiver. This phenomenon is known as ISI [19] which is illustrated in Figure 2.1-(a).

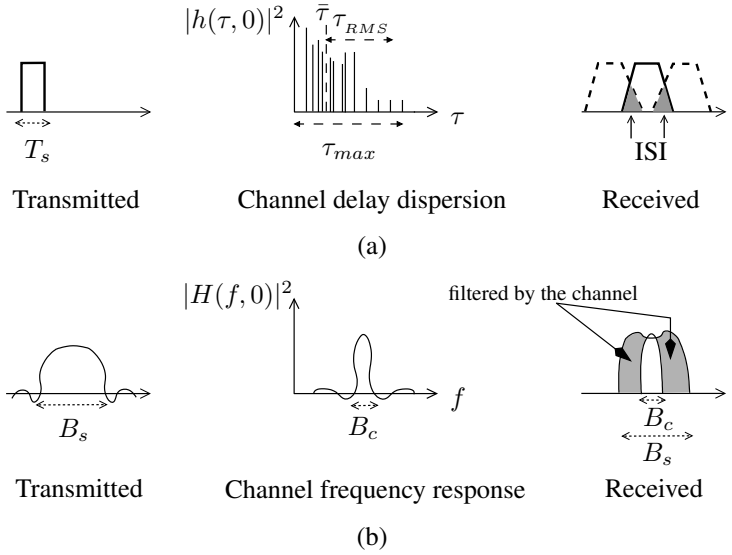

Figure 2.1: Wireless channel effect: (a) delay dispersion (b) frequency selectivity

Whereas the preceding metrics are in the relative-delay domain, channel fading may also be characterized in the spectral domain. Specifically, the coherence bandwidth, B_c, offers an alternative metric to the RMS-delay-spread, τ_{RMS}, to measure the channel's delay dispersion. The channel impulse response's Fourier transform gives the time-variant channel transfer function [17]:

$$\overline{H}(f,t) \;=\; \sum_{p=0}^{N_p-1} a_p(t) e^{j(2\pi(f_{D,p}t - f\tau_p(t)) + \varphi_p)}. \tag{2.5}$$

We define the channel frequency response's autocorrelation function as [20]:

$$R(\Delta f) \;=\; E\{\overline{H}(f,0)\overline{H}^*(f-\Delta f,0)\} \tag{2.6}$$

where $(\cdot)^*$ denotes the complex conjugate. The coherence bandwidth B_c measures the spectral width of $|R(\Delta f)|$ over which the channel is considered frequency flat. Note that

the frequency selectivity is relative to the transmitted signal bandwidth. In particular, if the channel's B_c is less than the transmitted signal bandwidth, the channel distorts the received signal at selected frequencies, as shown in Figure 2.1-(b). On the other hand, the channel does not affect the received signal, if its B_c is greater than the transmitted signal bandwidth.

Independently from delay dispersion and frequency selectivity, subscriber mobility causes frequency dispersion which in turn results in channel time selectivity. The time correlation function [20, 21]

$$R(\Delta t) \;=\; E\{\overline{H}(0,t)\overline{H}^{*}(0,t-\Delta t)\} \tag{2.7}$$

quantifies the time varying nature of the channel. From $R(\Delta t)$, the channel coherence time T_c can be obtained, and it is defined as the time duration over which the channel is essentially flat [17]. $R(\Delta t)$ Fourier transform is the channel doppler power spectrum that its correlation width is the B_d. If the channel impulse response changes rapidly within the symbol duration, i.e., $T_c < T_s$, the transmitted signal undergoes fast fading which leads to signal distortion [19], or the doppler spread B_d is greater than the transmitted signal bandwidth.

Communications engineers often discretize the continuous-time impulse response $h(t,\tau)$ of (2.1) to a very few discrete-time bins, for computational convenience in simulation studies. This results in the "tapped-delay-line" (TDL) model [22]:

$$h_{\mathrm{TDL}}(t,\tau) \;=\; \sum_{m=1}^{M} g_m(t)\delta\left(\tau-\tau_m(t)\right) \tag{2.8}$$

where M denotes the total number of taps, $\tau_m(t)$ symbolizes the mth tap's propagation delay, and $g_m(t)$ refers to the mth tap's complex-valued stochastic time-varying amplitude. The TDL model taps are represented by the vector $\mathbf{g}(t) = [g_1(t)\cdots g_m(t)\cdots g_M(t)]$.

2.1.1 Large-scale Fading

Unlike small-scale fading, large scale fading is distance dependant. As the receiver moves away from the transmitter, the received signal strength attenuates following the

inverse-power law:

$$H(f,t) = D^{-\kappa} \cdot \overline{H}(f,t) \tag{2.9}$$

where D denotes the distance between the transmitter and receiver in meters and κ is the path loss exponent.

To summarize,

- Delay dispersion results in frequency selective fading that alters the received signal waveform and hence causes performance degradation. This channel effect can be avoided by transforming the broadband signal into parallel narrowband signals with bandwidth smaller the the channel's B_c.
- Frequency dispersion smears the signal spectrum in the frequency domain. Also, cause time selectivity that varies the signal at a rate higher than the rate at which the channel can be accurately estimated. This can be taken care of by considering CSI inaccuracy.
- Large distance propagation attenuates the received signal strength. Thus, reduces the transmission rate by limiting the supportable modulation schemes. The adoption of cooperative relay technologies combats large scale fading.

2.2 Overview of OFDM and OFDMA

Based on the discussions in the previous section, the channel impairments significantly degrade the performance of BWA networks. Similar to any modulation technique, multi-carrier technologies try to approach the channel's capacity. For a specific channel condition and network architecture, one of the available techniques may perform better than others. The multi-carrier transmission is selected among others as a promising technique

for future communication due to its robustness against frequency selectivity for high-speed data communication, its maturity through the research and development for wireless LAN and terrestrial digital video transmission [23]. In the following subsections, we present an overview on OFDM and OFDMA multi-carrier transmitter and receiver structures along with detailed discussion on their operations. In addition, we present the basic operation of OFDMA MAC role in resource allocation.

2.2.1 Orthogonal Frequency Division Multiplexing (OFDM)

Frequency division multiplexing (FDM) first appeared in 1950s [23], however its implementation required multiple analog RF modules in each transceiver that made FDM impractical [21]. Recently, the implementation of IFFT/FFT and FDM ability in mitigating the channels ISI brought FDM back under light. While FDM major advantage is eliminating the ISI effect, it does not eliminate the ICI that rises due to closely packed multi-carriers. Alternatively, data symbols can be modulated on orthogonal multiple carriers to reduce Inter-Carrier Interference (ICI), which is termed orthogonal frequency division multiplexing (OFDM) [24].

For OFDM, the basic premise is to transmit a single high data rate signal (i.e., wide-band) on multiple orthogonal carriers at low data rate signals (i.e., narrow-band) [17, 23]. Figure 2.2 depicts a typical single subscriber OFDM transmitter and receiver block diagram and is used as a reference for discussing the basic operation of a system that implements OFDM or OFDMA at the PHY layer.

2.2.1.1 Transmitter

The high data rate stream is partitioned into I data blocks of N_{sc} length. The symbols are serial-to-parallel converted which increases the source symbol duration T_s to:

$$T_s^{'} = N_{sc}T_s. \tag{2.10}$$

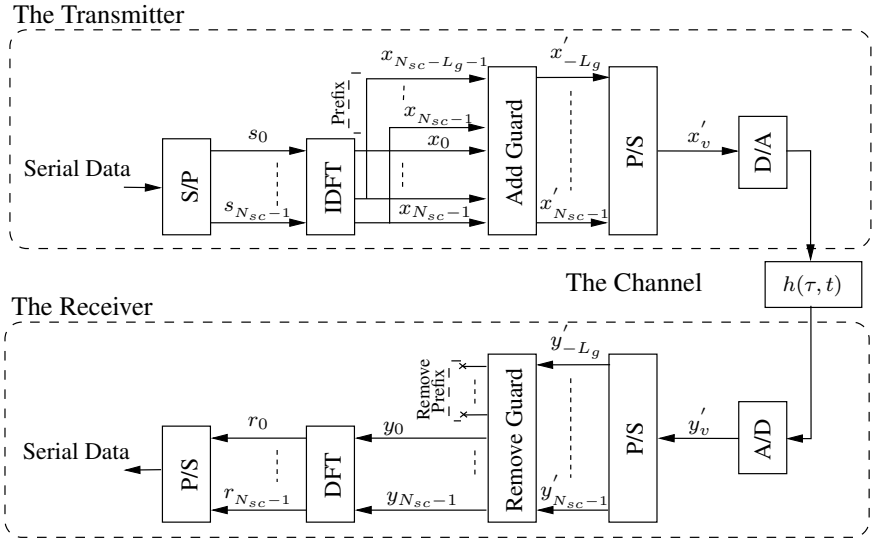

Figure 2.2: The PHY transmitter and receiver structure for OFDM.

Based on the channel characteristics presented in section 2.1, as the symbol duration increases, the ISI effect significantly decreases. Thus, the need for an equalizer at the receiver is eliminated which reduces the complexity of the receiver. After serial-to-parallel conversion, block i represents the OFDM symbol which consists of N_{sc} complex data symbols denoted by S_n, $n = 0, \ldots, N_{sc} - 1$. In other words, $S_{n,i}$ is the nth data symbol in the ith OFDM symbol. For simplicity, the ith index is dropped and we only refer to the S_n, $n = 0, \ldots, N_{sc} - 1$ sequence in each block (i.e., OFDM symbol) unless it is necessary. The complex data symbols are represented by the vector

$$\mathbf{s} = \left[s_0 \; s_1 \; \cdots \; s_{N_{sc}-1}\right]^T. \tag{2.11}$$

The OFDM is implemented by applying inverse discrete fourier transform (IDFT) to the data sequence S_n. The IDFT gives the following samples $x_v, \; v = 0, \cdots, N_{sc} - 1$ of each OFDM symbol [17]:

$$x_v \;\; = \;\; \frac{1}{N_{sc}} \sum_{n=0}^{N_{sc}-1} S_n e^{j\frac{2\pi nv}{N_{sc}}} \qquad v = 0, \cdots, N_{sc} - 1. \tag{2.12}$$

Using vector representation, the resulting time domain signal is given by

$$\begin{aligned} \mathbf{x} &= [x_0\, x_1\, \cdots\, x_{N_{sc}-1}]^T \\ &= \mathbf{Ws} \end{aligned} \tag{2.13}$$

where $\mathbf{W}$ is a $N_{sc} \times N_{sc}$ IDFT matrix that its columns correspond to the subcarriers to be modulated by the data. In particular, the matrix representation of $\mathbf{W}$ for $v = 0, \cdots, N_{sc}-1$ and $n = 0, \cdots, N_{sc}-1$ is given by

$$\mathbf{W} = \frac{1}{N_{sc}} \begin{bmatrix} 1 & 1 & \cdots & 1 \\ 1 & e^{j\frac{2\pi}{N_{sc}}} & \cdots & e^{j\frac{2\pi N_{sc}-1}{N_{sc}}} \\ 1 & \vdots & \ddots & \vdots \\ 1 & e^{j\frac{2\pi N_{sc}-1}{N_{sc}}} & \cdots & e^{j\frac{2\pi (N_{sc}-1)^2}{N_{sc}}} \end{bmatrix}. \tag{2.14}$$

Whereas serial-to-parallel conversion only reduces the ISI effect, cyclic extension of the symbol by inserting a guard interval T_g that is longer than the maximum channel dispersion time τ_{max} eliminates the residual ISI effect [17]. The sampled guard interval is a copy of $T_s^{'}$ last L_g samples[1]. Denote the cyclic extended OFDM symbol by:

$$T_s^{''} = T_s^{'} + T_g. \tag{2.15}$$

To eliminate ISI, the discrete length of the guard interval L_g has to be [17]:

$$\begin{aligned} L_g &= \left\lceil \frac{\tau_{max}}{T_s} \right\rceil \\ &= \left\lceil \frac{\tau_{max} N_{sc}}{T_s^{'}} \right\rceil \end{aligned} \tag{2.16}$$

After cyclic extension of the OFDM symbol, the time domain sampled sequence becomes:

$$x_v^{'} = \frac{1}{N_{sc}} \sum_{n=0}^{N_{sc}-1} S_n e^{j\frac{2\pi nv}{N_{sc}}} \qquad v = -L_g, \cdots, N_{sc}-1. \tag{2.17}$$

[1]Practically, the symbol source is continuous and guard insertion is archived by adjusting the starting phase and making the symbol period longer [25]

The matrix representation of the cyclic extended time domain OFDM Symbol is given by:

$$\begin{aligned} \mathbf{x}^{'} &= \left[x_{N_{sc}-L_g-1} \cdots x_{N_{sc}-1}\, x_0\, x_1 \cdots x_{N_{sc}-1}\right]^T. \\ &= \left[x^{'}_{-L_g} \cdots x^{'}_0 \cdots x^{'}_{N_{sc}-1}\right]^T \end{aligned} \tag{2.18}$$

After, parallel to series conversion, the $\mathbf{x}^{'}$ sequence is passed through digital-to-analog converter, then its output is transmitted to the wireless channel. Figure 2.3 depicts the time and frequency representation of an OFDM symbols and frames.

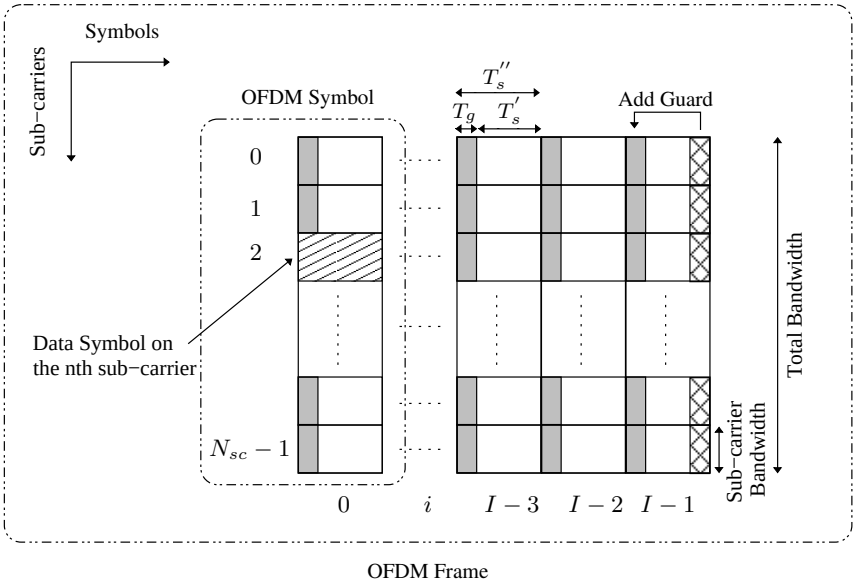

Figure 2.3: OFDM frame in time and frequency domains.

2.2.1.2 Channel

By implementing the OFDM multi-carrier modulation, the continuous channel transfer function (2.5) is sampled in time at OFDM symbol rate $1/T_s^{''}$ and in frequency at spacing

F_s. The discrete channel transfer function of multi-carrier systems is given by [17]:

$$\begin{aligned} H_{n,i} &= H(nF_s, iT_s^{''}) \\ &= \sum_{p=0}^{N_p-1} a_p(t) e^{j(2\pi(f_{D,p} iT_s^{''} - nFs\tau_p(t)) + \varphi_p)} \\ &= a_{n,i} e^{j\varphi_{n,i}}. \end{aligned} \tag{2.19}$$

A transmitted symbol on subcarrier n of the OFDM symbol i (Figure 2.3) is multiplied by the resulting fading amplitude $a_{n,i}$ and rotated by random phase $\varphi_{n,i}$ [17]. The multi-carriers gains can be represented by the following $N_{sc} \times N_{sc}$ channel matrix for the OFDM symbol i

$$\mathbf{H} = \begin{bmatrix} H_0 & 0 & \cdots & 0 \\ 0 & H_1 & & 0 \\ \vdots & & \ddots & \vdots \\ 0 & 0 & \cdots & H_{N_{sc}-1} \end{bmatrix}. \tag{2.20}$$

The OFDM symbol index i has been dropped for simplicity. Let h_v be the sampled L sequence of the channel impulse response $h(\tau, t)$ given in (2.1) at particular time t (i.e., $h_v = h(lT_s^{''}, iT_s^{''})$, $l = 0, \cdots, L = (\tau_{max}/T_s^{''})$) and represented by the vector **h**. Then, the above matrix **H** diagonal elements are the Discrete Fourier Transform (DFT) of channel discrete impulse response.

2.2.1.3 Receiver

After analog-to-digital conversion, the received sampled sequence $y_v^{'}$, $v = -L_g, \cdots, N_{sc}-1$ contains ISI in the first L_g samples that are discarded. The remaining sequence $0, \cdots, N_{sc}-1$ is demodulated by the DFT. The DFT demodulated multi-carrier sequence r_n, $n = 0, \cdots, N_{sc}-1$, consists of N_{sc} complex valued symbols [17]:

$$r_n = \sum_{n=0}^{N_{sc}-1} y_v e^{-j\frac{2\pi nv}{N_{sc}}}, \quad n = -0, \cdots, N_{sc}-1. \tag{2.21}$$

The matrix representation of the received data symbols is given by

$$\begin{aligned} \mathbf{r} &= [r_0\ r_1 \cdots r_{N_{sc}-1}]^T \\ &= \mathbf{W}^H \mathbf{y}. \end{aligned} \tag{2.22}$$

where the operator $(\cdot)^H$ denotes the matrix Hermitian and **y** is defined as $[y_0\ y_1 \cdots y_{N_{sc}-1}]^T$. Recall that x_v and y_v are the sampled sequences of the transmitted and received signals, respectively. The channel output (i.e., received signal) is related to the channel's impulse response and input (i.e., transmitted signal) by linear convolution denoted by $*$ as follows [21, 26]:

$$y_v = x_v * h_v \tag{2.23}$$

The DFT of x_v, h_v and y_v, are respectively denoted by s_n, H_n and r_n, $n = 0, \cdots, N_{sc}-1$. In frequency domain

$$r_n \neq s_n H_n \quad n = 0, \cdots, N_{sc} - 1 \tag{2.24}$$

because y_v is related to x_v and h_v by linear convolution [21]. However, the circular convolution is created for OFDM by appending the L_g samples ($x_{N_{sc}-L_g-1},\ x_{N_{sc}-L_g}, \cdots,\ x_{N_{sc}-1}$) to the sequence x_v. This circular convolution of the two periodic sequences is transformed in the product of their DFTs [21]:

$$r_n = H_n s_n \quad n = 0, \cdots, N_{sc} - 1 \tag{2.25}$$

which can be alternatively written as:

$$\mathbf{r} = \mathbf{Hs}. \tag{2.26}$$

Substituting equation (2.22) in the left-hand-side of equation (2.26) results in the following equations:

$$\begin{aligned} \mathbf{W}^H \mathbf{y}^T &= \mathbf{Hs} \\ \mathbf{H}^{-1} \mathbf{W}^H \mathbf{y}^T &= \mathbf{s} \end{aligned} \tag{2.27}$$

where $\mathbf{H}^{-1}$ is the matrix inverse[2]. The above result shows the major advantage of OFDM. Depending on the availability of the channel estimation matrix $\mathbf{H}$ and by the implementation of DFT, the transmitted symbols can be recovered.

2.2.2 Orthogonal Frequency Division Multiple Access (OFDMA)

Despite the advantages of OFDM in mitigating the channels's impairments as mentioned before, under-utilization of transmitter power and network subcarriers is its disadvantage. Particularly, when an OFDM transmitter accesses the channel in a time division manner (e.g., TDMA) the transmitter is forced to transmit on all available subcarriers N_{sc}, although it may require a less number of subcarriers to satisfy its transmission rate requirement. Consequently, the transmitter power consumption increases as the number of subcarriers increases. This disadvantage motivates the development of a PHY technology where transmitters are multiplexed in time and frequency, i.e., OFDMA. In this technology, the subscribers are exclusively assigned only a subset of the network available subcarriers in each time slot [2, 21]. The number of both time slots and subcarriers can be dynamically assigned to each subscriber; this is referred to as dynamic subcarrier assignment (DSA) which introduces multiuser diversity. The multiuser diversity gain arises from the fact that the utilization of given resources varies from one subscriber to another. A subcarrier may be in deep fading for one subscriber (e.g., the second subcarrier for subscriber X in Figure 2.4) while it's not for another subscriber (e.g., the same subcarrier for subscriber O). Allocating this particular subcarrier to the subscriber with higher channel gain permits higher transmission rate. To achieve multiuser diversity gain, a scheduler at the MAC sublayer is required to schedule subscribers in appropriate frequency and time slots.

[2]Note that the inverse of a diagonal matrix is a matrix with diagonal elements $\frac{1}{H_{n,n}}$ $n = 0, \cdots, N_{sc}-1$.

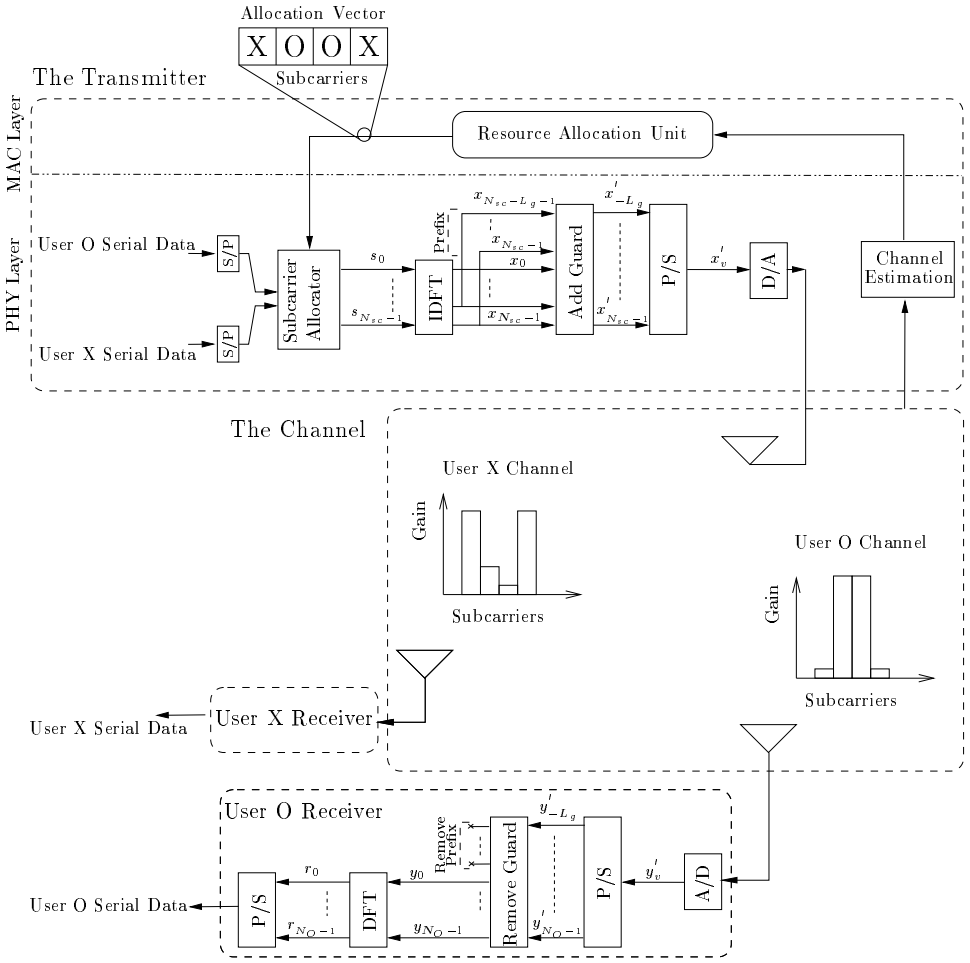

Figure 2.4: OFDMA transmitter and receiver's PHY structure and MAC operations

2.3 Relay Networks

Whereas OFDMA mitigates the channel small-scale fading (e.g., multipath caused ISI), it does not overcome the channel large-scale fading (i.e., propagation loss and shadowing). Relaying is a promising network architecture that overcomes challenges faced by conventional cellular networks. Relaying does not only provide radio coverage extension to cellular networks but also compacts shadowing, enhances capacity through exploiting spatial diversity, and effectively reduces the infrastructure deployment cost [27]. In addi-

tion, relaying is widely applicable in emergency civil networks[3] and military networks[4].

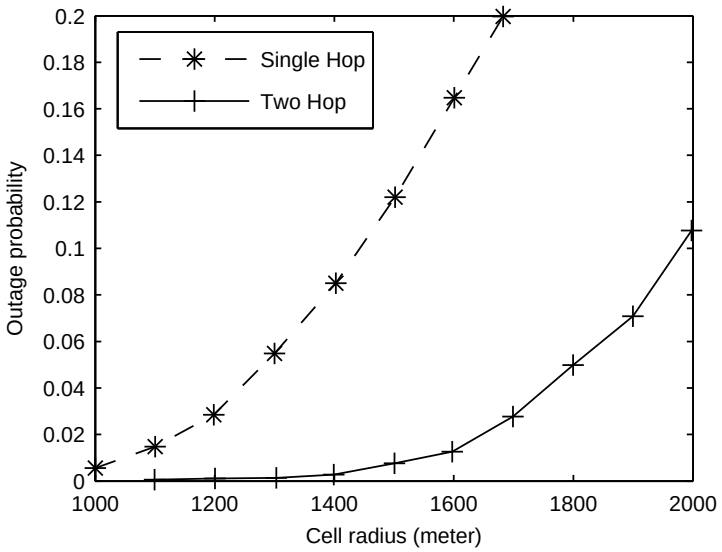

Figure 2.5: Cell radius dependant Outage probability (Figure 2 of [1])

The benefits of relaying are detailed in the following:

- **Wireless coverage extension**

  Broadband communication systems operating at high frequencies suffer distant dependant large scale fading [29] because of high penetration loss which results in a limited radio coverage range. Placing a relay station at distances where radio coverage is attenuated can relay a stronger signal (by employing a specific relaying schemes like AF and/or DF), hence it provides higher throughput to subscribers [29]. Relaying effectiveness in extending radio coverage was simulated in [1]. It simulates a single cell IEEE 802.16 network where subscribers communicate directly with the base station (e.g, single hop) or indirectly (e.g, two hop). Simulation results in Figure 2.5-(b) shows that the outage probability at 1600 meters can be decreased by 0.15 via relaying. Simulation results reported in [30] concurs. To

[3]Temporary formed networks to support areas of sport events or disaster.

[4]Examples can be found in [28].

illustrate relay networks efficiency in extending network coverage, we have simulated a wireless network coverage area with a IEEE 802.16 base station placed on the roof of CEIT building at the University of Waterloo (geographical coordinates $43°28'15"$N and $-80°32'2"$W) and a subscriber node placed at low elevation (i.e. -112 meters w.r.t to base station antenna hight) close to Grand-River as shown in Figure 2.6. The radio coverage results are produced using the Radio Mobile radio prediction software [31] with system settings based on the actual technical specification of the SIEMINS IEEE 802.16 base station [32] and SIEMINS Gigaset subscriber station [33]. The technical specifications of base-station, relay-station and subscriber-station are presented in Table 2.1. The topographic and elevation data were obtained from Natural Resources Canada. To serve the purpose of the illustration, the base station signal strength is restricted to the range (10 - 40dB). Green area in Figure 2.6 represents the geographical area covered with signal strength in this range. Subscribers in areas other than green area experience large scale fading rendering the signal strength to drop below 10dB threshold and communication can't be established with the base station. The 10dB is the minimum signal strength to support a specific modulation scheme. A Base station radio coverage can be extended by placing a relay station in the range of the base station coverage as shown in Figure 2.6. A relaying station is chosen to have the same technical specifications as the subscriber station to avoid the financial cost of unnecessary new base station. The new network coverage is represented by the green and yellow area.

- **Deployment cost reduction**

  While the base station connects to the backhaul network through wired connection (e.g., fiber-optic links), relay stations connect wirelessly to the base station [27]. This configuration eliminates the costs of backplane. Backplane cost includes, land-lines networks deployments cost, land lease or purchase to run links, construction, permitting, or the cost of using other service providers deployed networks. In sub-urban areas where land-line network deployment can be financially

expensive and the number of subscribers is not large enough to motivate such costly coverage extension, relay stations placement is cost effective alternative to placing a new base station.

- **Efficient utilization of resources**

  In cellular based radio systems efficient utilization of resources rely on intelligent allocation of frequencies, codes, or time slots. Resource reuse has been widely used to achieve the desired utilization. For instance, neighboring cells are assigned completely different frequency channels to avoid co-channel interference. However, distant cells can be assigned the same frequency channels as long as the distance is large enough to keep the interference within tolerable levels. Cell sectoring further reduces the co-channel interference by using directional antennas, each radiating within a specific sector. Hence, the interference is reduced to a fraction of the co-channel cells rather than the whole co-channel cells [34]. Similarly, relay stations radiate within a limited spatial area causing low co-channel interference to relay stations operating on the same resources (i.e., frequencies, codes, time slots).

Table 2.1: Technical specifications the subscriber, base and relay stations

Stations	Frequency Range (GHz)	Transmit Power (dBm)	Receiver Sensitivity (dBm)	Antenna Type	Antenna Gain (dB)	Antenna Azimuth (degrees)
Base	3.4 - 3.8	35	-100	Omni	35	n/a
Relay	3.4 - 3.8	27	-85	Yagi	9.5	160°
Subscriber	3.4 - 3.8	27	-85	Yagi	9.5	360°

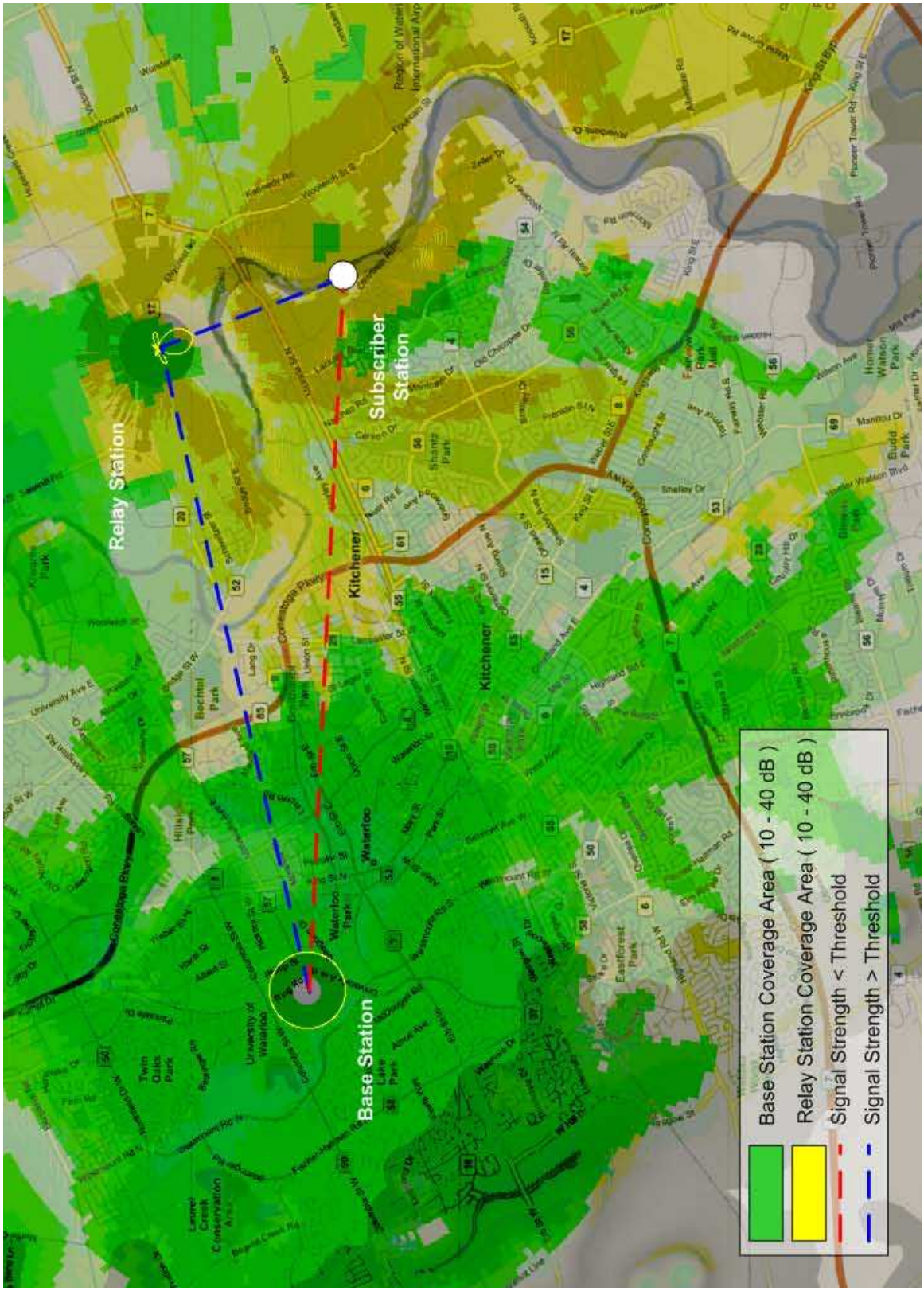

Figure 2.6: Illustration of a IEEE 802.16 base station and relay station radio coverage.

2.4 Literature Survey and Commonly Invoked Assumptions

Because of its desirable features presented and discussed in the previous section, OFDMA is being widely adopted in 4G networks. Prior to designing a resource allocation scheme, assumptions are made based on the considered network model [8]. In this section, major possible assumptions made in the literature on OFDMA resource allocation for such networks are presented. Figure 1.1 shows the above mentioned OFDMA based possible networks. In a single cell, the subscriber stations are randomly moving, nomadic, or fixed over the cell coverage area, relays are either mobile or fixed and the base station is fixed at the center of the cell. Subscriber stations can either directly communicate with the base station in PMP [35], or indirectly through one relay station [36–38] or more than one relay station [39–42].

The relay stations relay the information it receives from the base station to the nodes in the down-link or from subscriber stations to base station in the uplink by employing one of the available forwarding schemes. Alternatively, an adaptive forwarding scheme can be designed to adaptively cope with the varying network parameters. Under a specific network parameters like network topology, relay stations locations, and wireless channel condition, node to relay distance, one of the forwarding schemes out performs the others. A TDD transmission pattern is considered where a source node transmits to the relay station (in-direct communication) or to the base station (direct communication) in the first time frame and the relay station forwards the information in the next time frame [36–42]. In a multi-carrier systems, a relay station can either re-transmit the received data on the same subcarrier [39–41] or on a different subcarrier. While the former is simpler, the later allows the relay station to exploit the chance of transmitting on a different subcarrier with a higher gain. Following the definition of OFDMA, each subcarrier is exclusively assigned to one subscriber and relay pair or to subscriber and base station pair. However, each source can be assigned more than one subcarrier to satisfy its QoS requirements. The base station can allocate power uniformly to all subcarriers or adaptively according

to each subcarrier gain. In addition, transmitting subscriber stations can employ either adaptive modulation or non-adaptive modulation schemes.

The resource allocation unit at the base station allocate resources to subscriber stations and/or relay stations based on the above mentioned possible assumptions in addition to the following:

- The channel state information for each subcarrier between any communicating stations is either perfectly [21, 24, 35, 38–57] or imperfectly [58–60] available at the resource allocation unit.
- The channel experiences either fast fading (i.e., mobile subscriber stations) [49, 61–65] or slow fading (i.e., fixed subscriber stations) [21, 24, 35, 38–42, 52–57]. Hence, channel coefficients can be either be varying or constant during resource allocation.
- There exists a scheme to exchange the channel state and control information between the sources, relays and the base station.
- Subscribers' channel frequency response are independent [21, 24, 35, 38–57].

The above summarizes major assumptions made in the literature. Among these assumptions, we adopt practical ones in the design of resource allocation schemes. In particular, assumptions we adopt are as follows:

- Adaptive forwarding and modulation schemes are employed.
- The source and relay operate on the same subcarrier in a TDD fashion.
- Subcarriers are exclusively allocated to subscribers and relays.
- The CSI is imperfectly available at the RAU along with the estimation error statistics.
- The channel under goes either types of fading.

- There exist a scheme to exchange CSI between the RAU and subscribers.
- Subscribers channels are assumed independent.
- The resource allocation unit is assumed to have limited computational power which requires the development of low complexity resource allocation schemes.

Chapter 3

Ergodic Mutual Information of OFDMA-based Cooperative Networks

This chapter presents a novel approach to investigate ergodic mutual information of OFDMA-based SDF cooperative relay networks with CSI. Figure 3.1 illustrates a single cell scenario of OFDMA cooperative relay networks. The ergodic mutual information of single carrier and direct transmission are also investigated because they are special cases of OFDMA and cooperative relaying, respectively. Relay stations are either dedicated or non-dedicated (i.e., subscriber stations assisting other subscriber stations). The CSI imperfection is modeled as an additive random variable with known statistics. Numerical evaluations and simulations demonstrate that by considering the CSI imperfection based on a priori knowledge of the estimation error statistics, a substantial gain can be achieved in terms of ergodic mutual information which makes channel adaptive schemes closer to practical implementations.

Although extensive research has been published on relay networks, the inaccuracy of CSI remains a major obstacle for their practical implementation. The performance of multicarrier systems is severely degraded by considering an inaccurate and delayed CSI as perfect one [66–68], where the channel estimation error at the PHY layer propagates to higher layers, resulting in poor system performance. This practical implementation

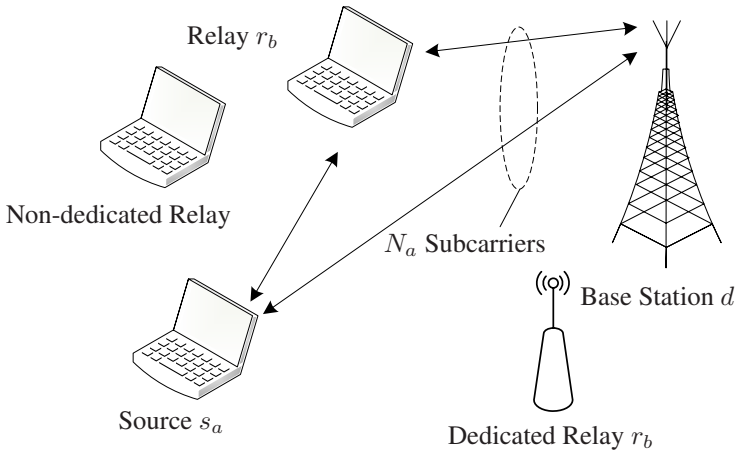

Figure 3.1: Illustration of an OFDMA-based cooperative relay network.

issue has motivated researchers working on different aspects of wireless networks design to consider estimation error in their design. For instance, A relay-precoder and decoder are jointly optimized for cooperative networks in [69]. In [70], a power loading scheme for data and pilots is proposed for OFDMA networks. Resource allocation (i.e., power, rate and beamforming) schemes are proposed for OFDMA PMP networks [71–73] and for cooperative networks [74]. The design of a spacetime constellation is considered in [75]. An extensive survey on the field of limited feedback across different systems and standards can be found in [76]. In all mentioned works, considering CSI imperfection improves performance in terms of various metrics as demonstrated by the reported simulation results, with the cost of design complexity. A specific type of wireless system may have complexity limitation where implementing such a design may degrade the overall performance. In addition, certain wireless systems' estimation errors may be minimal, and in these cases CSI imperfection becomes unnecessary. Therefore, evaluating the performance gain achieved by considering CSI imperfection due to channel estimation error is of great importance.

The aim of this chapter is to evaluate the ergodic mutual information of OFDMA-

based SDF networks when the CSI is treated as inaccurate, and a priori knowledge of the error statistics is available. The performance gain is measured in terms of a common metric, the ergodic mutual information, and the amount of channel estimation error is represented by the error statistics. The importance of the analytical results lies in the following:

- Given the estimation error statistics, the ergodic mutual information achieved by accounting for CSI inaccuracy can be evaluated. Thus, system designers can decide if considering CSI inaccuracy is worth the incurred computational complexity.
- Allocating resources (i.e, rate, power, subcarriers, and relay stations pairing) in OFDMA cooperative networks based on the proposed approach achieves a network ergodic mutual information close to the one that can be achieved if perfect CSI is available. In particular, a resource allocation problem can be formulated to maximize the evaluated ergodic mutual information while satisfying the network constraints [9].
- The considered system model is very general, such that the proposed approach can be applied to either uplink or downlink modes, dedicated or non-dedicated relays. Furthermore, although the evaluated ergodic mutual information is for SDF networks, it can be applied to direct transmission in PMP networks because it is a special case of SDF networks.

The remainder of the Chapter is organized as follows. Section 3.1 introduces the system model of the OFDMA cooperative relay network under consideration. The SDF ergodic mutual information is derived in Section 3.2. The performance improvement is evaluated in Section 3.3, followed by a summary in Section 3.4.

3.1 System Model

Consider a single cell scenario with one base station at the center of the cell, multiple relay stations, and multiple subscriber stations. Subscriber stations that are not trans-

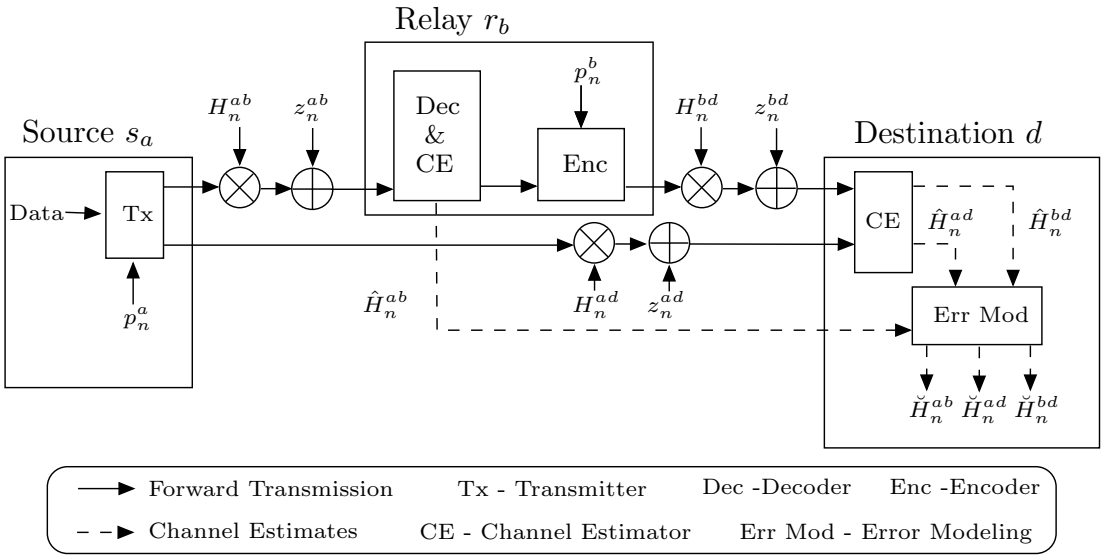

Figure 3.2: Illustrative SDF network with the actual, estimated and imperfect CSI on the three links in the uplink mode.

mitting can cooperate with other subscriber stations as relay stations (i.e., non-dedicated relays). There are A sources forming the set $\mathcal{A} = \{s_1, \cdots, s_a, \cdots, s_A\}$. The available B relays form the set $\mathcal{B} = \{r_1, \cdots, r_b, \cdots, r_B\}$. The destination is symbolized by d. The subscriber stations share a total of N_{sc} subcarriers available to the cell. The set of subcarriers is denoted by $\mathcal{N} = \{1, \cdots, n, \cdots, N_{sc}\}$. In OFDMA networks, a sub-set $\mathcal{N}_a$ [1] of the network subcarriers is exclusively assigned to a source-relay pair, as shown in Figure 3.1. We consider a frequency selective fading channel between any pair of communicating stations.

Although the presentation of the system model focuses on networks in uplink mode, the proposed approach can used to evaluate the ergodic mutual information of both uplink and downlink modes. An OFDMA frame consists of multiple time slots. An OFDMA symbol is transmitted on all assigned subcarriers during the same time slot [8]. Other schemes may use a full frame for broadcasting the signals to the relay and destination,

[1] The cardinality of the sub-set $\mathcal{N}_a$ is denoted by N_a.

and another frame for relaying, but the basic concept is the same. In SDF [6], the transmission frame is divided into two halves. During the first half, the relay r_b and destination d, respectively, receive the following OFDM signals

$$\mathbf{r}^{ab}[j] = \sqrt{\mathbf{P}^a[j]}\mathbf{H}^{ab}[j]\mathbf{s}[j] + \mathbf{z}^{ab}[j], \tag{3.1}$$

$$\mathbf{r}^{ad}[j] = \sqrt{\mathbf{P}^a[j]}\mathbf{H}^{ad}[j]\mathbf{s}[j] + \mathbf{z}^{ad}[j], \tag{3.2}$$

where $\sqrt{\mathbf{P}^a}[j]$ is a diagonal $N_a \times N_a$, and where $\sqrt{p_n^a[j]}$ for $n \in \mathcal{N}_a$ being the power allocated by a MAC resource allocation scheme to the ath source on the nth subcarrier during the jth slot. $\mathbf{H}^{bd} = diag\{\boldsymbol{\hbar}^{bd}[j]\}$ is the diagonal channel matrix that models the channel between the relay r_b and destination d; $\boldsymbol{\hbar}^{bd}[j]$ is a vector of $H_n^{bd}[j]$ for $n \in \mathcal{N}_a$, which is the nth subcarrier gain of the r_b to d channel during the jth slot[2]. $\mathbf{s}[j]$ denotes the data source symbols. The vectors $\mathbf{z}^{ab}$ and $\mathbf{z}^{ad}$, respectively, represent the additive noise at the source-to-relay and source-to-destination channels and are modeled as circularly symmetric complex Gaussian $\mathbf{z}^{ab} \sim \mathcal{CN}(\mathbf{0}, (\sigma_z^{ab})^2\mathbf{I})$ and $\mathbf{z}^{ad} \sim \mathcal{CN}(\mathbf{0}, (\sigma_z^{ad})^2\mathbf{I})$. In the second half, if the source-to-relay ergodic mutual information is greater than a threshold R, the relay cooperates with the source, and the destination receives the following OFDM signal:

$$\begin{aligned}\mathbf{r}^{bd}[j+\frac{1}{2}] = \sqrt{\mathbf{P}^b}[j+\frac{1}{2}](\sqrt{\mathbf{P}^a}[j+\frac{1}{2}])^{-1} \\ \times\mathbf{H}^{bd}[j+\frac{1}{2}]\hat{\mathbf{r}}^{ab}[j] + \mathbf{z}^{bd}[j+\frac{1}{2}],\end{aligned} \tag{3.3}$$

where T_f is the frame length and $\sqrt{\mathbf{P}^b}[j]$ is a diagonal matrix of $\sqrt{p_n^b[j]},\ n \in \mathcal{N}_a$ being the power allocated to the bth relay on the nth subcarrier during the jth slot. $\hat{\mathbf{r}}^{ab}[j]$ denotes the re-encoded signal by r_b. The additive noise vector at the relay-to-destination channel $\mathbf{z}^{bd}[j+\frac{T_f}{2}]$ is modeled as $\mathbf{z}^{bd} \sim \mathcal{CN}(\mathbf{0}, (\sigma_z^{bd})^2\mathbf{I})$. The destination d combines the received signals ($\mathbf{r}^{ad}[j]$ and $\mathbf{r}^{bd}[j+\frac{T_f}{2}]$) by employing one of the literature available

[2]The superscript $\cdot^{ab}$, $\cdot^{bd}$ and $\cdot^{ad}$, respectively, denote the link between a source s_a and a relay r_b, a relay r_b and a source s_a, and a source s_a and the destination d.

diversity combining schemes [6]. Conversely, if the mutual information of the s_a to r_b link is less than R, s_a continues transmitting to d without the cooperation of r_b.

The CSI is updated every OFDMA frame. As mentioned previously, the frame is divided into two sub-frames. At the beginning of the first half of the frame, a sequence of OFDM symbols are transmitted by the source s_a to the relay r_b and destination d for channel estimation. In the second sub-frame, the relay r_b transmits another set of training symbols for the destination d to estimate the channel. In addition, it forwards its estimate $\hat{\mathbf{H}}^{ab}$ of $\mathbf{H}^{ab}$ to the destination d which estimates $\mathbf{H}^{bd}$ and $\mathbf{H}^{ad}$ to obtain $\hat{\mathbf{H}}^{bd}$ and $\hat{\mathbf{H}}^{ad}$. The slot index (i.e., $[j]$) is dropped for simpler notation. Figure 3.2 shows modeling parameters of an illustrative SDF network.

Note that the channel matrices are diagonals of the subcarrier channel gain vectors, namely $\boldsymbol{\hbar}^{ab}$, $\boldsymbol{\hbar}^{ad}$ and $\boldsymbol{\hbar}^{bd}$. Let $\hat{\boldsymbol{\hbar}}^{ab}$, $\hat{\boldsymbol{\hbar}}^{ad}$ and $\hat{\boldsymbol{\hbar}}^{bd}$ be their estimates available at the receiver, respectively. Before the next frame estimates arrive, they are treated as deterministic [77] and their delay and estimation error are modeled by $\tilde{\boldsymbol{\hbar}}^{ab}$, $\tilde{\boldsymbol{\hbar}}^{ad}$ and $\tilde{\boldsymbol{\hbar}}^{bd}$ [58]; delay error represents the time difference between the instant the channel is estimated and the instant it is considered by the channel adaptive scheme, during which the channel may change. Hence, given the channel estimates $\hat{\boldsymbol{\hbar}}^{ab}$, $\hat{\boldsymbol{\hbar}}^{ad}$ and $\hat{\boldsymbol{\hbar}}^{bd}$, the imperfect CSI for the three links (i.e., s_a to r_b, s_a to d and r_b to d) are modeled, respectively, as follows:

$$\breve{\boldsymbol{\hbar}}^{ab} = \hat{\boldsymbol{\hbar}}^{ab} + \tilde{\boldsymbol{\hbar}}^{ab}; \tag{3.4}$$

$$\breve{\boldsymbol{\hbar}}^{ad} = \hat{\boldsymbol{\hbar}}^{ad} + \tilde{\boldsymbol{\hbar}}^{ad}; \tag{3.5}$$

$$\breve{\boldsymbol{\hbar}}^{bd} = \hat{\boldsymbol{\hbar}}^{bd} + \tilde{\boldsymbol{\hbar}}^{bd}. \tag{3.6}$$

Assuming a Rayleigh channel and AWGN noise [78], $\breve{\boldsymbol{\hbar}}^{ab}$, $\breve{\boldsymbol{\hbar}}^{ad}$ and $\breve{\boldsymbol{\hbar}}^{bd}$, respectively, are $\sim \mathcal{CN}(\hat{\boldsymbol{\hbar}}^{ab}, \boldsymbol{\Sigma}_{\tilde{\boldsymbol{\hbar}}^{ab}})$, $\sim \mathcal{CN}(\hat{\boldsymbol{\hbar}}^{ad}, \boldsymbol{\Sigma}_{\tilde{\boldsymbol{\hbar}}^{ad}})$ and $\sim \mathcal{CN}(\hat{\boldsymbol{\hbar}}^{bd}, \boldsymbol{\Sigma}_{\tilde{\boldsymbol{\hbar}}^{bd}})$ where $\boldsymbol{\Sigma}_{\tilde{\boldsymbol{\hbar}}^{ab}}$, $\boldsymbol{\Sigma}_{\tilde{\boldsymbol{\hbar}}^{ad}}$ and $\boldsymbol{\Sigma}_{\tilde{\boldsymbol{\hbar}}^{bd}}$ are the error covariance matrices [58, 79–84]. The estimation errors on different subcarriers are independent; hence, the covariance matrices are scalar multiples of the identity matrix. Therefore, $\boldsymbol{\Sigma}_{\tilde{\boldsymbol{\hbar}}^{ab}} = (\tilde{\sigma}_{\epsilon}^{ab})^2\mathbf{I}$, $\boldsymbol{\Sigma}_{\tilde{\boldsymbol{\hbar}}^{ad}} = (\tilde{\sigma}_{\epsilon}^{ad})^2\mathbf{I}$, and $\boldsymbol{\Sigma}_{\tilde{\boldsymbol{\hbar}}^{bd}} = (\tilde{\sigma}_{\epsilon}^{bd})^2\mathbf{I}$ where $(\tilde{\sigma}_{\epsilon}^{ab})^2$, $(\tilde{\sigma}_{\epsilon}^{ad})^2$, and $(\tilde{\sigma}_{\epsilon}^{bd})^2$ are the delay and estimation error variances.

Hence, the nth subcarrier[3] imperfect CSI ($[\breve{\boldsymbol{\hbar}}^{ab}]_n = \breve{H}_n^{ab}$, $[\breve{\boldsymbol{\hbar}}^{ad}]_n = \breve{H}_n^{ad}$, and $[\breve{\boldsymbol{\hbar}}^{bd}]_n = \breve{H}_n^{bd}$) are, respectively, modeled as $\sim \mathcal{CN}(\hat{H}_n^{ab}, (\tilde{\sigma}_\epsilon^{ab})^2)$, $\sim \mathcal{CN}(\hat{H}_n^{ad}, (\tilde{\sigma}_\epsilon^{ad})^2)$ and $\sim \mathcal{CN}(\hat{H}_n^{bd}, (\tilde{\sigma}_\epsilon^{bd})^2)$. Therefore, their squares follow non-central Chi-square probability density functions (PDFs) given by [85] as follows:

$$f_X(x) = \frac{1}{(\tilde{\sigma}_\epsilon^{ad})^2} e^{-\frac{(|\hat{H}_n^{ad}|^2 + x)}{(\tilde{\sigma}_\epsilon^{ad})^2}} \mathfrak{I}_0\left(2\sqrt{\frac{|\hat{H}_n^{ad}|^2 x}{(\tilde{\sigma}_\epsilon^{ad})^4}}\right); \tag{3.7}$$

$$f_Y(y) = \frac{1}{(\tilde{\sigma}_\epsilon^{ab})^2} e^{-\frac{(|\hat{H}_n^{ab}|^2 + y)}{(\tilde{\sigma}_\epsilon^{ab})^2}} \mathfrak{I}_0\left(2\sqrt{\frac{|\hat{H}_n^{ab}|^2 y}{(\tilde{\sigma}_\epsilon^{ab})^4}}\right); \tag{3.8}$$

$$f_Z(z) = \frac{1}{(\tilde{\sigma}_\epsilon^{bd})^2} e^{-\frac{(|\hat{H}_n^{bd}|^2 + z)}{(\tilde{\sigma}_\epsilon^{bd})^2}} \mathfrak{I}_0\left(2\sqrt{\frac{|\hat{H}_n^{bd}|^2 z}{(\tilde{\sigma}_\epsilon^{bd})^4}}\right), \tag{3.9}$$

where $\mathfrak{I}_0(\cdot)$ is the zeroth-order modified Bessel function of the first kind. The random variables $|\breve{H}_n^{ad}|^2$, $|\breve{H}_n^{ab}|^2$ and $|\breve{H}_n^{bd}|^2$ are, respectively, denoted by X, Y and Z for simpler notation.

3.2 SDF Ergodic Mutual Information

The SDF mutual information for deterministic and perfectly known CSI is given by equation [6]:

$$\overline{I}_{n,a,b}^{SDF} = \begin{cases} \frac{1}{2}\log\left(1 + \frac{2p_n^a |\hat{H}_n^{ad}|^2}{(\sigma_z^{ad})^2}\right), & \frac{1}{2}\log\left(1 + \frac{2p_n^a |\hat{H}_n^{ab}|^2}{(\sigma_z^{ab})^2}\right) \leq R \quad (3.10a) \\ \frac{1}{2}\log\left(1 + \frac{2p_n^a |\hat{H}_n^{ad}|^2}{(\sigma_z^{ad})^2} + \frac{2p_n^b |\hat{H}_n^{bd}|^2}{(\sigma_z^{bd})^2}\right), & \frac{1}{2}\log\left(1 + \frac{2p_n^a |\hat{H}_n^{ab}|^2}{(\sigma_z^{ab})^2}\right) > R. \quad (3.10b) \end{cases}$$

[3] $[\boldsymbol{x}]_n$ denotes the nth element of vector $\boldsymbol{x}$.

When the imperfection of CSI is considered, the channel gains are random variables and the ergodic mutual information becomes a function of them; thus, (3.10) becomes

$$E\left[I_{n,a,b}^{SDF}\right] = \begin{cases} E\left[I_n^{ad}|I_n^{ab}\right], & Pr\left\{I_n^{ab} \leq R\right\} \quad (3.11a) \\ E\left[I_n^{abd}|I_n^{ab}\right], & Pr\left\{I_n^{ab} > R\right\}, \quad (3.11b) \end{cases}$$

where $E\left[I_n^{ad}|I_n^{ab}\right]$ is the ergodic mutual information of the direct transmission and $E\left[I_n^{abd}|I_n^{ab}\right]$ is the cooperation ergodic mutual information, $Pr\left\{I_n^{ab} \leq R\right\}$ is the probability that the information on the source-to-relay link is less than or equal to a threshold R. With the PDF of $|\breve{H}_n^{ad}|^2$, $|\breve{H}_n^{ab}|^2$ and $|\breve{H}_n^{bd}|^2$, we evaluate the ergodic mutual information of SDF, $E\left[I_{n,a,b}^{SDF}\right]$. In the following, we focus on the mutual information at the subcarrier level; to do so, the subcarrier index n is removed.

3.2.1 Direct and Cooperative Transmission Probabilities: $Pr\left\{I^{ab} \leq R\right\}$ and $Pr\left\{I^{ab} > R\right\}$

The random variable mutual information between s_a and r_b that is a function of the imperfect CSI random variable Y is given by [58]

$$I^{ab} = \frac{1}{2}\log_e\left(1 + \frac{2p^a Y}{(\sigma_z^{ab})^2}\right), \quad (3.12)$$

then,

$$Pr\left\{I^{ab} \leq R\right\} = \int_0^R f_{I^{ab}}(i)di, \quad (3.13)$$

where $f_{I^{ab}}(i)$ is the PDF of I^{ab}. Define the strictly increasing function $g(y) = \frac{1}{2}\log_e(1 + \frac{2p^a y}{(\sigma_z^{ab})^2})$, then $f_{I^{ab}}(i)$ is

$$f_{I^{ab}}(i) = f_Y\left(g^{-1}(i)\right)\left|\frac{dg^{-1}(i)}{di}\right|, \quad (3.14)$$

where $g^{-1}(\cdot)$ is the inverse function given by

$$\begin{aligned} i &= g(y) && (3.15) \\ &= \frac{1}{2}\log_e(1 + \frac{2p^a y}{(\sigma_z^{ab})^2}) && (3.16) \\ g^{-1}(y) &= \frac{(e^{2i}-1)(\sigma_z^{ab})^2}{2p^a}. && (3.17) \end{aligned}$$

Hence,

$$\frac{dg^{-1}(i)}{di} = \frac{(\sigma_z^{ab})^2 e^{2i}}{2p^a}. \tag{3.18}$$

Therefore, the distribution $f_{I^{ab}}(i)$ is

$$f_{I^{ab}}(i) = \frac{(\sigma_z^{ab})^2 e^{2i}}{2p^a(\tilde{\sigma}_\epsilon^{ab})^2} e^{-\frac{|\hat{H}^{ab}|^2 + \frac{(\sigma_z^{ab})^2(e^{2i}-1)}{2p^a}}{(\tilde{\sigma}_\epsilon^{ab})^2}} \mathfrak{I}_0\left(2\sqrt{\frac{|\hat{H}^{ab}|^2(\sigma_z^{ab})^2(e^{2i}-1)}{2p^a(\tilde{\sigma}_\epsilon^{ab})^4}}\right), \tag{3.19}$$

which can be written as

$$f_{I^{ab}}(i) = 2\zeta e^{2i-\eta-\zeta(e^{2i}-1)} \mathfrak{I}_0\left(2\sqrt{\eta\zeta(e^{2i}-1)}\right), \tag{3.20}$$

for $\eta = \frac{|\hat{H}^{ab}|^2}{(\tilde{\sigma}_\epsilon^{ab})^2}$ and $\zeta = \frac{(\sigma_z^{ab})^2}{2p^a(\tilde{\sigma}_\epsilon^{ab})^2}$. By the transformation $i' = (e^{2i}-1)$, substituting the series representation of $\mathfrak{I}_0(\cdot)$ [[86], 8.447(1)] into (3.20) and (3.20) into (3.13) gives

$$Pr\left\{I^{ab} \leq R\right\} = \int_0^{e^{2R}-1} e^{-\eta-\zeta i'} \mathfrak{I}_0\left(2\sqrt{\eta\zeta i'}\right) di' \tag{3.21}$$

$$= \int_0^{e^{2R}-1} e^{-\eta-\zeta i'} \sum_{k=0}^{\infty} \frac{(\eta\zeta i')^k}{(k!)^2} di'. \tag{3.22}$$

Now, integrating by parts for $u = \sum_{k=0}^{\infty} \frac{(\eta\zeta i')^k}{(k!)^2}$ and $dv = e^{-\zeta i'}$ gives

$$= \zeta e^{-\eta}\left[\frac{e^{-\zeta i'}}{-\zeta} \sum_{k=0}^{\infty} \frac{(\eta\zeta i')^k}{(k!)^2}\right]_0^{e^{2R}-1} - \int_0^{e^{2R}-1} \frac{e^{-\zeta i'}}{-\zeta} \sum_{k=1}^{\infty} \frac{\eta^k \zeta^k (i')^{k-1}}{k!(k-1)!} di'. \tag{3.23}$$

By repeating the integration by parts infinity times, we arrive at

$$= e^{-\eta}\left[\sum_{m=0}^{\infty}\left(-e^{-\zeta(e^{2R}-1)} \sum_{k=m}^{\infty} \frac{\eta^k(\zeta(e^{2R}-1))^{k-m}}{k!(k-m)!}\right) + \frac{\eta^m}{m!}\right], \tag{3.24}$$

and when the index k is replaced by $k' = k - m$, (3.24) becomes

$$= e^{-\eta}\left[\sum_{m=0}^{\infty}\left(-e^{-\zeta(e^{2R}-1)} \sum_{k'=0}^{\infty} \frac{\eta^{k'+m}(\zeta(e^{2R}-1))^{k'}}{(k'+m)!k'!}\right) + \frac{\eta^m}{m!}\right]. \tag{3.25}$$

Rearranging the absolutely convergent series [87], the above integral in (3.22) evaluates to

$$= e^{-\eta}\left[\sum_{m=0}^{\infty} -e^{-\zeta(e^{2R}-1)}\sum_{k'=0}^{m}\frac{\eta^m(\zeta(e^{2R}-1))^{k'}}{m!k'!}+\frac{\eta^m}{m!}\right]. \tag{3.26}$$

By substituting back the values of η and ζ, (3.26) becomes

$$\begin{aligned} Pr\left\{I^{ab}\leq R\right\} = e^{-\frac{|\hat{H}^{ab}|^2}{(\tilde{\sigma}_\epsilon^{ab})^2}}\Bigg[\sum_{m=0}^{\infty}\Bigg(-e^{-\left(\frac{(\sigma_z^{ab})^2}{2p^a(\tilde{\sigma}_\epsilon^{ab})^2}\right)(e^{2R}-1)} \\ \times\sum_{k'=0}^{m}\frac{\left(\frac{|\hat{H}^{ab}|^2}{(\tilde{\sigma}_\epsilon^{ab})^2}\right)^m\left(\left(\frac{(\sigma_z^{ab})^2}{2p^a(\tilde{\sigma}_\epsilon^{ab})^2}\right)(e^{2R}-1)\right)^{k'}}{m!k'!}\Bigg) \\ +\frac{\left(\frac{|\hat{H}^{ab}|^2}{(\tilde{\sigma}_\epsilon^{ab})^2}\right)^m}{m!}\Bigg]. \end{aligned} \tag{3.27}$$

Hence, $Pr\left\{I^{ab}>R\right\}$ can be simply found from (3.27) by

$$Pr\left\{I^{ab}>R\right\} = 1 - Pr\left\{I^{ab}\leq R\right\}. \qquad \square \tag{3.28}$$

3.2.2 Conditional Direct Transmission Ergodic Mutual Information, $E\left[I^{ad}|I^{ab}\right]$

If the mutual information of the s_a to r_b channel is less than the threshold, R, the relay does not cooperate and the source transmits directly to the destination, d. The random variable I^{ad} is a function of the imperfect CSI random variable X (i.e., $|\breve{H}^{ad}|^2$) and defined as follows:

$$I^{ad} = \frac{1}{2}\log_e\left(1+\frac{2p^aX}{(\sigma_z^{ad})^2}\right). \tag{3.29}$$

The PDF of the random variable $Q = \frac{2p^aX}{(\sigma_z^{ad})^2}$ is

$$f_Q(q) = \frac{1}{\Omega_Q^2}e^{-\frac{\alpha_Q^2+q}{\Omega_Q^2}}\mathfrak{I}_0\left(2\sqrt{\frac{\alpha_Q^2 q}{\Omega_Q^4}}\right), \tag{3.30}$$

where $\frac{1}{\Omega_Q^2} = \frac{(\sigma_z^{ad})^2}{2p^a(\tilde{\sigma}_\epsilon^{ad})^2}$ and $\alpha_Q^2 = \frac{2p^a|\hat{H}^{ad}|^2}{(\sigma_z^{ad})^2}$. By substituting the series representation of $\mathfrak{I}_0(\cdot)$ ([86], 8.447(1)) in (4.8), we obtain

$$f_Q(q) = \frac{1}{\Omega_Q^2} e^{-\frac{\alpha_Q^2+q}{\Omega_Q^2}} \sum_{t=0}^{\infty} \frac{\alpha_Q^{2t} q^t}{\Omega_Q^{4t}(t!)^2}. \tag{3.31}$$

Given the PDF $f_Q(q)$, the ergodic mutual information for direct communication can be written as

$$E\left[I^{ad}|I^{ab}\right] = \int_0^{\infty} \frac{1}{2}\log_e(1+q) f_Q(q) dq \tag{3.32}$$

$$= \frac{e^{-\frac{\alpha_Q^2}{\Omega_Q^2}}}{2\Omega_Q^2} \sum_{t=0}^{\infty} \frac{\alpha_Q^{2t}}{\Omega_Q^{4t}(t!)^2} \int_0^{\infty} \log_e(1+q) e^{-\frac{q}{\Omega_Q^2}} q^t dq. \tag{3.33}$$

By ([86], 4.222(8)), we obtain

$$E\left[I^{ad}|I^{ab}\right] = \frac{e^{-\frac{\alpha_Q^2}{\Omega_Q^2}}}{2\Omega_Q^2} \sum_{t=0}^{\infty} \frac{\alpha_Q^{2t}\Omega_Q^{2(t+1)}}{\Omega_Q^{4t}(t!)^2} \sum_{m=0}^{t} \frac{t!}{(t-m)!} \times \left[\frac{(-1)^{t-m-1}}{\Omega_Q^{2(t-m)}} e^{\frac{1}{\Omega_Q^2}} Ei\left(\frac{-1}{\Omega_Q^2}\right) + \sum_{j=1}^{t-m} \frac{(j-1)!}{-\Omega_Q^{2(t-m-j)}}\right], \tag{3.34}$$

where $Ei(\cdot)$ is the exponential integral function. □

3.2.3 Conditional Cooperative Transmission Ergodic Mutual Information $E\left[I^{abd}|I^{ab}\right]$

In cooperative networks, diverse assumptions can be made about the network parameters and will result in different expressions of $E\left[I^{abd}|I^{ab}\right]$. This subsection presents $E\left[I^{abd}|I^{ab}\right]$ for a general case which is flexible enough to capture the ergodic mutual information of any scenario of SDF networks. In particular, the three links are treated independently such that their power allocations, channel gains and estimation errors statistics are independent. Networks in uplink mode with equal power allocation to source and relay in a pair, and equal estimation error parameters at the relay-to-destination and

source-to-destination links are considered a special case. For this special case, the sum of non-central Chi-square distribution can be simplified, which in turn simplifies the general expression of cooperative transmission mutual information.

3.2.3.1 A General Case

Define the random variables $W = \frac{2p^b Z}{(\sigma_z^{bd})^2}$, $S = Q + W$ and

$$I^{abd} = \frac{1}{2}\log_e\left(1 + \frac{2p^a X}{(\sigma_z^{ad})^2} + \frac{2p^b Z}{(\sigma_z^{bd})^2}\right), \tag{3.35}$$

where the PDF of Z is given by (3.9). The PDF of Q was found in (4.8) and the PDF of W is given by

$$f_W(w) = \frac{(\sigma_z^{bd})^2 e^{-\frac{|\hat{H}^{bd}|^2 + \frac{(\sigma_z^{bd})^2 w}{2p^b}}{(\tilde{\sigma}_\epsilon^{bd})^2}}}{2p^b(\tilde{\sigma}_\epsilon^{bd})^2}\mathfrak{I}_0\left(2\sqrt{\frac{|\hat{H}^{bd}|^2(\sigma_z^{bd})^2 w}{2p^b(\tilde{\sigma}_\epsilon^{bd})^4}}\right). \tag{3.36}$$

The distribution of the sum of none-central Chi square random variables is given by [88]

$$\begin{aligned} f_S(s) = {} & \frac{1}{2\eta_W^2}\left(\frac{s}{\alpha_Q^2}\right)^{1/2} e^{\frac{-s}{2\eta_Q^2}} e^{-\frac{1}{2}\left(\frac{\alpha_Q^2}{\eta_Q^2} + \frac{\alpha_W^2}{\eta_W^2}\right)} \\ & \times \sum_{i=0}^{\infty}\sum_{l=0}^{\infty} \frac{\Gamma(i+l+1)}{i!l!\Gamma(l+1)}\left(\frac{\sqrt{s}\alpha_W^2\eta_Q^2}{2\alpha_Q\eta_W^4}\right)^l \\ & \times \left(\frac{\sqrt{s}(\eta_W^2 - \eta_Q^2)}{\alpha_Q\eta_W^2}\right)^i \mathfrak{I}_{i+l+1}\left(\frac{\sqrt{s}\alpha_Q}{\eta_Q^2}\right), \end{aligned} \tag{3.37}$$

where $\alpha_Q^2 = \frac{2p^a|\hat{H}^{ad}|^2}{(\sigma_z^{ad})^2}$, $\eta_Q^2 = \frac{p^a(\tilde{\sigma}_\epsilon^{ad})^2}{(\sigma_z^{ad})^2}$, $\alpha_W^2 = \frac{2p^b|\hat{H}^{bd}|^2}{(\sigma_z^{bd})^2}$,$\eta_W^2 = \frac{p^b(\tilde{\sigma}_\epsilon^{bd})^2}{(\sigma_z^{bd})^2}$, and $\Gamma(\cdot)$ is the Gamma function. Given the distribution of the sum random variable, S, the ergodic mutual information can be evaluated as follows:

$$E\left[I^{abd}|I^{ab}\right] = \int_0^\infty \frac{1}{2}\log_e(1+s)f_S(s)ds. \tag{3.38}$$

After writing the Bessel function in its series representation and by using ([86], 8.444(8)), the ergodic mutual information in (3.38) evaluates to the following rearranged series

$$
\begin{aligned}
E\left[I^{abd}|I^{ab}\right] &= \frac{1}{4\eta_W^2\alpha_Q} e^{-\frac{1}{2}\left(\frac{\alpha_Q^2}{\eta_Q^2}+\frac{\alpha_W^2}{\eta_W^2}\right)} \\
&\times \sum_{j=0}^{\infty}\sum_{v=0}^{j}\sum_{o=0}^{j-v} \frac{\Gamma(o+v+1)}{o!v!\Gamma(v+1)} \left(\frac{\alpha_W^2\eta_Q^2}{2\alpha_Q^2\eta_W^4}\right)^v \left(\frac{\eta_W^2-\eta_Q^2}{\alpha_Q\eta_W^2}\right)^o \\
&\times \frac{\left(\frac{\alpha_Q^2}{\eta_Q^2}\right)^{2j-o-v+1}\left(2\eta_Q^2\right)^{j+2}}{(j-o-v)!\Gamma(j+2)} \sum_{m=0}^{j+1}\frac{(j+1)!}{(j+1-m)!} \\
&\times \left[\frac{(-1)^{j-m+1}e^{\frac{1}{2\eta_Q^2}}}{(2\eta_Q^2)^{j-m+1}} Ei(\frac{-1}{2\eta_Q^2}) + \sum_{t=1}^{j-m+1}\frac{(t-1)!}{(2\eta_Q^2)^{j-m-t}}\right].\square
\end{aligned} \tag{3.39}
$$

3.2.3.2 A Special Case

Because the destination, d, is common to both r_b to d and s_a to d links, the estimation and delay errors, and the additive noise variances are equal (i.e., $(\sigma_z^{ad})^2 = (\sigma_z^{bd})^2$ and $(\tilde{\sigma}_\epsilon^{ad})^2 = (\tilde{\sigma}_\epsilon^{bd})^2$). In cooperative networks that have the relay r_b as one of the subscriber stations assisting another subscriber station, the source and the relay can be assumed to be transmitting at equal power, i.e., $p^a = p^b$; thus, $\theta_Q = \theta_W$. Both $f_Q(q)$ and $f_W(w)$ can be mapped to the type-one Bessel function PDF [89], respectively, for $\theta_Q = \frac{(\sigma_z^{ad})^2}{2p^a(\tilde{\sigma}_\epsilon^{ad})^2}$, $\beta_Q^2 = \frac{4|\hat{H}^{ad}|^2(\sigma_z^{ad})^2}{2p^a(\tilde{\sigma}_\epsilon^{bd})^4}$ and $\lambda_Q = 1$, and $\theta_W = \frac{(\sigma_z^{bd})^2}{2p^b(\tilde{\sigma}_\epsilon^{bd})^2}$, $\beta_W^2 = \frac{4|\hat{H}^{bd}|^2(\sigma_z^{bd})^2}{2p^b(\tilde{\sigma}_\epsilon^{bd})^2}$ and $\lambda_W = 1$. By the reproductive property of Bessel function random variables [90], the PDF of S reduces to

$$
f_S(s) = \frac{2\theta_S^2}{\beta_S} e^{\frac{-\beta_S^2}{4\theta_S}} s^{\frac{1}{2}} e^{-\theta_S s} \sum_{k=0}^{\infty} \frac{\left(\sqrt{\beta_S^2 s/4}\right)^{2k+1}}{k!(k+1)!}, \tag{3.40}
$$

where $\theta_S = \theta_Q = \theta_W$ (i.e., common variance), and $\beta_S^2 = \beta_Q^2 + \beta_W^2$. Given the PDF of the sum random variable S in (3.40), the ergodic mutual information is written as

$$\begin{aligned} E\left[I^{abd}|I^{ab}\right] &= \int_0^\infty \frac{1}{2}\log_e(1+s) f_S(s) ds. \\ &= \frac{\theta_S^2}{\beta_S} e^{\frac{-\beta_S^2}{4\theta_S}} \sum_{k=0}^{\infty} \frac{\left(\frac{\beta_S}{2}\right)^{2k+1}}{k!(k+1)!} \int_0^\infty s^{k+1} e^{-\theta_S s} \log_e(1+s) ds. \end{aligned} \tag{3.41}$$

Using [[86], 8.444(8)], equation (3.41) after rearangement of terms becomes

$$\begin{aligned} E\left[I^{abd}|I^{ab}\right] &= \frac{e^{-\frac{\beta_S^2}{4\theta_S}}}{\beta_S} \sum_{k=0}^{\infty} \frac{\theta_S^{-k}(\frac{\beta_S}{2})^{2k+1}}{k!} \sum_{m=0}^{k+1} \frac{1}{(k-m+1)!} \\ &\times \left[\frac{(-1)^{k-m}}{\left(\frac{1}{\theta_S}\right)^{k-m+1}} e^{\theta_S} Ei(-\theta_S) + \sum_{l=1}^{k-m+1} \frac{(l-1)!}{\left(\frac{-1}{\theta_S}\right)^{k-m-l+1}} \right]. \square \end{aligned} \tag{3.42}$$

The SDF ergodic mutual information on each subcarrier is obtained by substituting the direct transmission probability (3.27) and cooperative transmission probability (3.28), the direct transmission ergodic mutual information (3.34), and the cooperative transmission ergodic mutual information (3.39) or (3.42) in

$$E\left[I_{n,a,b}^{SDF}\right] = E\left[I^{ad}|I^{ab}\right] Pr\left\{I^{ab} \leq R\right\} + E\left[I^{abd}|I^{ab}\right] Pr\left\{I^{ab} > R\right\}. \tag{3.43}$$

Although equation (3.43) is specific to each subcarrier assigned to a subscriber-relay pair, it can be generalized to capture the network ergodic mutual information as follows:

$$E\left[I_{\text{Net}}^{SDF}\right] = \sum_{n=1}^{N_{sc}} \sum_{a=1}^{A} \sum_{b=1}^{B} E\left[I_{n,a,b}^{SDF}\right]. \tag{3.44}$$

3.3 Performance Evaluations

Performance evaluations are presented over two subsections. The first deals with a numerical evaluations that compare the analytically evaluated ergodic mutual information from (3.43) to that from (3.10) by numerically varying various network parameters. The second provides simulations in which the ergodic mutual information is evaluated for simulated CSI and compared to the analytical results.

3.3.1 Numerical Evaluations

Numerical evaluations illustrate the substantial gain achieved when the CSI imperfection is considered. In addition, they highlight the dependency of the SDF network's mutual information on the CSI accuracy at the three links (i.e., s_a to r_b, s_a to d and r_b to d) as network parameters vary. Consider an SDF network with a subscriber station, a relay station and a destination. Numerical evaluations focus on comparing two scenarios. The *first scenario* represents networks that allocate resources based on the assumption that the received CSI for each subcarrier is perfect, i.e., $|\hat{H}_n^{ab}|^2 = |H_n^{ab}|^2$, $|\hat{H}_n^{ad}|^2 = |H_n^{ad}|^2$ and $|\hat{H}_n^{bd}|^2 = |H_n^{bd}|^2$ in Figure 3.2. Under this scenario, the per-subcarrier mutual information expected to be achieved, $\overline{I}_{n,a,b}^{SDF}$, is given in equation (3.10). The *second scenario* represents more practical networks, in which the estimates of the channels are considered inaccurate, and the inaccuracy is characterized by prior knowledge of the error statistics as in (3.4), (3.5) and (3.6). Based on $|\breve{H}_n^{ab}|^2$, $|\breve{H}_n^{ad}|^2$ and $|\breve{H}_n^{bd}|^2$, Figure 3.2, the source achieves the ergodic mutual information $E\left[I_{n,a,b}^{SDF}\right]$ derived in equation (3.43) on each subcarrier assigned to it.

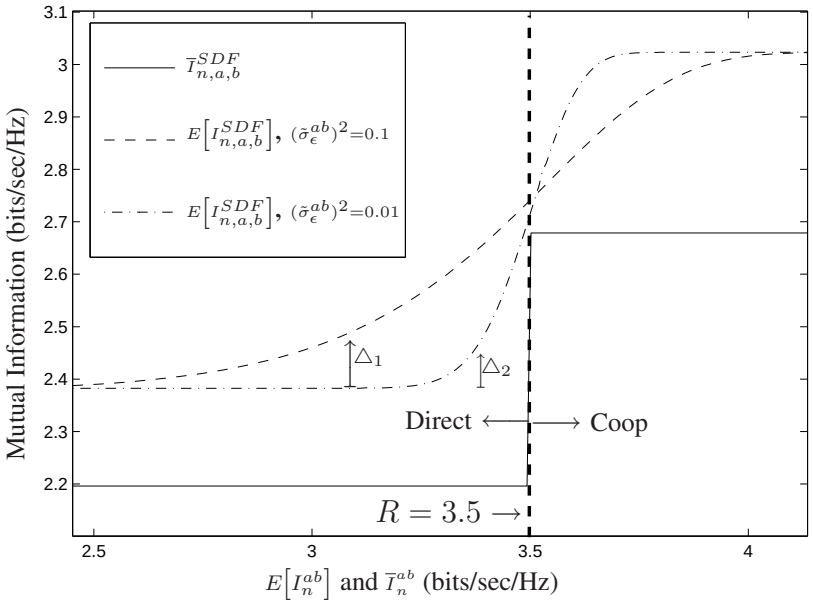

Figure 3.3: Change in mutual information as the direct (i.e., s_a to r_b) mutual information increases.

Increasing the signal-to-noise ratio (SNR) on the s_a to r_b link from 3 dB to 23 dB increases the source-to-relay mutual information, represented by the horizontal axis in Figure 3.3. Thus, s_a switches from direct transmission mode to the cooperative mode at the threshold, R, as shown in Figure 3.3 for $(\tilde{\sigma}_{\epsilon}^{ad})^2 = (\tilde{\sigma}_{\epsilon}^{bd})^2 = 0.1$ and equal SNR of 10 dB on the s_a to d and r_b to d links. The cooperation decision is based on the deterministic (i.e., $\overline{I}_n^{ab}$) and ergodic (i.e., $E\left[I_n^{ab}\right]$) mutual information on the s_a to r_b link in the first and second scenario, respectively. Thus, considering an inaccurate channel estimate as a perfect one leads to the wrong decision, as is evident from Figure 3.3. In particular, because of the estimation error, the first scenario subscriber stations do not cooperate, although the actual channel condition is at a cooperation permissible level. On the other hand, the second scenario networks consider the error and take advantage of the channel gain increase, which translates to higher mutual information as indicated by $\triangle_1$ and $\triangle_2$ in Figure 3.3. It is obvious that greater mutual information can be achieved by the second scenario networks in either cooperative or direct transmission modes.

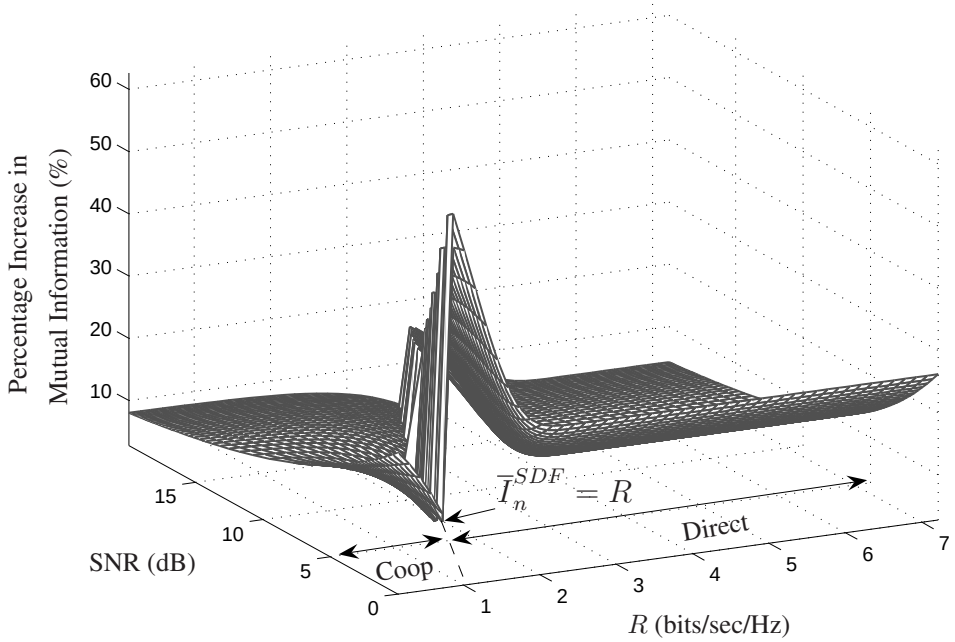

Figure 3.4: Percentage increase in mutual information when CSI imperfection is taken into account in both cooperative (Coop) and direct (Direct) transmission modes.

Figure 3.4 shows the percentage increase in the mutual information achieved, $\frac{E\left[I_{n,a,b}^{SDF}\right]-\overline{I}_{n,a,b}^{SDF}}{\overline{I}_{n,a,b}^{SDF}}$ %, when the CSI uncertainty is considered at the receiver as the SNR on the three links varies and the threshold R increases for equal error variances, $(\tilde{\sigma}_{\epsilon}^{ab})^2 = (\tilde{\sigma}_{\epsilon}^{ad})^2 = (\tilde{\sigma}_{\epsilon}^{bd})^2 = 0.01$. Although the estimation error is more significant at high SNR compared to low SNR [66], the percentage increase in mutual information is more pronounced at low SNR than at high SNR. This observation is explained as follows: the large gain achieved by considering the second scenario relative to the mutual information of the first scenario at high SNR is less than the small gain achieved by considering the second scenario relative to the mutual information of the first scenario at low SNR. The sharp increase seen in Figure 3.4 is due to the difference in transmission modes of each scenario. In other words, the first scenario r_b switches to direct transmission mode based on the poor estimate $|\hat{H}_n^{ab}|^2$, while the second scenario r_b remains in the cooperation mode based on a better estimate, $|\breve{H}_n^{ab}|^2$, than $|\hat{H}_n^{ab}|^2$.

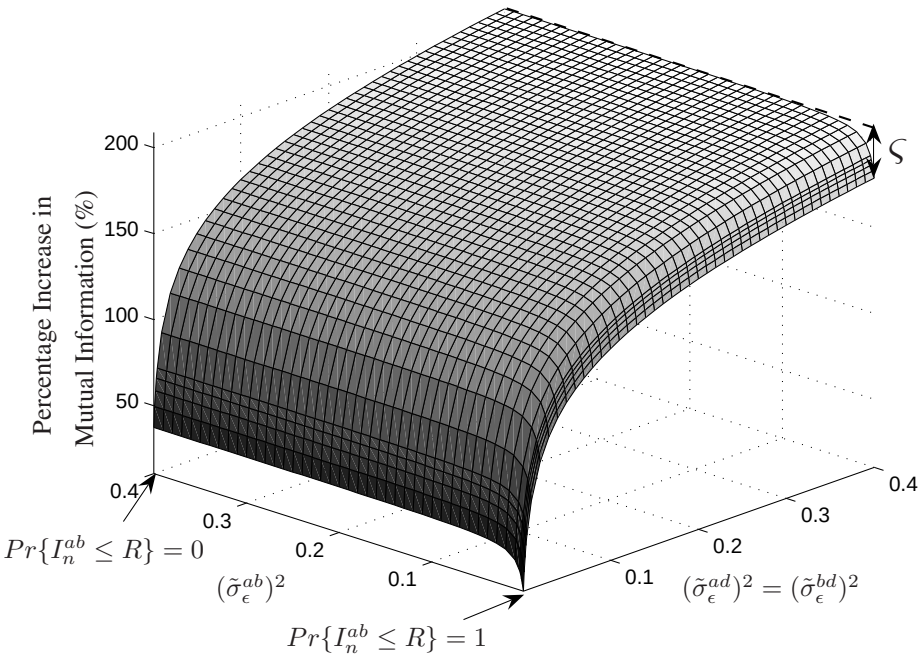

Figure 3.5: Effect of CSI inaccuracy on the ergodic mutual information.

To investigate the impact of the three links' CSI imperfection on the ergodic mutual information, Figure 3.5 shows the ergodic mutual information gain achieved in the second scenario relative to first scenario as the three estimation errors' variances increase for a constant SNR of 10 dB on the three links. Since the estimation error at the relay affect the transmission mode decision (i.e., cooperative vs. direct), as $(\tilde{\sigma}_{\epsilon}^{ab})^2$ increases, the cooperative transmission probability increases, resulting in a gain denoted by ς over the direct transmission. The increase in $(\tilde{\sigma}_{\epsilon}^{ad})^2$ and $(\tilde{\sigma}_{\epsilon}^{bd})^2$ affects both cooperative and direct transmissions ergodic mutual information; hence, the second scenario achieves larger gain over the first scenario as the estimation error increases.

3.3.2 Simulations

Whereas the previous numerical evaluations focused on evaluating the gain achieved by considering the CSI imperfection, the following simulations demonstrate that with the knowledge of estimation error statistics and CSI estimates, channel adaptive schemes can achieve an ergodic mutual information close to that would be attained if the perfect CSI made available through adopting the presented analytical results. A frequency selective Rayleigh distributed channel is modeled via a six taps channel model. The number of subcarriers is simulated to be 128 in all simulations. The statistical properties of the perfect, estimated and imperfect CSI for the three links are detailed in section 3.1. The following discussion compares the ergodic mutual information attained for direct and cooperative modes over a range of power-to-noise ratio for the following cases:

(i) The CSI is simulated to be perfectly known (i.e, H^{bd} and H^{ad}) and the ergodic mutual information is evaluated over 1000 channel realizations.

(ii) The estimates of CSI (i.e, $\hat{H}^{bd}$ and $\hat{H}^{ad}$) are the only knowns while the estimation error variances (i.e., $(\tilde{\sigma}_{\epsilon}^{ad})^2$ and $(\tilde{\sigma}_{\epsilon}^{bd})^2$) are simulated to be 0.1, 0.3 or 0.5. The ergodic mutual information is evaluated over 1000 channel realizations.

(iii) The estimates of CSI (i.e., $\hat{H}^{bd}$ and $\hat{H}^{ad}$) are known and the estimation error is

taken into consideration. The worst estimation error variances of (ii) is considered (i.e., $(\tilde{\sigma}_{\epsilon}^{ad})^2 = (\tilde{\sigma}_{\epsilon}^{bd})^2 = 0.5$) where the ergodic mutual information is evaluated analytically by (3.34) for the direct mode and by (3.42) or (3.39) for the cooperative mode.

Note that the source-to-relay mutual information I^{ab} in (3.11) in SDF networks only determines the probability of direct and cooperative but not the ergodic mutual information in either of the modes; thus, it is not considered in the following simulations.

Figure 3.6 shows the ergodic mutual information of the cooperative mode. (sim) and (ana) denote simulated and analytically evaluated ergodic mutual information, respectively. It can be clearly observed that the ergodic mutual information (dashed, dotted and dashed-dotted lines) decreases with the channel estimation mismatch increase that is represented by the estimation error variance increase from 0.1 to 0.5 when the estimation error is ignored (case (ii)). However, with the analytically evaluated expression, and the knowledge of the channel estimates and error statistics, the ergodic mutual information (solid line, case (iii)) is close to the one attained when the perfect CSI is available (marked by $+$, case (i)).

Networks with a dedicated relay station have a high channel gain on the relay-to-base station link because the relay station is fixed and its position is optimized by network planers. Therefore, the channel can be tracked easily and the estimation performance improves. In addition, dedicated relay stations have more relaxed power constraints than non-dedicated ones that are often battery powered. This scenario is simulated by setting $\frac{p^b}{(\sigma_z^{bd})^2}$ to a high value (e.g., 20 dB) and the estimation error variance to a low value (e.g., $(\tilde{\sigma}_{\epsilon}^{bd})^2 = 0.01$). Figure 3.7 shows the ergodic mutual information of this scenario. It demonstrates that the estimation error effect is larger at high SNR than at low SNR, which concurs with an observation made earlier. Using similar plots, network designers can answer questions about the significance of CSI imperfection effect in the power operation region of their designed transmitters. As in Figure 3.6, Figure 3.7 shows that the analytically evaluated ergodic mutual information captures the ergodic mutual information that can be achieved if the perfect CSI is made available. Thus, adopting the

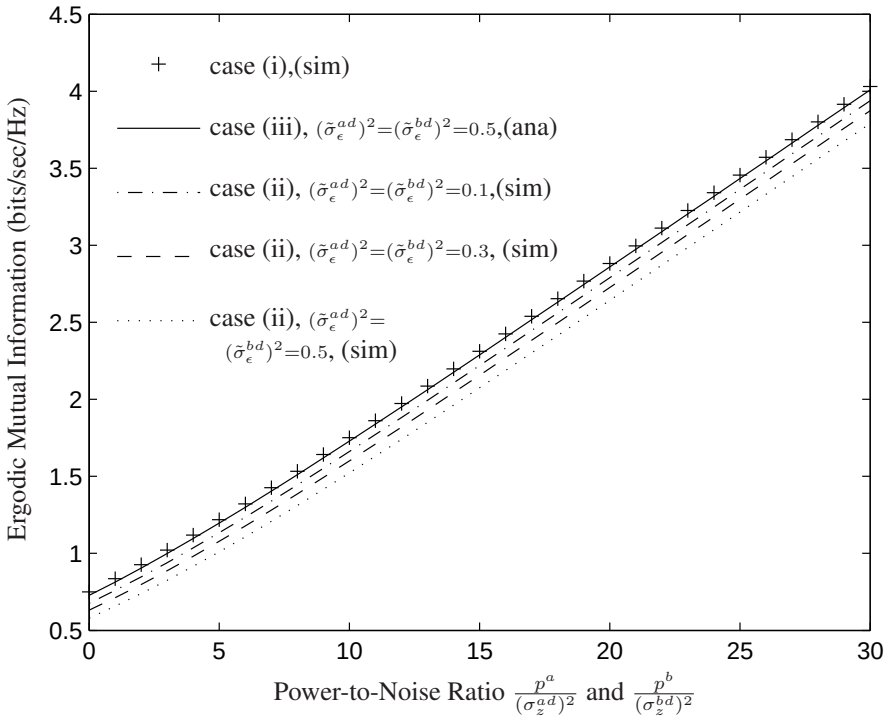

Figure 3.6: Ergodic mutual information of the cooperative mode.

proposed approach in channel adaptive schemes greatly reduces the performance degradation caused by channel estimation inaccuracy. An example of utilizing the analytical results in resource allocation for OFDMA networks is presented in chapter 4.

3.4 Summary

We have proposed an approach to investigate the ergodic mutual information of OFDMA-based SDF cooperative relay networks with imperfect CSI. A quantitative measure of the gain in ergodic mutual information attained by considering the CSI imperfection was presented. Numerical evaluations show that by considering the CSI imperfection, the ergodic mutual information can be increased over a large range of SNR; however, the relative increase is more tangible at low SNR than that at high SNR. Furthermore,

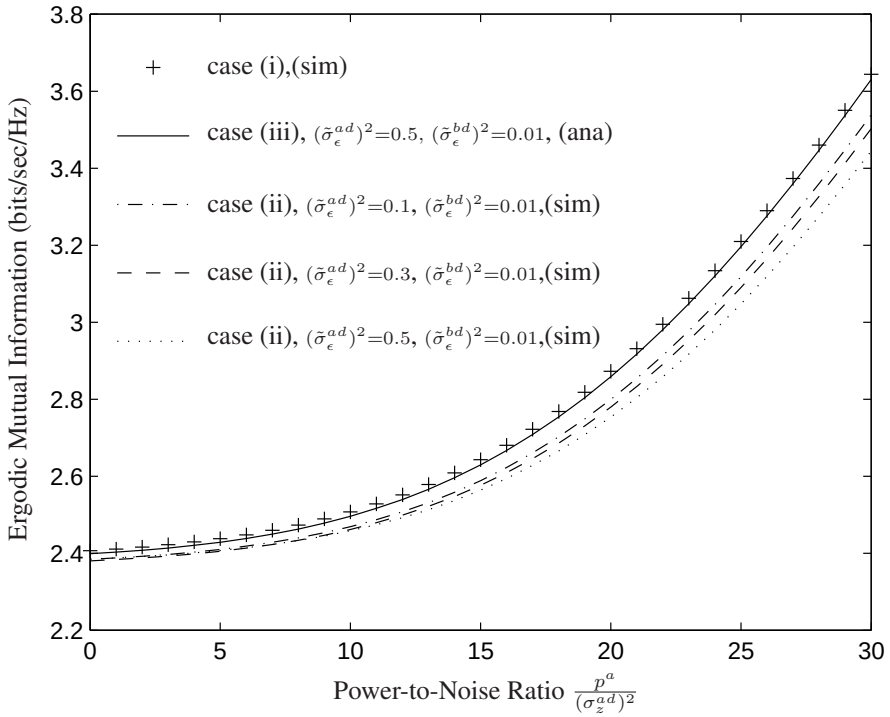

Figure 3.7: Ergodic mutual information of the cooperative mode for dedicated relays where $\frac{p^b}{(\sigma_z^{bd})^2}$ is prefixed to 20 dB.

channel adaptive schemes can achieve an ergodic mutual information close to the one achieved if perfect estimates of CSI are available. Therefore, until designed resource allocation schemes consider channel estimates error, they remain far from being practically implementable and unlikely to achieve their claimed performance in real networks.

Chapter 4

Resource Allocation for OFDMA-based PMP Multiservice Networks

This chapter presents a novel scheme for the allocation of subcarriers, rate and power in orthogonal OFDMA networks. The scheme addresses practical implementation issues of resource allocation in OFDMA networks: inaccuracy of CSI available to the RAU and diversity of subscribers' quality of service (QoS) requirements. In addition to embedding the effect of CSI imperfection in the evaluation of subscribers' expected rate, the resource allocation problem is posed as a NUM one which is solved via decomposing it into a hierarchy of subproblems. These subproblems coordinate their allocations to achieve a final allocation that satisfies aggregate rate constraints imposed by the call admission control (CAC) unit and OFDMA-related constraints. Complexity analysis shows that the proposed scheme is computationally efficient. In addition, performance evaluation findings support our theoretical claims: a substantial data rate gain can be achieved by considering the CSI imperfection and multiservice classes can be supported with QoS guarantees.

Although most recent research works have posed the resource allocation problem of OFDMA networks as NUM problem [42, 91–94], they depend too heavily on the accuracy of CSI and overlook the availability of the allocated throughput. Works in

[42, 92, 94] have generally focused on maximizing the sum of utilities, without considering the limit imposed by the CAC unit on each service aggregate rate. In other words, the higher the channel gain and the available power, the higher the throughput granted to subscribers. However, in multiservice networks, the aggregate rate allocated to subscribers of each service cannot exceed the prescribed partition of the network throughput, especially when subscribers have diverse QoS requirements. For example, a particular group of subscribers may be more demanding than the rest of the subscribers, which results in an allocation of the network resources to the former and leaves the latter unsupported. Limiting the aggregate rate that the group of demanding subscribers receive imposes fairness among supported classes and guarantees QoS for each service. Although works in [91, 92, 95] propose joint resource allocation and CAC schemes that avoid over using the network throughput by partitioning it over the supported services, the CSI in these schemes is assumed to be perfectly known. However, such perfection is rare and the performance of multi-carrier systems is severely degraded by considering an inaccurate and delayed CSI as perfect, and allocating resources based on it [66–68].

The main focus of this chapter is the resource allocation for OFDMA-based networks with imperfect CSI and multiple classes of services that demand diverse QoS requirements. Allocating resources for OFDMA networks is cross-layer in nature; the PHY layer feeds the CSI of all subscribers to the RAU at the MAC layer which, in turn, allocates resources. Inaccuracy of the reported CSI is modeled as an additive random variable with a known distribution, based on which the expected rate is evaluated. Power allocation is performed by inverting the expected rate function. The OFDMA resource allocation problem is combinatorial in nature with a nonconvex structure; thus, it cannot be solved by convex[1] optimization methods. However, as the number of subcarriers becomes infinitely large, the duality gap tends to zero[2]; hence, the nonconvex problem can be solved in the dual domain [98]. With this dual approach, decomposition methods for NUM [97] can be applied to solve the problem under consideration. Solutions

[1] A function f is convex if for all $x, y \in$ domain of f and $\theta \in [0, 1]$, $\theta x + (1-\theta)y \in$ Domain of f and $f(\theta x + (1-\theta)y) \leq \theta f(x) + (1-\theta)f(y)$ [96, 97].

[2] Zero duality gap implies that both the primal and the dual problems have the same optimal value [98].

obtained via decomposition have the inherent property of being implementable in both a distributed and a centralized manner; we adopt the centralized implementation and highlight subroutines of the proposed scheme that are distributable. The proposed scheme is presented for OFDMA systems in the downlink mode and modifications can be extended for uplink resource allocation.

The remainder of the chapter is organized as follows. Section 4.1 introduces the system model of the OFDMA-based PMP network under consideration. The expected data rate for imperfect CSI is presented in Section 4.2. Mathematical formulation of the resource allocation problem along with the proposed scheme is presented in Section 4.3. Computational complexity is analyzed in Section 4.4. The performance of the proposed scheme is evaluated in Section 4.5, and followed by a summary in Section 4.6.

4.1 System Model

The system model of PMP networks is considered a special case of the cooperative relay networks system model presented in Section 3.1 because the relay does not exist in PMP network and only direct transmissions are allowed. Thus, the notation of the source to destination $(\cdot)^{ad}$ is replaced with $(\cdot)^{s}$ in this chapter for notational brevity. In addition, the source to relay and relay to destination related modeling in Section 3.1 is removed which reduces the system model to PMP networks presented here.

We consider a single cell scenario of a PMP network. The network consists of one BS at the center of the cell and multiple subscriber stations. There are S subscriber stations forming the set $\mathcal{S} = \{1, \cdots, s, \cdots, S\}$. The subscriber stations share a set of N_{sc} subcarriers available to the cell. In OFDMA networks, a sub-set $\mathcal{N}_s$ [3] of the network subcarriers is exclusively assigned to one subscriber station. Although, for simplicity, the general presentation focuses on the downlink mode, the proposed resource allocation scheme is generally applicable to both uplink and downlink modes, as will be shown later.

[3]The cardinality of the sub-set $\mathcal{N}_s$ is denoted by N_s.

The network supports L QoS classes. Network parameters related to the lth class are denoted by a superscript $^{(l)}$. For example, the set of subscriber stations that subscribe for the lth class is denoted by $\mathcal{S}^{(l)}$. A utility function, $U^s(\overline{r}^s)$, models the sth subscriber station's satisfaction of the expected data rate, $\overline{r}^s$, assigned to it. The characteristics of utility functions depend on the class of service that each subscriber station opts for. We consider a frequency selective fading channel between any pair of communicating

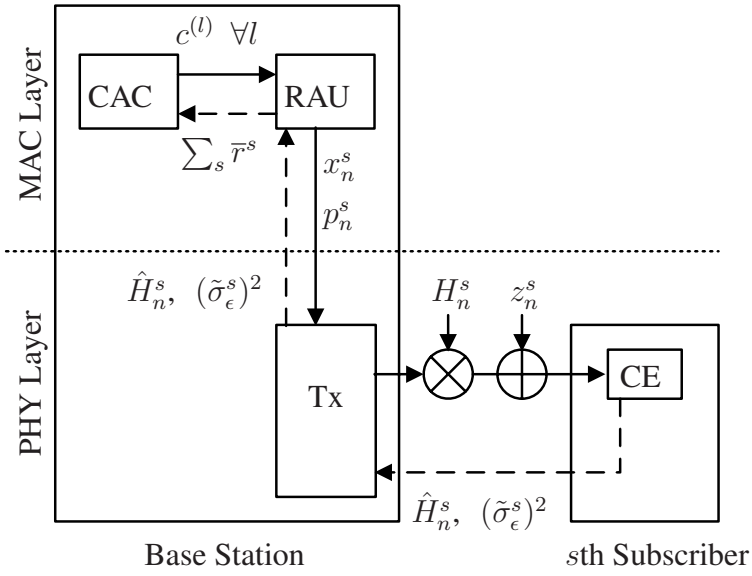

Figure 4.1: Illustrative PMP network of one subscriber station and a base station showing various components involved in resource allocation. Tx and CE, respectively, stand for transmitter and channel estimator.

stations. In OFDMA, the subband bandwidth is smaller than the channel coherence bandwidth; therefore, each subcarrier experiences flat fading. During the jth slot, the sth subscriber receives the following OFDM signals:

$$\mathbf{y}^s[j] = \sqrt{\mathbf{P}^s[j]}\mathbf{H}^s[j]\mathbf{x}[j] + \mathbf{z}^s[j], \tag{4.1}$$

where $\sqrt{\mathbf{P}^s}[j]$ is a diagonal $N_s \times N_s$, matrix of $p_n^s[j]$ $\forall n \in \mathcal{N}_s$ which is the power allocated by the MAC resource allocation scheme to the sth subscriber on the nth subcarrier

during the jth slot. $\mathbf{H}^s[j]$ is a diagonal matrix of the channel gains, and $\mathbf{x}[j]$ denotes the data source symbols. The vector $\mathbf{z}^s$ represents the additive noise, which is modeled as circularly symmetric complex Gaussian random variable $\mathbf{z}^s \sim \mathcal{CN}(\mathbf{0}, (\sigma_z^s)^2\mathbf{I})$.

The CSI is updated every OFDMA frame. At the beginning of the frame, a sequence of OFDM symbols is transmitted by the BS to the subscribers for channel estimation [52]. Each subscriber estimates the channel and forwards its estimate, $\hat{\mathbf{H}}^s$, of the perfect CSI, $\mathbf{H}^s$, to the BS. The slot index, $[j]$, is dropped for notational convenience. Note that the matrix of channel gains is a diagonal of the subcarriers' channel gain vector, $\boldsymbol{\hbar}^s$. Let $\hat{\boldsymbol{\hbar}}^s$ be its estimate available at the RAU; before the next frame estimates arrive, the current frame estimates are treated as deterministic [77], and their delay and estimation error are modeled by $\tilde{\boldsymbol{\hbar}}^s$. Hence, given the channel estimate $\hat{\boldsymbol{\hbar}}^s$, the imperfect CSI can be modeled as

$$\breve{\boldsymbol{\hbar}}^s = \hat{\boldsymbol{\hbar}}^s + \tilde{\boldsymbol{\hbar}}^s, \tag{4.2}$$

and assumed to be $\sim \mathcal{CN}(\hat{\boldsymbol{\hbar}}^s, \boldsymbol{\Sigma}_{\tilde{\boldsymbol{\hbar}}^s})$. The matrix $\boldsymbol{\Sigma}_{\tilde{\boldsymbol{\hbar}}^s}$ is the error covariance matrix that captures the quality of the channel estimation [58, 82, 99]. We assume that the estimation errors on different subcarriers are independent; thus, $\boldsymbol{\Sigma}_{\tilde{\boldsymbol{\hbar}}^s} = (\tilde{\sigma}_\epsilon^s)^2\mathbf{I}$, where $(\tilde{\sigma}_\epsilon^s)^2$ is the estimation error variance. The nth subcarrier[4] imperfect CSI ($[\breve{\boldsymbol{\hbar}}^s]_n = \breve{H}_n^s$) is modeled as $\sim \mathcal{CN}(\hat{H}_n^s, (\tilde{\sigma}_\epsilon^s)^2)$. Therefore, its square follows a non-central chi-square PDF given by [85]

$$f_X(x) = \frac{1}{(\tilde{\sigma}_\epsilon^s)^2} e^{-\frac{(|\hat{H}_n^s|^2 + x)}{(\tilde{\sigma}_\epsilon^s)^2}} \mathfrak{I}_0\left(2\sqrt{\frac{|\hat{H}_n^s|^2 x}{(\tilde{\sigma}_\epsilon^s)^4}}\right), \tag{4.3}$$

where $\mathfrak{I}_0(\cdot)$ is the zeroth-order modified Bessel function of the first kind. The random variable $|\breve{H}_n^s|^2$ is denoted by X for notational convenience. Figure 4.1 shows the above-mentioned modeling parameters on an illustrative PMP network.

[4] $[\boldsymbol{x}]_n$ denotes the nth element of vector $\boldsymbol{x}$.

4.2 Expected Rate with Imperfect CSI

The BS receives a deterministic channel gain estimate of each subcarrier, $\hat{H}_n^s$, and the estimation error statistical information. Based on the model in (4.2), the mutual information is a function of the imperfect CSI random variable X (i.e., $|\breve{H}_n^s|^2$), which can be written as

$$I_n^s = \log_e \left(1 + \frac{p_n^s X}{(\sigma_z^s)^2}\right). \tag{4.4}$$

Equation (4.4) is similar to equation (3.29) in chapter 3. Nevertheless, the mutual information is hard to achieve in practice especially in the network under consideration where adaptive modulation and coding (AMC) is adopted. In the following we show how the bit error probability, P_b, is incorporated in equation (4.4). The P_b is given by [35, 100–102]:

$$P_b \approx 0.2 \exp\left[\frac{1.5 \frac{p_n^s X}{(\sigma_z^s)^2}}{M-1}\right], \tag{4.5}$$

where M is the constellation size. By assuming "$=$" instead of "$\approx$" in (4.5) and solving for M, we obtain:

$$M = \left(1 + \frac{1.5}{-\ln(5P_b)} \frac{p_n^s X}{(\sigma_z^s)^2}\right) \tag{4.6}$$

The adaptive modulation transmission rate as a function of P_b can be obtained by substituting (4.6) in $r_n^s = \log_e M$ as follows:

$$r_n^s = \log_e \left(1 + \frac{p_n^s X}{\triangle(\sigma_z^s)^2}\right), \tag{4.7}$$

where $\triangle = \frac{-\ln(5P_b)}{1.5}$. The PDF of the random variable $Q' = \frac{p_n^s X}{\triangle(\sigma_z^s)^2}$ is given by

$$f_{Q'}(q) = \frac{1}{\Omega_{Q'}^2} e^{-\frac{\theta_{Q'}^2 + q}{\Omega_{Q'}^2}} \mathfrak{I}_0\left(2\sqrt{\frac{\theta_{Q'}^2 q}{\Omega_{Q'}^4}}\right), \tag{4.8}$$

where $\frac{1}{\Omega_{Q'}^2} = \frac{\triangle(\sigma_z^s)^2}{2p_n^s(\tilde{\sigma}_\epsilon^s)^2}$ and $\theta_{Q'}^2 = \frac{p_n^s|\hat{H}^s|^2}{\triangle(\sigma_z^s)^2}$. By substituting the series representation of $\mathfrak{I}_0(\cdot)$ ([86], 8.447(1)) in (4.8), we obtain

$$f_{Q'}(q) = \frac{1}{\Omega_{Q'}^2} e^{-\frac{\theta_{Q'}^2 + q}{\Omega_{Q'}^2}} \sum_{t=0}^{\infty} \frac{\theta_{Q'}^{2t} q^t}{\Omega_{Q'}^{4t} (t!)^2}. \tag{4.9}$$

Given the PDF $f_{Q'}(q)$, the expected achievable rate can be written as

$$E\left[r_n^s\right] = E\left[\log_e(1+Q')\right] \tag{4.10}$$

$$= \int_0^\infty \log_e(1+q) f_{Q'}(q) dq \tag{4.11}$$

$$= \frac{e^{-\frac{\theta_{Q'}^2}{\Omega_{Q'}^2}}}{2\Omega_{Q'}^2} \sum_{t=0}^{\infty} \frac{\theta_{Q'}^{2t}}{\Omega_{Q'}^{4t}(t!)^2} \int_0^\infty \log_e(1+q) e^{-\frac{q}{\Omega_{Q'}^2}} q^t dq. \tag{4.12}$$

By ([86], 4.222(8)), we obtain

$$E\left[r_n^s\right] = \frac{e^{-\frac{\theta_{Q'}^2}{\Omega_{Q'}^2}}}{2\Omega_{Q'}^2} \sum_{t=0}^{\infty} \frac{\theta_{Q'}^{2t}\Omega_{Q'}^{2(t+1)}}{\Omega_{Q'}^{4t}(t!)^2} \sum_{m=0}^{t} \frac{t!}{(t-m)!} \times \left[\frac{(-1)^{t-m-1}}{\Omega_{Q'}^{2(t-m)}} e^{\frac{1}{\Omega_{Q'}^2}} Ei\left(\frac{-1}{\Omega_{Q'}^2}\right) + \sum_{j=1}^{t-m} \frac{(j-1)!}{-\Omega_{Q'}^{2(t-m-j)}} \right], \tag{4.13}$$

where $Ei(\cdot)$ is the exponential integral function.

Given the expected data rate to be supported, the power allocation phase of the proposed scheme requires solving (4.13) for p_n^s, which is computationally extensive. Alternatively, after evaluating (4.13) off-line, the expected achievable rate can be represented by a simpler function that can be efficiently inverted for power. Note that $E[\log_e(1+x)] \approx E[\log_e(x)] + \vartheta(x)$, where $\vartheta(x)$ is an approximation error correction term which approaches zero for large values of x. Similarly, (4.10) can be written as

$$E\left[r_n^s\right] = E\left[\log_e(1+Q')\right] \tag{4.14}$$

$$\backsimeq E\left[\log_e(Q')\right] + \vartheta\left(p_n^s\right) \tag{4.15}$$

$$\backsimeq \log_e\left(\frac{|\hat{H}_n^s|^2}{(\tilde{\sigma}_\epsilon^s)^2}\right) - Ei\left(\frac{-|\hat{H}_n^s|^2}{(\tilde{\sigma}_\epsilon^s)^2}\right) + \log_e\left(\frac{(\tilde{\sigma}_\epsilon^s)^2}{\triangle(\sigma_z^s)^2}\right) + \log_e\left(p_n^s\right) + \vartheta\left(p_n^s\right), \tag{4.16}$$

where $E\left[\log_e(Q')\right]$ is given in [103], and $\vartheta\left(p_n^s\right) = \alpha(\hat{H}_n^s, (\tilde{\sigma}_\epsilon^s)^2) \times \left(p_n^s\right)^{-\beta(\hat{H}_n^s, (\tilde{\sigma}_\epsilon^s)^2)} + \gamma(\hat{H}_n^s, (\tilde{\sigma}_\epsilon^s)^2)$ is an approximation error correction term. The parameters α, β and γ are

found by curve fitting the difference $E\left[r_n^s\right] - E\left[\log_e(Q')\right]$ to a power decaying function; $E\left[r_n^s\right]$ is evaluated by (4.13). These parameters are stored in lookup tables for a range of practical values of $|\hat{H}_n^s|^2$ and $(\tilde{\sigma}_\epsilon^s)^2$. Rearranging equation (4.16) results in the following:

$$\log_e\left(p_n^s\right) + \vartheta\left(p_n^s\right) \backsimeq -\log_e\left(\frac{|\hat{H}_n^s|^2}{(\tilde{\sigma}_\epsilon^s)^2}\right) + Ei\left(\frac{-|\hat{H}_n^s|^2}{(\tilde{\sigma}_\epsilon^s)^2}\right) - \log_e\left(\frac{(\tilde{\sigma}_\epsilon^s)^2}{\triangle(\sigma_z^s)^2}\right) + E\left[r_n^s\right]. \tag{4.17}$$

Note that the R.H.S of (4.17) is a function of $|\hat{H}_n^s|^2$ and $(\tilde{\sigma}_\epsilon^s)^2$, which are known deterministic values to the RAU. For notational convenience, we denote the constant term $-\log_e\left(\frac{|\hat{H}_n^s|^2}{(\tilde{\sigma}_\epsilon^s)^2}\right) + Ei\left(\frac{-|\hat{H}_n^s|^2}{(\tilde{\sigma}_\epsilon^s)^2}\right) - \log_e\left(\frac{(\tilde{\sigma}_\epsilon^s)^2}{\triangle(\sigma_z^s)^2}\right)$ by Ψ. The required power to support the expected rate $E\left[r_n^s\right]$ for given $|\hat{H}_n^s|^2$ and $(\tilde{\sigma}_\epsilon^s)^2$ is found by Maple[5] to be

$$p_n^s = exp\left\{\frac{W_0(-\beta\alpha e^{\beta(E[r_n^s]-\gamma-\Psi)}) + \beta(E\left[r_n^s\right]-\gamma-\Psi)}{\beta}\right\}, \tag{4.18}$$

where $W_0(\cdot)$ is the Lambert's W function given by $W_0(\cdot) = \sum_{i=1}^{\infty} \frac{(-i)^{i-1}}{i!}(\cdot)^i$.

4.3 Problem Formulation and Solutions

We formulate the resource allocation problem as a constrained NUM problem, where the objective function is a maximization of the sum of the subscribers' utility functions. The constraints are related to the specifications of the network under consideration, namely, the per-service allocated aggregate rate limit, power limitation and exclusive subcarrier assignment. Let $x_n^s \in \{0,1\}$ where $x_n^s = 1$ means that the nth subcarrier is allocated to the sth subscriber and $x_n^s = 0$ otherwise. Furthermore, let $\overline{r}^s$ be the expected rate allocated to the sth subscriber of the subcarriers assigned to it (i.e., $\mathcal{N}_s$); mathematically $\overline{r}^s = \sum_{n\in\mathcal{N}_s} E\left[r_n^s\right]$. The CAC unit receives the allocation results from the RAU and updates the RAU with the throughput partitioning results, $c^{(l)}\ \forall l$ (Figure 4.1). The CAC schemes available in the literature (e.g., [91, 93, 95, 104]) can be applied here. In the

[5]Maplesoft, version 11.02.

downlink mode, the power available to the network is limited by the BS power, which is denoted by P_{BS}. Mathematically, the optimization problem is

$$\max_{x_n^s, p_n^s} \quad \sum_s U^s(\overline{r}^s) \tag{4.19}$$

$$\text{s.t.} \quad \sum_{s \in \mathcal{S}^{(l)}} \overline{r}^s \leq c^{(l)} \qquad \forall l \tag{4.20}$$

$$\sum_s x_n^s \leq 1 \qquad \forall n \tag{4.21}$$

$$\sum_s \sum_{n=1}^{N_{sc}} p_n^s \leq P_{BS} \tag{4.22}$$

$$x_n^s \in \{0, 1\}. \tag{4.23}$$

The set of constraints in (4.20) limits the lth class subscribers' allocated aggregate expected rate to $c^{(l)}$. Constraints in (4.21) satisfy the exclusive subcarrier allocation of OFDMA [8]. Constraint (4.22) limits the total power allocated to P_{BS}.

The resource allocation problem is combinatorial in nature due to the subcarrier exclusive assignment constraint, which results in a nonconvex feasible space. Generally, solving nonconvex problems in the dual domain provides only an upper bound that is at a distance from the optimum known as the "duality gap". However, resource allocation for multicarrier transmissions is a special case in which the duality gap becomes zero as the number of subcarriers approaches infinity [98]. In networks with a number of subcarriers as small as 64, a duality gap of less than 10^{-5} can be achieved, which is acceptable in practice [79]. These results suggest solving the problem in the dual domain. One of the effective methods for solving NUM problems is dual decomposition, where the dual problem is decomposed into multiple subproblems that are easier to solve than the primal. The master dual problem sets the prices for resources and reports them to the decomposed subproblems, which in turn decide the amount of resources to be consumed [97].

A Lagrangian is formed by relaxing the constraints in (4.20) as follows

$$D(\overline{r}^s, \boldsymbol{\lambda}) = \sum_l \left[\sum_{s \in \mathcal{S}^{(l)}} \left[U^s(\overline{r}^s) - \lambda^{(l)} \overline{r}^s \right] + \lambda^{(l)} c^{(l)} \right], \tag{4.24}$$

where $\lambda^{(l)} \geq 0 \ \ \forall l$ are the classes' set of Lagrange multipliers (i.e., prices). If the lth class throughput is over utilized, $\lambda^{(l)}$ increases, and the converse is true. The problem can be solved by solving its dual:

$$\begin{aligned} \min_{\boldsymbol{\lambda}} \quad & d(\boldsymbol{\lambda}) \\ \text{s.t.} \quad & \boldsymbol{\lambda} \geq \mathbf{0}, \end{aligned} \tag{4.25}$$

where $d(\boldsymbol{\lambda}) = \min_{\overline{r}^s} D(\overline{r}^s, \boldsymbol{\lambda})$ and $\boldsymbol{\lambda}$ is a vector of $\lambda^{(l)} \ \ \forall l$. The Lagrange multipliers are updated with the following subgradient method for each multiplier [97, 98, 105]:

$$\lambda^l(t+1) = \left[\lambda^l(t) - \kappa \left(c^{(l)} - \sum_{s \in \mathcal{S}^{(l)}} \overline{r}^{s\star}(\lambda^l(t)) \right) \right]^+, \tag{4.26}$$

where $\kappa = \frac{0.1}{\sqrt{t}}$ is a diminishing step size, $[\cdot]^+$ denotes $\max(\cdot, 0)$ and t is the iteration index. Here, $\overline{r}^{s\star}(\lambda^l(t))$ is the optimum value obtained by solving the following problem for a given $\lambda^{(l)} \ \ \forall l$:

$$\max_{x_n^s, p_n^s} \quad \sum_l \sum_{s \in \mathcal{S}^{(l)}} \left[U^s(\overline{r}^s) - \lambda^{(l)} \overline{r}^s \right] \tag{4.27}$$

$$\text{s.t.} \quad \sum_s x_n^s \leq 1 \qquad \forall n \tag{4.28}$$

$$\sum_s \sum_{n=1}^{N_{sc}} p_n^s \leq P_{BS} \tag{4.29}$$

$$x_n^s \in \{0, 1\}. \tag{4.30}$$

The problem in (4.27) can be rewritten by introducing the set of auxiliary variables $b^s \ \ \forall s$ as follows:

$$\max_{x_n^s, p_n^s} \quad \sum_l \sum_{s \in \mathcal{S}^{(l)}} \left[U^s(b^s) - \lambda^{(l)} b^s \right] \tag{4.31}$$

$$\text{s.t.} \quad \sum_s x_n^s \leq 1 \qquad \forall n \tag{4.32}$$

$$\sum_s \sum_{n=1}^{N_{sc}} p_n^s \leq P_{BS} \tag{4.33}$$

$$x_n^s \in \{0, 1\} \tag{4.34}$$

$$\overline{r}^s \geq b^s \qquad \forall s. \tag{4.35}$$

Constraint (4.35) is relaxed by forming the Lagrangian

$$W(b^s, \lambda^{(l)}, \delta^s) = \sum_l \sum_{s \in \mathcal{S}^{(l)}} \left[U^s(b^s) - \lambda^{(l)} b^s + \delta^s \left(\overline{r}^s - b^s \right) \right], \tag{4.36}$$

where δ^s is the Lagrange multiplier associated with the sth subscriber. δ^s demands a rate allocation for the sth subscriber. The dual problem[6] is given by

$$\begin{aligned} \min_{\boldsymbol{\lambda}, \boldsymbol{\delta}} \quad & w(\boldsymbol{\lambda}, \boldsymbol{\delta}) && (4.37) \\ \text{s.t.} \quad & \text{constraints } (4.32) - (4.34) \\ & \boldsymbol{\lambda} \geq \mathbf{0} && (4.38) \\ & \boldsymbol{\delta} \geq \mathbf{0}, && (4.39) \end{aligned}$$

where $w(\boldsymbol{\lambda}, \boldsymbol{\delta}) = \max_{b^s} W(b^s, \lambda^{(l)}, \delta^s)$. The dual problem can be separated into two problems [42]. The first is a utility maximization problem:

$$w'(\boldsymbol{\lambda}, \boldsymbol{\delta}) = \max_{b^s} \sum_l \sum_{s \in \mathcal{S}^{(l)}} \left[U^s(b^s) - \lambda^{(l)} b^s - \delta^s b^s \right], \tag{4.40}$$

and the second is a subcarrier, rate and power allocation problem

$$\begin{aligned} w''(\boldsymbol{\delta}) \; = \; & \max_{p_n^s, x_n^s} \sum_l \sum_{s \in \mathcal{S}^{(l)}} \delta^s \overline{r}^s && (4.41) \\ \text{s.t.} \quad & \sum_s x_n^s \leq 1 \qquad \forall n && (4.42) \\ & \sum_s \sum_{n=1}^{N_{sc}} p_n^s \leq P_{BS} && (4.43) \\ & x_n^s \in \{0, 1\}. && (4.44) \end{aligned}$$

Note that each of the dual problems (4.40) and (4.41) can be individually solved to obtain their optimums (i.e., $b^{s^\star}$ and $\overline{r}^{s^\star}$) while being coordinated by the master dual problem (4.37) (Figure 4.2). Multipliers $\delta^s \;\; \forall s$ are updated iteratively at each iteration $\dot{t}$ by the subgradient method

$$\delta^s(\dot{t}+1) = \left[\delta^s(\dot{t}) + \dot{\kappa} \left(b^{s^\star}(\delta^s(\dot{t})) - \overline{r}^{s^\star}(\delta^s(\dot{t})) \right) \right]^+, \tag{4.45}$$

[6] $\boldsymbol{\delta}$ denotes a vector of $\delta^s \;\; \forall s$.

where $\dot{\kappa}$ is a diminishing step size. At each iteration, $b^{s^\star}(\delta^s(\dot{t}))$ is obtained for each subscriber by maximizing (4.40) for b^s where the utility functions are assumed to be concave. The coupling constraints (4.42) and (4.43) pose complication in solving (4.41). However, relaxing constraint (4.43) decouples the problem into multiple per-subcarrier subproblems, which also satisfies (4.42). Therefore, a Lagrangian can be formed:

$$Z(\overline{r}^s, p_n^s, \boldsymbol{\delta}, \upsilon) = \sum_l \sum_{s \in \mathcal{S}^{(l)}} \delta^s \sum_n^{N_s} E[r_n^s] + \upsilon(P_{BS} - \sum_s \sum_{n=1}^{N_{sc}} p_n^s). \tag{4.46}$$

The Lagrange multiplier υ is interpreted as the price of using P_{BS}. Let $\min_{\boldsymbol{\delta},\upsilon} z(\boldsymbol{\delta}, \upsilon) = \max_{p_n^s, x_n^s} Z(\overline{r}^s, p_n^s, \boldsymbol{\delta}, \upsilon)$. Because the duality gap is zero, the dual problem

$$\min_{\boldsymbol{\delta},\upsilon} \quad z(\boldsymbol{\delta}, \upsilon) \tag{4.47}$$

$$\text{s.t.} \quad \sum_s x_n^s \leq 1 \quad \forall n \tag{4.48}$$

$$x_n^s \in \{0, 1\} \tag{4.49}$$

$$\boldsymbol{\lambda} \geq \mathbf{0} \tag{4.50}$$

$$\upsilon \geq 0, \tag{4.51}$$

is now decoupled into N_{sc} maximization subproblems,

$$\arg\max_s \ \delta^s E[r_n^s] - \upsilon \, p_n^s \qquad \forall \, n. \tag{4.52}$$

For each expected rate, $E[r_n^s]$, to be supported, the required power, p_n^s, is obtained by (4.18). These maximization subproblems are solved per-subcarrier. In other words, the subcarrier is exclusively assigned to the sth subscriber that maximizes (4.52) on that particular subcarrier; thus, constraint (4.42) is also satisfied. $\boldsymbol{\delta}$ is passed down from (4.37) and υ is updated by the following subgradient method:

$$\upsilon(\ddot{t}+1) = \left[\upsilon(\ddot{t}) - \ddot{\kappa}\left(P_{BS} - \sum_s \sum_n^{N_{sc}} p_n^{s^\star}(\upsilon(\ddot{t}))\right)\right]^+, \tag{4.53}$$

where $\ddot{\kappa}$ is the step size and $\ddot{t}$ is the iteration index. $p_n^{s^\star}(\upsilon(\ddot{t}))$ is obtained by solving the per-subcarrier problems (4.52) for a specific $\upsilon(\ddot{t})$. Figure 4.2 shows the decomposition of the master dual problem into a hierarchy of subproblems and the interaction among them.

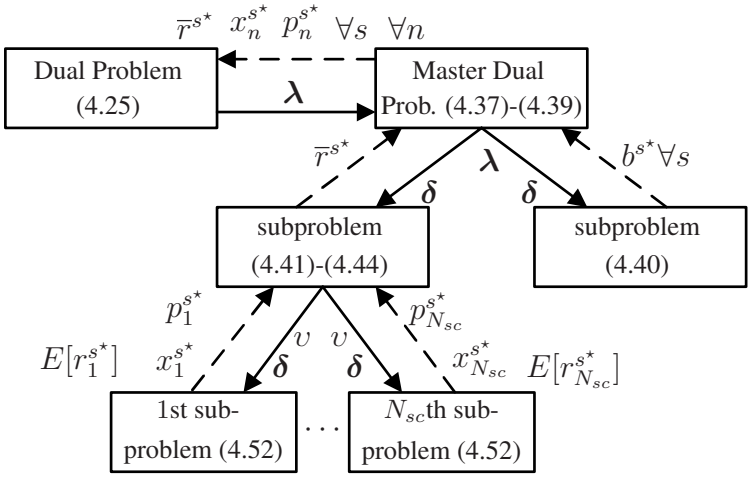

Figure 4.2: Hierarchy of decomposed dual problem.

Based on the mathematical formulations and derivations presented above, the pseudocode of the proposed scheme is outlined in Algorithm 1. The Algorithm inputs are: the necessary parameters to solve equations (4.18) and (4.40), imperfect CSI, estimation error statistics, capacity partitions and maximum transmission power. The outputs include power, rate and subcarriers allocation. The scheme is divided into two phases: a pre-optimization phase and an optimization phase. The pre-optimization phase prepares the possible expected rate levels, K, and their corresponding power allocations, by (4.18), based on the received imperfect CSI, lines 2 to 9. This phase can be implemented in both a centralized manner, as in lines 2 to 9 at the BS, or in a distributed manner by which each subscriber searches the lookup tables for α, β and γ, evaluates the required power allocations, and reports them to the BS. Either of the implementations provides the same result, but questions arise about how much computation the subscriber station can perform and how much reporting overhead the feedback channel can support. Hence, it's a trade-off between computational complexity at the BS and the feedback reporting overhead.

In the optimization phase, the power, rate and subcarrier allocations are optimized while satisfying the network constraints. In the following, the network constraints along

Algorithm 1 Pseudocode of the proposed scheme

Pre-optimization phase
for $s = 1$ to S **do**
    for $n = 1$ to N_{sc} **do**
        Search lookup tables for α, β and γ
        for k=1 to K **do**
            Solve (4.18) for p_n^s
        end for
    end for
end for

Optimization phase
Initialize $\lambda^l \; \forall l$
Initialize $\delta^s \; \forall s$
for $s = 1$ to S **do**
    Solve the derivative of (4.40) for $b^{s^\star}$
    $b^{s^\star} \leftarrow b^s$
end for
Initialize υ
for $n = 1$ to N_{sc} **do**
    $\arg\max_s \; \delta^s E[r_n^s] - \upsilon \, p_n^s$
    $s^\star \leftarrow s$
    Allocate nth subcarrier
    $\mathcal{N}_{s^\star} \leftarrow \mathcal{N}_{s^\star} \cup \{n\}$
    Allocate power
    $p_n^{s^\star} \leftarrow p_n^s$
end for
update $\upsilon(\ddot{t}+1) =$

$$\left[\upsilon(\ddot{t}) - \ddot{\kappa}\left(P_{BS} - \sum_s \sum_n^{N_{sc}} p_n^{s^\star}(\upsilon(\ddot{t}))\right)\right]^+$$

Repeat lines 17 to 23 until convergence
$\overline{r}^{s^\star} \leftarrow \sum_n^{N_s} E[r_n^s] \quad \forall s$
update $\delta^s(\dot{t}+1) =$

$$\left[\delta^s(\dot{t}) + \dot{\kappa}\left(b^{s^\star}(\delta^s(\dot{t})) - \overline{r}^{s^\star}(\delta^s(\dot{t}))\right)\right]^+$$

Repeat lines 12 to 26 until convergence
update $\lambda^l(t+1) =$

$$\left[\lambda^l(t) - \kappa\left(c^{(l)} - \sum_{s\in\mathcal{S}^{(l)}} \overline{r}^{s^\star}(\lambda^l(t))\right)\right]^+$$

Repeat lines 11 to 28 until convergence

with their related subroutines in Algorithm 1 are discussed:

- *A subcarrier is exclusively allocated to one subscriber.* In lines 18 to 23, each subcarrier is allocated to the subscriber that maximizes the term $\delta^s E[r_n^s] - \upsilon\, p_n^s$ by searching over a matrix of supported expected rate levels for all subscribers. The required power to support the granted rate is allocated to the subscriber on the nth subcarrier, line 22. Note that the cardinality of the set $\mathcal{N}_s$ is denoted by N_s, which is the number of subcarriers allocated to the sth subscriber.

- *The aggregate rate allocated to the lth service is limited to a partition of the throughput $c^{(l)}$.* The Lagrange multiplier $\lambda^{(l)}$ represents the price of utilizing $c^{(l)}$. As the scheme evolves, over utilizing $c^{(l)}$ increases $\lambda^{(l)}$, and the converse is true, line 29. The unavailability of throughput for a specific class of service l is signalled via $\lambda^{(l)}$ to line 14, where the minimum rate (i.e., axillary variable b^s) to be allocated to the subscribers is obtained. For example, let the utility function be the concave function $U^s(b^s) = \varsigma \log(b^s)$; therefore, solving the derivative of (4.40), for each term of the summation gives $b^s = \frac{\varsigma}{\lambda^{(l)} + \delta^s}$. Hence, an increase in $\lambda^{(l)}$ decreases b^s, and the scheme tends to allocate a lower rate to subscribers of the lth class of service by reducing the demand variable (i.e., Lagrange multiplier δ^s), line 27.

- *Total allocated power is limited to the base station power P_{BS} in the downlink mode and the power allocated to each subscriber is limited to its specific power constraint, P_s, in the uplink mode.* Power supply is controlled by the Lagrange multiplier, υ, line 24. If the base station power is over utilized, the price, υ, increases resulting in a decrease in the term $\arg\max_s\ \delta^s E[r_n^s] - \upsilon\, p_n^s$. Thus, the scheme tends to allocate a lower rate, which requires less power. In the uplink mode, the allocated power to each subscriber is constrained by its maximum available power (i.e., device battery power), denoted by P_s. Therefore, the constraint in (4.22) is replaced with $\sum_{n \in \mathcal{N}_s} p_n^s \leq P_s$, and the subgradient algorithm in line 24

is replaced with

$$\upsilon^s(\ddot{t}+1) = \left[\upsilon^s(\ddot{t}) - \ddot{\kappa}\left(P_s - \sum_{n\in\mathcal{N}_s} p_n^{s\star}(\upsilon^s(\ddot{t}))\right)\right]^+ \quad \forall s. \tag{4.54}$$

Thus, each subscriber has a specific multiplier υ^s that prices the supply of its power.

4.4 Complexity Analysis

Computational complexity is a major factor in implementing resource allocation schemes for OFDMA networks. However, the resource allocation problem for OFDMA networks is known to be NP-hard as shown in Appendix A and obtaining an exhaustive search allocation is computationally impossible for large number of subcarriers. The exclusive subcarrier assignment constraint makes the problem a complex combinatorial one that becomes harder when the power and per-service aggregate rate constraints are considered. The proposed scheme is low in computational complexity due to the adopted decomposition approach. The following complexity analysis estimates the execution time of the proposed scheme in relation to the input size.

Let T_{24}, T_{27} and T_{29} be, respectively, the number of iterations required for each of the the subgradient methods in line 24, 27 and 29 of the Algorithm 1 to converge. Also, let J be the length of the lookup table (line 4). It can be seen that the pre-optimization phase is $\mathcal{O}(SN_{sc}(J+K))$. Starting with the most inner loop (lines 18 to 23) each cycle of the N_{sc} cycles requires KS comparisons, and it takes T_{24} for convergence resulting in $\mathcal{O}(T_{24}N_{sc}KS)$. The loop in lines 13 to 16 is $\mathcal{O}(S)$ because it cycles S times. Thus, the optimization phase is $\mathcal{O}(T_{27}T_{29}(S+T_{24}N_{sc}KS))$. Therefore, the overall resource allocation scheme complexity is $\mathcal{O}(SN_{sc}(J+K)) + \mathcal{O}(T_{27}T_{29}(S+T_{24}N_{sc}KS))$. Whereas an exhaustive search for allocating subcarriers and rates only is exponential (i.e., $\mathcal{O}((KS)^{N_{sc}})$), the proposed scheme is linear (i.e., $\mathcal{O}(T_{24}KSN_{sc})$) in terms of the

number of subcarriers[7] available to the cell, which implies a major reduction in the computational complexity. Although the complexity has been reduced, a stoping criteria needs to be defined to stop the algorithm before the CSI changes. The change in CSI depends on how fast is the channel varying in real time. Defining a stoping criteria requires the implementation of the Algorithm in hardware which will be addressed in our future work.

4.5 Performance Evaluations

Simulations are presented in this section to evaluate the proposed scheme's performance in terms of the expected rate gain achieved by considering the CSI imperfection at the MAC layer, the performance in limiting the allocated classes expected rate to a partition of throughput specified by the CAC scheme, and the satisfaction of OFDMA constraints.

A frequency selective fading and Rayleigh distributed channel is simulated based on a six-tap time varying model. A 512 discrete Fourier transform (512-DFT) of the delay tap gains generates 512 subcarriers CSI. The subscribers' channels experience distance dependent fading that follows the power inverse law [19]. In our simulation, the path loss exponent is set to 2. In the network under consideration, the RAU knows the estimated CSI of each subcarrier, $\hat{H}_n^s$, for each particular subscriber, s, in addition to the estimation error variance $(\tilde{\sigma}_\epsilon^s)^2$. Various network parameters' distributions and assumptions are stated in the system model (Section 4.1).

Figure 4.3 shows the expected rate achieved by one subscriber station over 500 samples of the channel for a range of power-to-noise ratio, $p_n^s/(\sigma_z^s)^2$. In order to show the gain achieved by considering the channel estimation error, three scenarios are studied.

1- In the first scenario, the RAU has perfect knowledge of the CSI (i.e., H_n^s) which is shown to achieve the highest expected rate, but not possible in practice.

[7] In OFDMA networks, the number of subcarriers can be as large as 2048.

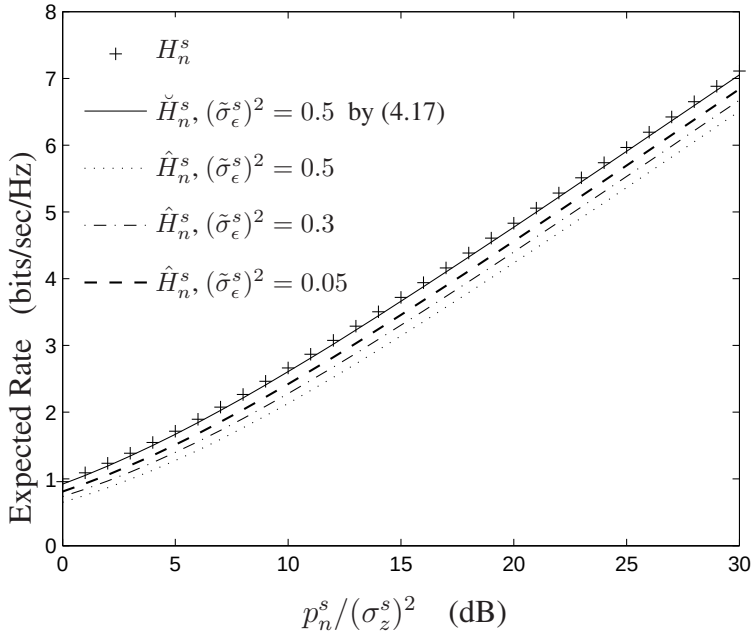

Figure 4.3: Expected rate achieved given perfect CSI, H_n^s (first scenario), estimated CSI with error ignored, $\hat{H}_n^s$ (second scenario), and estimated CSI with error considered, $\breve{H}_n^s$ (third scenario - proposed)

2- In the second scenario, the RAU assumes the estimate, $\hat{H}_n^s$, to be perfect and ignores the estimation and delay error.

The expected rate decreases as the estimation error variance increases as shown by lines labeled as $\hat{H}_n^s, (\tilde{\sigma}_\epsilon^s)^2 = 0.05,\ 0.3$ and 0.5 in Figure 4.3. Note that the plots are in bits/sec/Hz; thus, the difference between the expected rate for the above two scenarios is scaled by the transmission bandwidth. Therefore, as the transmission bandwidth increases, the loss in expected rate increases in the second scenario.

3- The third scenario represents our proposed model where the RAU has knowledge of the estimate $\hat{H}_n^s$ and the estimation error statistics, $(\tilde{\sigma}_\epsilon^s)^2 = 0.5$.

Based on this knowledge and equation (4.18), the expected rate (solid line in Figure 4.3)

is close to the one achieved when the RAU has perfect knowledge of the CSI as in the first scenario (line marked with $+$).

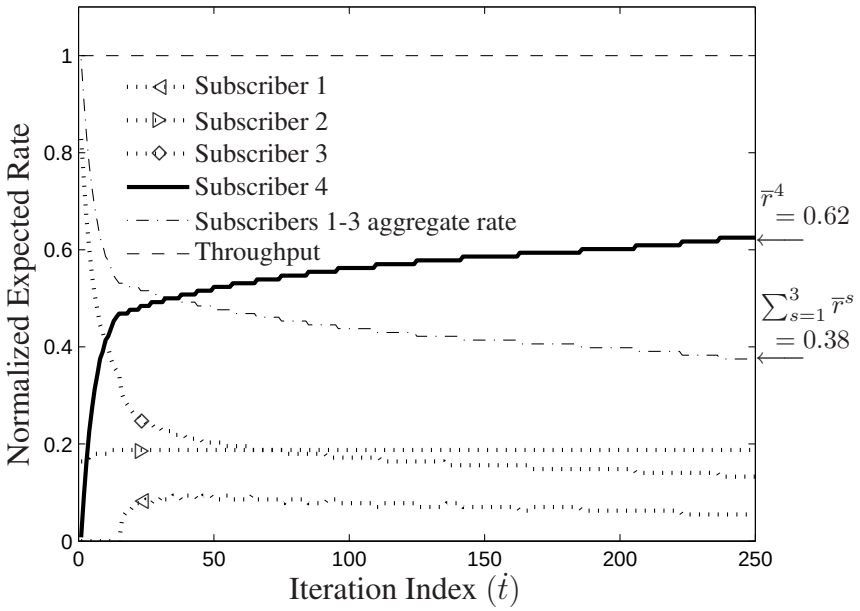

Figure 4.4: Expected rate allocated as the scheme evolves without classes aggregate rates limit constraints.

Whereas the above simulation shows how a substantial rate gain can be achieved by considering the CSI imperfection, in the following, we show how the proposed resource allocation scheme maintains the aggregate rate limit for each service class in a multiservice network. In addition to the above mentioned PHY layer simulation setup, consider a cell with four subscribers that are randomly distributed in the cell. The BS offers two classes of service; three of the subscribers subscribe to the first class, $\{s \in \mathcal{S}^{(1)} : s = 1, 2, 3\}$, and the fourth subscriber subscribes to the second class, $\{s \in \mathcal{S}^{(2)} : s = 4\}$. The first class subscribers are considered to be less demanding for rate than the second class subscribers. Thus, the first class and second class subscribers are considered to, respectively, have the following utility functions $U^s(\overline{r}^s) = \log(\overline{r}^s)$ for $s = 1, 2, 3$ and $U^4(\overline{r}^{\,4}) = 15\log(\overline{r}^{\,4})$. Intuitively, a large amount of resources is

expected to be allocated to the fourth subscriber station if constraints are not imposed on each class aggregate rate. This scenario is simulated by setting the Lagrange multipliers of problem (4.37) to zero, i.e., $\boldsymbol{\lambda} = \mathbf{0}$. Figure 4.4 shows the expected rates allocated to subscribers. Subscribers 1-3 subscribe to class 1 while subscriber 4 subscribe to class 2. The rates are normalized to the network throughput over this allocation instance. It is clearly observed that the scheme allocates 62% of the network throughput to the demanding subscriber (i.e, second class subscriber) while it allocates only 38% to the three subscribers of the first class as shown by their aggregate rate, $\sum_{s\in\mathcal{S}^{(1)}} \overline{r}^s = 0.38$, when the scheme converges. In this scenario, the scheme allocates even higher rate if the demanding subscribers have better channel condition than the rest which may result in not supporting the less demanding subscribers. The difference among the rates allocated to the first class subscribers is due to the difference in their subcarriers gains. Our proposed scheme constrains the aggregate rate allocated to each class subscriber to its limit reported by the CAC scheme while satisfying the power and subcarriers exclusive allocation constraints.

Consider that the CAC scheme limits the first class aggregate rate to 80% and the second class to 20%, (i.e., $c^{(1)} = 0.8$ and $c^{(2)} = 0.2$). We re-run the simulation with the same network parameters (i.e., utility functions, channels, subscribers) while $\boldsymbol{\lambda}$ is evaluated by (4.37). Figure 4.5 shows the expected rates allocated to subscribers when limits are imposed on the classes aggregate rates. Subscribers 1-3 subscribe to class 1 while subscriber 4 subscribes to class 2. We observe that, at convergence, the rate allocated to the demanding subscriber is reduced from 62% to 20%. The 42% that became available is now shared among the first class subscribers; thus, their aggregate rate increases from 38% to 80%. Both classes allocated rates are limited to their capacities specified by the CAC scheme that satisfies the QoS requirements of each class of service. In both scenarios, the proposed scheme exclusively allocates each subcarrier to one subscriber and maintains a limit of P_{BS} on the power allocated to all subscribers.

Next, we demonstrate the performance of the proposed scheme on the uplink mode. We consider a single cell with six subscriber stations. The first three subscribers are

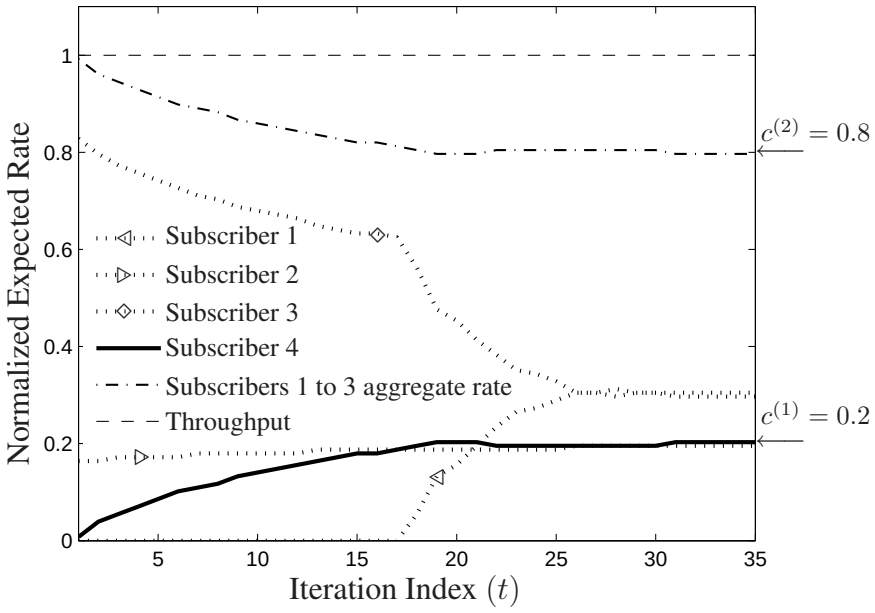

Figure 4.5: Expected rate allocated as the scheme evolves with classes aggregate rates limit constraints (proposed scheme).

more demanding than the last three; thus, their utility functions are considered to be, respectively, $U^s(\overline{r}^s) = 5\log(\overline{r}^s)$ for $s = 1, 2, 3$ and $U^s(\overline{r}^s) = \log(\overline{r}^s)$ for $s = 4, 5, 6$. In addition, they subscribe to two different classes, $\{s \in \mathcal{S}^{(1)} : s = 1, 2, 3\}$ and $\{s \in \mathcal{S}^{(2)} : s = 4, 5, 6\}$. In the uplink mode, each subscriber has a power constraint which corresponds to its battery available power (i.e., P_s); thus, the power allocated to each subscriber has to be limited to P_s. Subscribers are simulated to have equal power constraints for simplicity. The first and second class of service aggregate rates, determined by the CAC scheme, are assumed to be $c^{(1)} = 60\%$ and $c^{(1)} = 40\%$, respectively.

Figure 4.6 shows the evolutions of expected rate allocation for each subscriber and the aggregate rate for each class. Similar to the downlink mode, the presented scheme limits the aggregate rate of each class to the partition of the throughput allocated to it. It is observed that the convergence speed for uplink is slower than that for downlink, shown

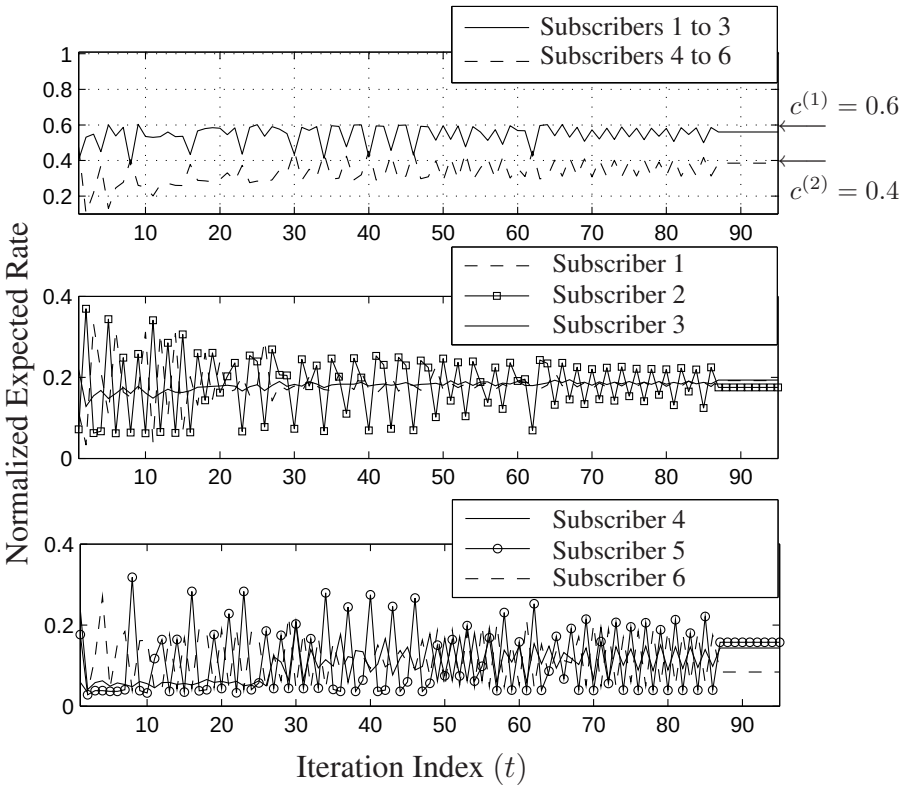

Figure 4.6: Normalized expected rate allocated as the scheme evolves to each class (top sub-figure), subscribers of class one (middle sub-figure) and subscribers of class two (bottom sub-figure).

in Figure 4.5. This decrease in convergence speed is due to the increase in the number of power constraints in uplink compared to downlink. To investigate the exclusive subcarrier assignment, the checkerboard plot in Figure 4.7 shows that each subcarrier of the 512 subcarriers is allocated to a subscriber station; black areas indicate the range of subcarriers allocated to a subscriber station. Similar performance in allocating subcarriers has also been observed for the downlink mode. In addition, the normalized power allocated to each subscriber (i.e., $\frac{\sum_{n\in\mathcal{N}_s} p_n^s}{P_s}$ for $s = 1 \cdots 6$) is shown in Figure 4.8. It can be seen that the power allocated to each subscriber never exceeds its power limit, P_s for $s = 1 \cdots 6$. The power allocated to some subscribers is more than the power allocated to

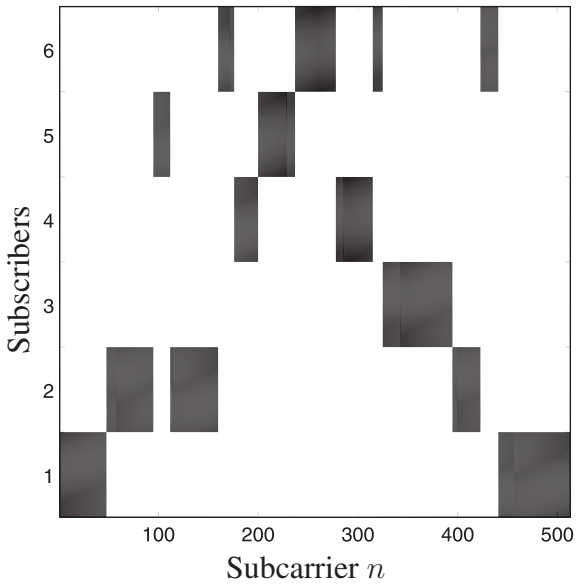

Figure 4.7: Subcarriers allocation to each subscriber at convergence.

the rest because of their low channel gain on their allocated subcarriers.

4.6 Summary

A novel resource allocation scheme for OFDMA-based PMP networks has been proposed. The proposed scheme solves the resource allocation problem in the dual domain by decomposing it into several subproblems at the MAC layer while considering channel estimation and delay errors at the PHY layer. In addition to satisfying OFDMA network constraints (i.e., exclusive subcarrier and maximum power allocations), the proposed scheme maintains the classes aggregate expected rate limits, imposed by a CAC unit, to satisfy the QoS requirements of each class. Simulation results are given to demonstrate that a significant gain can be achieved by taking the CSI imperfection into consideration.

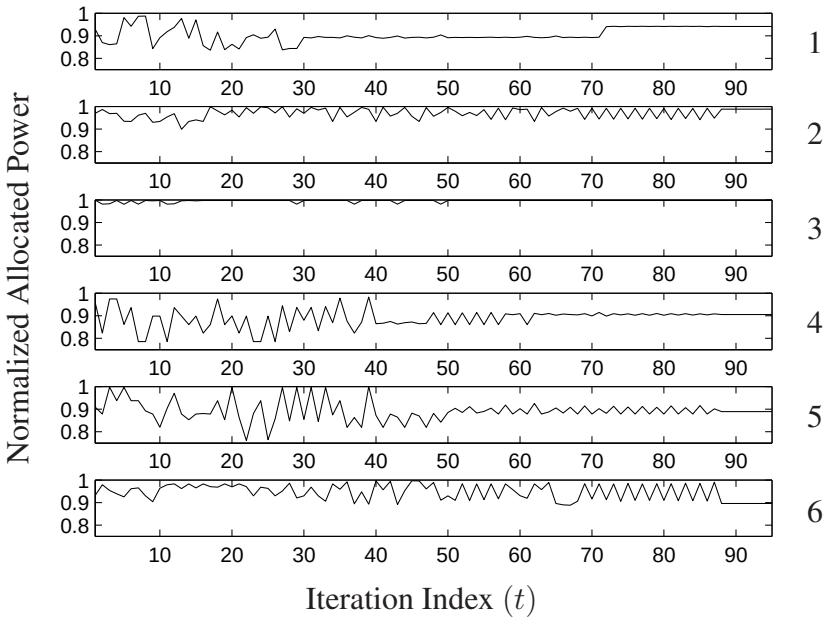

Figure 4.8: Normalized allocated power to each subscriber station in the uplink mode (i.e., $\frac{\sum_{n\in\mathcal{N}_s} p_n^s}{P_s}$ for $s = 1 \cdots 6$) as the scheme evolves. Numbers on the right indicate the subscriber index.

Chapter 5

Power Allocation for Single Carrier Cooperative Networks

In this chapter, we consider power allocation in cooperative networks with inaccurate CSI. The channel estimation error is embedded in the power allocation model which results in an uncertain linear and time varying system. Based on this system, a robust and constrained Kalman filtering (RCKF) scheme which adapts the allocated power to channel variation while satisfying the average bit error probability (BEP) requirements of each subscriber is developed. The proposed scheme's low complexity, robustness to CSI inaccuracy and adaptive responsiveness to changes in BEP requirements make it practical for real network implementation. Simulation results show that the proposed scheme converges to the optimal allocation with light computational burden despite the inaccuracy in the received CSI.

A cooperative network creates a virtual multiple input scenario to facilitate diversity reception in order to yield cooperative diversity (CD) gain when multiple antennas are not feasible for a communication terminal. Cooperation not only replicates multiple-input multiple-output (MIMO) transmissions but also outperforms it in palliating shadowing effects because the antennas of the source and its cooperating partner has a larger

separation distance than the antennas housed at one subscriber as in MIMO systems. In addition, scatterers in the vicinity of the source and its cooperating partner may be different; however, in MIMO systems the antennas are surrounded by the same scatterers. The CD gain reduces transmission power and allows increasing the code rate which, in turn, increases spectral efficiency [106]. In addition, the increase in spectral efficiency decreases retransmissions which results in lower delays. Cooperative networks improve the performance through adaption to network conditions (i.e., subscribers' channel gains, battery life) by choosing between with or without cooperation [107]. It is shown in [108] that cooperation offers an opportunity for diversity detection in cognitive radio networks. Because of these features, cooperative technologies have received great attention from both the research community and industry. For example, cooperative technologies are adopted in both the Broadband Wireless Access Networks IEEE 802.16j and the 3rd Generation Partnership Project Long Term Evolution (3GPP-LTE) [3] standards.

In [109], a bandwidth and energy efficient CD system using quadrature signaling for a two-subscriber cooperation paradigm is proposed. Quadrature signaling is achieved by transmitting in the in-phase and quadrature components of a quadrature amplitude modulation scheme. With quadrature signaling, instead of expanding the bandwidth or reducing the effective data rate of the cooperative system, the signal constellation of the modulation scheme is expanded to accommodate the transmissions by the partner. Since each subscriber employs its own multiple access channel to send both its and the partner's signals to the destination, quadrature signaling eliminates the need to use the partners' multiple access channels, and thereby reduces the additional synchronization normally required in schemes such as distributed space-time block coding (DSTBC) in which the signal from both subscribers should be received coherently. It is shown that the CD system in [109] can achieve diversity order of two.

Wireless mobile devices are normally battery powered. It is important to minimize the energy consumption in order to maximize the lifetime of the device without recharging or replacing the battery. The error probability of a CD system primarily depends on the quality of the inter-subscriber channel and subscriber-to-destination channel, and the

transmission power of the cooperating subscribers. To minimize the requested power for a guaranteed error probability, the transmission power should be optimally allocated to both the source and the relay according to the channel qualities and the CD system employed. Various power allocation schemes [42, 110–114] have been proposed for cooperative relay networks. However, these works assume the CSI to be perfectly known and ignores the effect of CSI inaccuracy with the exception of a limited number of reported results (e.g., [115, 116]). Our previous investigation [12] shows the CSI inaccuracy significantly affects cooperative networks performance. Generally, the performance of the CD systems is optimized using power allocation among the source and the partner based on the channel CSI, fed back from respective receivers. The destination must have the knowledge of CSI between the source and the potential relays to select a partner. The fading channel is time varying and the CSI received from the feedback message is not accurate at the time instant it is used because of the the channel estimation and processing errors, and transmission delays. Thus, it becomes of great importance to consider channel estimation error in the design of CD related schemes like power allocation which is the focus of this work.

In addition to overlooking the CSI inaccuracy, literature available power allocation schemes (e.g., [117, 118]) for relay networks are designed under the assumption that the source and relay power are constrained by a total power constraint. However, our system model represents a practical scenario in which the source and relay have individual power constraints that correspond to their individual batteries' power. The need for a practical scheme has motivated us to apply Kalman filtering in the context of power allocation because Kalman filter (KF) has been shown to be practical and implementable in numerous applications like space-craft navigation for the Apollo space program, nuclear power plant instrumentation, manufacturing, etc. [119]. In wireless communication related schemes, KF has been widely applied, for instance, in channel estimation [120], mobility estimation [121], interference estimation and power allocation [122, 123], and adaptive beamforming [124].

In this chapter, we propose a novel power allocation scheme for CD systems in which

the CSI estimate is inaccurate and the permissible computational complexity is low. The proposed scheme allocates the minimum power for a cooperating pair of subscribers while satisfying their average BEP requirements. Based on our previous results [109] which show that the optimal allocation is obtained by satisfying the constraints with equalities and the robust Kalman filter proposed in [125], the proposed approach converts the power allocation problem to a robust estimation problem. In particular, the power allocation process over frames is modeled as a first order autoregressive process [123]. The autoregressive process parameters (i.e., weights) vary over frames following state-space equations that describe the system. These state-space equations differs from state-space equation considered in conventional Kalman filtering problems in two aspects: First, the prediction and output matrices are uncertain due to CSI inaccuracy. Second, the output equation is constrained by target average SNRs that satisfies the average BEP. In this context, the robust and constrained Kalman filter estimates the weights that minimize the sum of allocated power and satisfy a predefined average BEP. Robust Kalman filters perform state estimation for linear models with uncertainty [125] and constrained Kalman filters estimate the states of a systems with a constraint imposed on the output equation (a.k.a measurement equation) [124, 126, 127]. The estimation error for Rayleigh channels and AWGN noise has been shown to be Gaussian [12, 58, 78]; however, in this work we consider a practical situation where the distribution of the error is unknown. The distribution of the estimation error is assumed to be uniformly distributed in a given range centered around zero. The proposed scheme is semi-distributed in the sense that different operations are performed at the subscribers and the base stations which coordinate the exchange of information among subscribers.

The notation used in this chapter is as follows. $\mathbf{O}$ is the identity matrix of the appropriate size. Boldface upper-case and non-italicized letters and symbols denote matrices while boldface italicized letters and symbols denote vectors.

The remainder of the chapter is organized as follows. Section 5.1 describes the system model. The problem formulation and proposed power allocation scheme are presented in Section 5.2. Simulations results are presented in Section 5.3. Finally, the

chapter is concluded in Section 5.4.

5.1 System Description

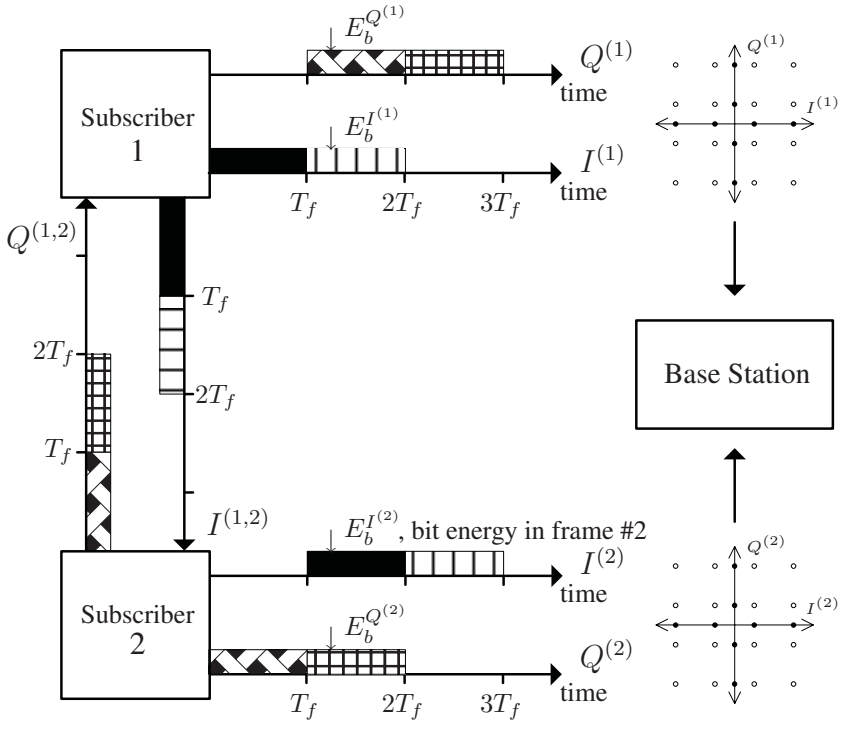

Figure 5.1: Illustrative CD network of a cooperating pair, subscriber-1 and subscriber-2, and a base station showing the time line of frames sourcing and relaying on each of the subscribers channels.

We consider a single-carrier wireless network where the base station (BS) of a radio cell supports multiple subscribers. Each subscriber is capable of cooperating with another subscriber (i.e., cooperation between two active subscribers). A cooperating partner for a subscriber is pre-selected by the RAU [7]. The partner forwards the frame if it was correctly received. The BS and each of the subscribers has a single antenna. The uplink signals (transmitted by the sender and relayed by the partner) are combined at the

BS using maximal ratio combining (MRC). The cooperative diversity scheme thus emulates a "two inputs one output" (2I1O) situation. The inter-subscriber and subscriber-to-BS channels are assumed to exhibit time selective and frequency non-selective Rayleigh fading and to be independent of each other. The channel is considered quasi-static so that channel variation over a frame duration is negligible. The BS receives a inaccurate CSI estimate of the subscriber-1-to-subscriber-2 channel while each subscriber receives an inaccurate estimate of the CSI on the subscriber-i-to-BS channel, $i \in \{1, 2\}$ in each frame from the BS. We make the assumption that the inter-subscriber channels are symmetric for simplicity but the proposed scheme can be applied in networks with asymmetric inter-subscriber channels. In addition, the BS evaluates the average channel gains over a window of frames. Based on the received inaccurate CSI and the target SNR to be maintained, each of the subscribers allocates its transmission power (for both sourcing and relaying channels) such that a pre-defined average BEP is supported.

To facilitate the proposed power allocation scheme presented in Section 5.2, we summarize the M-QAM cooperative diversity scheme under consideration and its performance in terms of average BEP [109].

5.1.1 Cooperative Diversity Scheme Under Consideration

Consider a cooperative diversity scheme based on M-QAM signaling in which a subscriber (the sender) cooperates with another subscriber (the partner) to transmit signals in the uplink of an infrastructure based network. Cooperating subscribers transmit their own and the partner's signals simultaneously using quadrature signaling. In quadrature signaling, we assign the in-phase channels at both subscribers (i.e., $I^{(1)}$, $I^{(2)}$ and $I^{(1,2)}$) to subscriber-1 and the quadrature channels (i.e., $Q^{(1)}$, $Q^{(2)}$ and $Q^{(1,2)}$) to subscriber-2 [109].

Figure 5.1 shows the frames of symbols broadcasted by subscriber-1 on $I^{(1)}$ and $I^{(1,2)}$ to the BS and subscriber-2, respectively. Subscriber-2, then relays the information in the next frame to the BS on $I^{(2)}$. For example, subscriber-1 broadcast the solid black

frame on $I^{(1)}$ and $I^{(1,2)}$. Then, subscriber-2 transmits the received solid black frame on $I^{(2)}$ to the BS. The same applies when subscriber-2 broadcasts its frames on $Q^{(2)}$ and $Q^{(1,2)}$ which are relayed by subscriber-1 on $Q^{(1)}$. The signals transmitted by the sender and relayed by the partner are combined at the BS receiver using maximal ratio combining. Figure 5.1 also shows the constellation plot with the in-phase and quadrature components of each subscriber; the inter-subscriber constellation plot was omitted for space limitations.

Since subscriber-1 and subscriber-2 use the in-phase and the quadrature components of the M-QAM modulation, respectively, each subscriber equivalently employs $\sqrt{M}$-PAM modulation. In the uplink receiver of both subscribers, the in-phase and quadrature components are demodulated separately and the detected and regenerated partner's frame is forwarded to the BS if the frame is detected error free.

Let the baseband equivalent received signals from subscriber-i, $i \in \{1, 2\}$, at the BS be denoted as $r^{i,B}(t)$, where t is the discrete symbol's time index. Similarly, subscriber-i's uplink signal received by subscriber-j, $j \in \{1, 2\}$ and $i \neq j$, is denoted as $r^{i,j}(t)$. From the system model, $r^{i,B}(t)$ and $r^{i,j}(t)$ can be written as

$$r^{i,B}(t) = h^{i,B}(t)s^{i}(t) + \eta^{i,B}(t) \tag{5.1}$$

$$r^{i,j}(t) = h^{i,j}(t)s^{i}(t) + \eta^{i,j}(t), \tag{5.2}$$

where the channel gain between subscriber-i and the BS is denoted by $h^{i,B}(t)$ and that from subscriber-i to subscriber-j by $h^{i,j}(t)$. When the inter-subscriber channel is symmetric, the coefficients of fading channel are equal (i.e., $h^{i,j}(t) = h^{j,i}(t)$). The processes $\eta^{i,B}(t)$ and $\eta^{i,j}(t)$ are additive noise at the respective receivers and assumed to be zero mean circularly symmetric, complex Gaussian distribution with variance $N_0/2$ per dimension, where N_0 is the one-sided power spectral density of white Gaussian noise. Subscriber-1's and subscriber-2's symbols, $sy^{(i)}(t)\ \ i \in \{1, 2\}$, are chosen from an M-QAM signal constellation similar to that shown in Figure 5.1. In a particular frame, f,

the symbols can be written as:

$$sy^{(1)}(t) = \varpi \left[\sqrt{E_b^{I^{(1)}}} a^{(1)}(t) + \imath \sqrt{E_b^{Q^{(1)}}} \bar{a}^{(2)}(t - T_f) \right] \tag{5.3}$$

$$sy^{(2)}(t) = \varpi \left[\sqrt{E_b^{I^{(2)}}} \bar{a}^{(1)}(t - T_f) + \imath \sqrt{E_b^{Q^{(2)}}} a^{(2)}(t) \right], \tag{5.4}$$

where $\varpi = \sqrt{\log_2 M}$, $\imath$ is the the imaginary unit, T_f is the frame duration, $E_b^{I^{(i)}}$ is the energy spent per bit at subscriber-i on the $I^{(i)}$ channel and $E_b^{Q^{(i)}}$ is the bit energy at subscriber-i on the $Q^{(i)}$ channel. $E_b^{I^{(i)}}$ remains constant for the frame duration. $a^{(i)}(t)$ is the $\sqrt{M}$-PAM information symbol of subscriber-i. $\bar{a}^{(i)}(\cdot)$ is the corresponding reproduced symbol at the partner, given by

$$\bar{a}^{(i)}(t) = \arg \min_{\bar{a}^{(i)} \in S_{\sqrt{M}}} \left(\chi^i \{ \hat{h}^{*^{i,j}}(t) r^{i,j}(t) \} \right), \tag{5.5}$$

where $\hat{h}^{i,j}$ is the estimate of $h^{i,j}$, and $\chi^1 = \Re$ and $\chi^2 = \imath$. $S_{\sqrt{M}}$ is the set of $\sqrt{M}$-PAM information symbols. At the BS, if each subscriber relays the partner's information, the signals received from both subscribers are combined using MRC. From the above description of the CD scheme, an inaccurate channel estimate affects the demodulation, symbol regeneration, power allocation and partner selection, and hence the performance of CD systems.

5.1.2 Average Bit Error Probability

In [109], we derived the analytical BEP performance of the M-QAM CD system under consideration. For the subscriber-1-to-BS, $\Upsilon^{(1)}$, subscriber-2-to-BS, $\Upsilon^{(2)}$, and subscriber-1-to-subscriber-2, $\Upsilon^{(1,2)}$ average SNRs, the BEP of subscriber-1 employing 4-QAM and 16-QAM signaling, respectively, were found to be ([109], (8) and (11))

$$\begin{aligned} P_b = (1 - P_{FEP}) \frac{1}{2} \Big(& g(\Upsilon^{(1)}, \Upsilon^{(2)}) \cdot z(\Upsilon^{(1)}) \\ & + g(\Upsilon^{(2)}, \Upsilon^{(1)}) \cdot z(\Upsilon^{(2)}) \Big) + \frac{1}{2} P_{FEP} \cdot z(\Upsilon^{(1)}), \end{aligned} \tag{5.6}$$

and

$$P_b = \frac{1}{8}(1 - P_{FEP}) \Big(g(\Upsilon^{(1)}, \Upsilon^{(2)}) \cdot d(1) + g(\Upsilon^{(2)}, \Upsilon^{(1)}) \cdot d(2) \Big) + \frac{1}{8} P_{FEP} \cdot d(1), \tag{5.7}$$

where $g(x, y) = \frac{x}{x-y}$ and $z(x) = 1 - \sqrt{\frac{x}{2+x}}$. Also, $d(i) = \big(4 - 3\mu^{(i)}(4,0) - 2\mu^{(i)}(4,1) + \mu^{(i)}(4,2)\big)$ where $\mu^{(i)}(x, y) = \sqrt{\frac{3\log_2 x.(2y+1)^2 \Upsilon^{(i)}}{2(x^2-1)+3\log_2 x.(2y+1)^2 \Upsilon^{(i)}}}$ $i \in \{1, 2\}$. Note that for subscriber-2 BEP, the above parameters are interchanged. The P_{FEP} for 4-QAM and 16-QAM are given respectively by

$$P_{FEP} \approx \sum_{N_{e|b}=1}^{Sym} \frac{1}{2} \left(1 - \sqrt{\frac{\Upsilon^{(1,2)} N_{e|b}}{2 + \Upsilon^{(1,2)} N_{e|b}}} \right), \tag{5.8}$$

and

$$P_{FEP} \approx \sum_{N_{e|b}=1}^{Sym} \frac{1}{8} \Bigg(4 - 3\sqrt{\frac{\Upsilon^{(1,2)} N_{e|b}}{5 + \Upsilon^{(1,2)} N_{e|b}}} - 2\sqrt{\frac{9\Upsilon^{(1,2)} N_{e|b}}{5 + 9\Upsilon^{(1,2)} N_{e|b}}} + \sqrt{\frac{25\Upsilon^{(1,2)} N_{e|b}}{5 + 25\Upsilon^{(1,2)} N_{e|b}}} \Bigg), \tag{5.9}$$

where $N_{e|b}$ is the number of symbol errors in a frame due to error in the b-th bit of the symbol and Sym is the number of symbols in a frame.

5.2 Problem Formulation and Proposed Power Allocation Scheme

The power allocation problem is posed as a minimization of the power consumption of both the source and relay while satisfying the average BEP requirements, $\varepsilon^{(1)}$ and $\varepsilon^{(2)}$. Mathematically, the power allocation problem can be written as follows:

$$\min \quad E_b^{I^{(i)}} + E_b^{Q^{(i)}} \quad i \in \{1, 2\} \tag{5.10}$$

$$\text{s.t.} \quad P_b^{(i)} \leq \varepsilon^{(i)} \quad i \in \{1, 2\}, \tag{5.11}$$

where $\varepsilon^{(i)}$ $i \in \{1, 2\}$ is the required BEP of subscriber-i. Although the proposed scheme essentially allocates bit energy, power allocation is obtained by simply multiplying the allocated bit energy by the number of bits in a frame and averaging over the frame duration since the bit energy is constant over a frame duration. Whereas the power allocation problem under consideration can be optimally solved for each frame, the resultant computational complexity will be prohibitively high. Computationally complex power allocation schemes are impractical in real networks because of the long computation time required to obtain an optimal solution during which the channel gain will likely be changed. Low complexity schemes are preferred, especially for distributed implementations in which subscribers have limited computational power. In addition to our results reported in [109], research works in [128, 129] show that the optimal solution is obtained when the constraints in (5.11) are satisfied with equalities. The proposed scheme achieves the optimal allocation through satisfying these constraints with equality. The required low complexity and the fact that an optimal solution can be obtained by satisfying the average BEP constraints with equality motivated us to adopt a state estimation technique with low implementation complexity and the average of its state estimates converges to the actual state's average [119]. The Kalman filter has these properties.

The BEP of 4-QAM and 16-QAM CD was given in (5.6) and (5.7), respectively. Note that the required average BEP (i.e., $\varepsilon^{(1)}$ and $\varepsilon^{(2)}$) of the subscribers can be achieved by maintaining their required average SNRs. These SNRs are defined as the target SNRs and denoted by $\Upsilon^{(1)}|\varepsilon^{(i)}$, $\Upsilon^{(2)}|\varepsilon^{(i)}$ and $\Upsilon^{(1,2)}|\varepsilon^{(i)}$, respectively, for $i \in \{1, 2\}$. Thus, for each cooperating pair, there are 6 SNRs to be maintained. For example, given $\varepsilon^{(1)}$ and $\varepsilon^{(2)}$ (e.g., 10^{-3}) to be satisfied, the target SNRs can be numerically solved by inverting equation (5.6) or (5.7). The complexity of such inversion is not a concern since it is performed off-line and the number of supported BEPs is limited. Therefore, they are not computed during power allocation but rather available in lookup tables at the BS. Based on the channel estimates available at the BS it looks up the target SNRs and reports them to the subscribers.

In our cooperative network, subscriber-1 (i.e., the source) broadcasts its signal to

subscriber-2 (i.e., partner) and to the BS during the same frame. With the assumption made earlier that each subscriber has a single antenna, evaluation of the transmission power at subscriber-1 for example, that maintains the target SNRs $\Upsilon^{(1)}|_{\mathcal{E}^{(1)}}$ on $I^{(1)}$ and $\Upsilon^{(1,2)}|_{\mathcal{E}^{(1)}}$ on $I^{(1,2)}$ over the same frame duration is impossible unless the condition

$$\frac{\Upsilon^{(1)}|_{\mathcal{E}^{(1)}}}{\Upsilon^{(1,2)}|_{\mathcal{E}^{(1)}}} = \frac{\overline{h}^{(1)}}{\overline{h}^{(1,2)}} \tag{5.12}$$

is satisfied. $\overline{h}^{I^{(1)}}$ and $\overline{h}^{I^{(1,2)}}$ are the average channel gains over a window of frames on $I^{(1)}$ and $I^{(1,2)}$, respectively (see proof given in Appendix B). Therefore, in the broadcast phase of the transmission, power allocation satisfies the target average SNR on one of the broadcast channels also satisfies the target average SNR on the other, if and only if the relation in (5.12) is satisfied. This condition can be easily satisfied after inverting either (5.6) or (5.7) offline.

Because each subscriber maintains its target SNR (i.e., the ones obtained by inverting (5.6) or (5.7)) separately, power can be allocated in a distributed manner at each subscriber. This allows us to present the proposed scheme in the sequel for one of the cooperating subscribers, say subscriber-1; power allocation at subscriber-2 can be similarly done.

The power allocation problem in (5.10) and (5.11) is converted to a robust and constrained Kalman state estimation problem. Power allocation is considered to be a first order autoregressive linear and time-varying process whose parameters are updated according to a set of state-space equations [123]. The allocated bit energy in the next frame, $f+1$, is a weighted version of the bit energy allocated in the f-th frame, which can be written as

$$\underbrace{\begin{bmatrix} E_{b_{f+1}}^{I^{(1)}} \\ E_{b_{f+1}}^{Q^{(1)}} \end{bmatrix}}_{\boldsymbol{E}_{b_{f+1}}^{(1)}} = \underbrace{\begin{bmatrix} E_{b_f}^{I^{(1)}} & 0 \\ 0 & E_{b_f}^{Q^{(1)}} \end{bmatrix}}_{\text{diag}\left(\boldsymbol{E}_{b_f}^{(1)}\right)} \underbrace{\begin{bmatrix} w_f^{I^{(1)}} \\ w_f^{Q^{(1)}} \end{bmatrix}}_{\boldsymbol{w}_f} \tag{5.13}$$

The weighting factors $w_f^{I^{(1)}}$ and $w_f^{Q^{(1)}}$ are updated from one frame to the next such that

they decrease if the estimate of SNR increase and the converse is true in order to maintain the target SNRs.

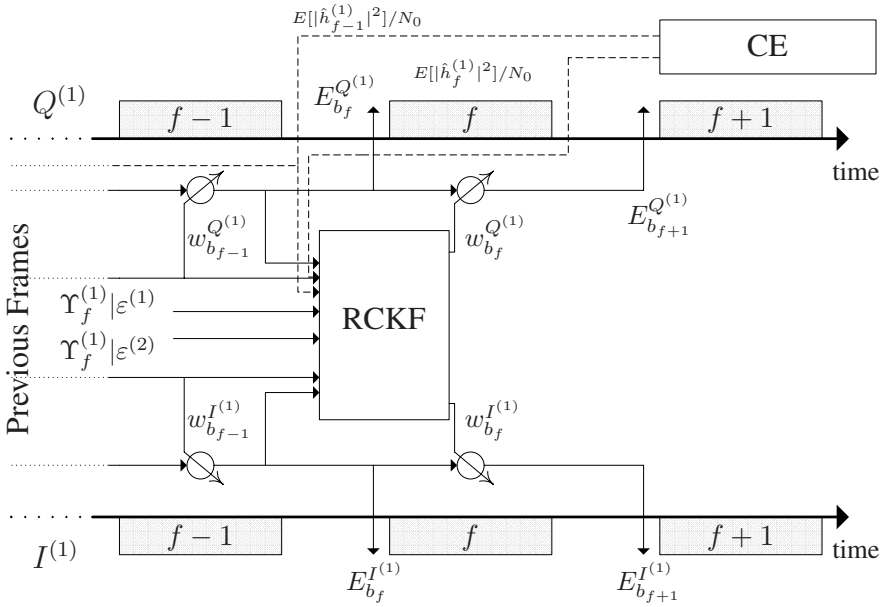

Figure 5.2: Block diagram of the proposed scheme at subscriber-1 showing power allocation for the frame $f+1$. CE stands for channel estimator.

Figure 5.2 shows a block diagram of the proposed scheme representing different modeling parameters and power allocation evolution over frames. The parameters cross the time axes in Figure 5.2 to indicate the time instant at which they are received or generated. The BS estimates the CFC and demodulates the received signals. Based on the estimated CFC, the CSI, $E[|\hat{h}_f^{(1)}|^2]/N_0$, can be calculated at the BS and fed back to subscriber-1. The CSI can be sent through a dedicated feedback channel or placed in the header of the next frame after the estimation in the downlink. The accuracy of the CSI depends on the CFC estimation error, averaging window size of CSI, signal processing delays and feedback delays. Therefore, it is imperative to consider CSI estimation inaccuracy in evaluating the weighting factors. Note that the estimate received at the end of the f-th frame (i.e., $E[|\hat{h}_f^{(1)}|^2]/N_0$) was generated from pilot symbols inserted in the

f-th frame (Figure 5.2); thus, it is an estimate of the channel during the f-th frame transmission. With the knowledge of the bit energy that was allocated in the f-th frame, the estimated average SNRs,

$$\bar{\gamma}_f^{I^{(1)}} = \frac{E_{b_f}^{I^{(1)}} E[|\hat{h}_f^{(1)}|^2]}{N_0} \text{ and } \bar{\gamma}_f^{Q^{(1)}} = \frac{E_{b_f}^{Q^{(1)}} E[|\hat{h}_f^{(1)}|^2]}{N_0}, \tag{5.14}$$

can be evaluated. This completes the information required to write the state (i.e., weights vector) prediction equation,

$$\boldsymbol{w}_f = \boldsymbol{\Pi}_{f-1}\boldsymbol{w}_{f-1} + \boldsymbol{\Lambda}_{f-1}\boldsymbol{z}_{f-1}. \tag{5.15}$$

The actual state transition matrix is given by

$$\boldsymbol{\Pi}_{f-1} = \begin{bmatrix} \frac{\bar{\gamma}_{f-1}^{I^{(1)}} + \delta\bar{\gamma}_{f-1}^{I^{(1)}}}{\bar{\gamma}_f^{I^{(1)}} + \delta\bar{\gamma}_f^{I^{(1)}}} & 0 \\ 0 & \frac{\bar{\gamma}_{f-1}^{Q^{(1)}} + \delta\bar{\gamma}_{f-1}^{Q^{(1)}}}{\bar{\gamma}_f^{Q^{(1)}} + \delta\bar{\gamma}_f^{Q^{(1)}}} \end{bmatrix}, \tag{5.16}$$

where $\delta\bar{\gamma}_f^{(1)}$ denotes the estimation error in the SNR, the error distribution is considered to be uniformly distributed in a given range as will be shown later. Incorporating the estimation error in the transition matrix makes the proposed approach resilient to estimation error. The modeling errors are denoted by the vector of Gaussian random variables $\boldsymbol{z}_f = [z_f^{I^{(1)}} \; z_f^{Q^{(1)}}]^T$ with zero mean and known covariance matrix $\boldsymbol{Z}_f$ [123]. $\boldsymbol{\Lambda}_f$ models how the Gaussian modeling errors affect the system; in equation (5.15) $\boldsymbol{\Lambda}_{f-1} = \mathbf{O}$. In this modeling, the weights adapt to channel variation to satisfy the equality constraints which achieve the target SNRs $\boldsymbol{\Upsilon}_f = \left[\Upsilon_f^{(1)}|\varepsilon^{(1)} \; \Upsilon_f^{(1)}|\varepsilon^{(2)}\right]^T$ or $\boldsymbol{\Upsilon}_f = \left[\Upsilon_f^{(1,2)}|\varepsilon^{(1)} \; \Upsilon_f^{(1)}|\varepsilon^{(2)}\right]^T$. As mentioned earlier, the sequence of power allocations (over multiple frames) that maintains an average SNR of $\Upsilon^{(1)}|\varepsilon^{(1)}$ on $I^{(1)}$ is the same sequence that maintains an average SNR of $\Upsilon^{(1,2)}|\varepsilon^{(1)}$ on $I^{(1,2)}$ and vice versa if the condition in (5.12) is satisfied. We choose to allocate power based on the weaker link required SNR, $\Upsilon_f^{(1)}|\varepsilon^{(1)}$, because the inter-subscriber link is always stronger since pairing is performed by the RAU; thus, $\boldsymbol{\Upsilon}_f = \left[\Upsilon_f^{(1)}|\varepsilon^{(1)} \; \Upsilon_f^{(1)}|\varepsilon^{(2)}\right]^T$. These target SNRs are incorporated in the output equation (a.k.a measurement equation) as fixed outputs,

$$\boldsymbol{\Upsilon}_f = \boldsymbol{\Xi}_f\boldsymbol{w}_f + \boldsymbol{v}_f. \tag{5.17}$$

In equation (5.17) the actual output matrix is,

$$\boldsymbol{\Xi}_f = \begin{bmatrix} \bar{\gamma}_f^{I^{(1)}} + \delta\bar{\gamma}_f^{I^{(1)}} & 0 \\ 0 & \bar{\gamma}_f^{Q^{(1)}} + \delta\bar{\gamma}_f^{Q^{(1)}} \end{bmatrix}. \tag{5.18}$$

The output error is modeled by $\boldsymbol{v}_f = [v_f^{I^{(1)}}\ v_f^{Q^{(1)}}]^T$ which is a vector of Gaussian random variables with zero mean and known covariance matrix $\boldsymbol{V}_f$. In conventional Kalman estimation system equations, this output error models the measurement error; however, in this constrained system equation (i.e., equation (5.17)), this error is added with a very small variance to avoid singular[1] matrices [130]. At any frame, $\boldsymbol{v}_f$ and $\boldsymbol{z}_f$ are assumed uncorrelated. It is imperative to stress on the difference between the state-space modeling for conventional Kalman filter and the above modeling. In the above output equation (5.17), the output is a predefined vector (i.e., the target SNRs); whereas in the conventional state-space modeling, the output is a mapped measurement vector of the actual states.

The estimation error is commonly modeled as Gaussian error which is true for Rayleigh channels and AWGN noise. In some practical situations, the estimation error distribution is unknown and can be considered uniformly distributed in a given range [131]. In other words, all values of error are equally probable and centered around zero. Because of the recursive nature of the above system equations (i.e., (5.15) and (5.17)), the uncertainties in the products $\boldsymbol{\Xi}_f\boldsymbol{\Pi}_{f-1}$ and $\boldsymbol{\Xi}_f\boldsymbol{\Lambda}_{f-1}$ are the ones that affect the estimation of $\boldsymbol{w}_f$ rather than the uncertainty in the individual matrices $\boldsymbol{\Pi}_{f-1}$, $\boldsymbol{\Xi}_f$ or $\boldsymbol{\Lambda}_{f-1}$ [125]. Hence, we focus on the uncertainty in the products $\boldsymbol{\Xi}_f\boldsymbol{\Pi}_{f-1}$ and $\boldsymbol{\Xi}_f\boldsymbol{\Lambda}_{f-1}$ which can be written as

$$[\delta\boldsymbol{\Xi}_f\boldsymbol{\Pi}_{f-1}\ \delta\boldsymbol{\Xi}_f\boldsymbol{\Lambda}_{f-1}] = \mathbf{M}\boldsymbol{\Delta}_f\left[\boldsymbol{\xi}^{\Pi}\boldsymbol{\xi}^{\Lambda}\right]. \tag{5.19}$$

$\boldsymbol{\Delta}_f$ is a diagonal matrix of arbitrary and unknown contractions $|\Delta_f^{(1)}| \leq 1$. $\mathbf{M}$, $\boldsymbol{\xi}^{\Pi}$ and $\boldsymbol{\xi}^{\Lambda}$ are perturbation modeling parameters that are known and given by

$$\mathbf{M} = \begin{bmatrix} M^{(1)} & 0 \\ 0 & M^{(1)} \end{bmatrix},\ \ \boldsymbol{\xi}^{\Pi} = \boldsymbol{\xi}^{\Lambda} = \begin{bmatrix} \xi^{(1)} & 0 \\ 0 & \xi^{(1)} \end{bmatrix}. \tag{5.20}$$

[1] A singular matrix is a square matrix that does not have an inverse.

These constant parameters model how matrices $\boldsymbol{\Xi}_f\boldsymbol{\Pi}_{f-1}$ and $\boldsymbol{\Xi}_f\boldsymbol{\Lambda}_{f-1}$ are affected by the contractions and they may vary from one channel estimation algorithm to the other. Such perturbation modeling is common for uncertain systems [122, 132].

Equations (5.15) and (5.17) form a state-space description of a discrete and linear-time-varying (LTV) system. The matrices $\delta\boldsymbol{\Xi}_f\boldsymbol{\Pi}_{f-1}$ and $\delta\boldsymbol{\Xi}_f\boldsymbol{\Lambda}_{f-1}$ capture the uncertainties of the SNR while the output equation (5.17) constrains the output to the target SNRs. The uncertainty in the system matrices and the constraints incorporated in the output equation call for adopting a robust [125, 133, 134] and constrained [130] Kalman filtering technique in order to estimate the weights vector, $\boldsymbol{w}_f$. In the sequel, a constrained version of the robust Kalman filter ([125], Table I) is applied in the context of power allocation for cooperative networks with inaccurate CSI. Each of the subscribers forms the estimate of the average SNR, $\breve{\boldsymbol{\Xi}}_f = \text{diag}([\bar{\gamma}_f^{I^{(1)}}\ \bar{\gamma}_f^{Q^{(1)}}])$ which is an inaccurate version of $\boldsymbol{\Xi}_f$. With the previous frame's SNR, $\breve{\boldsymbol{\Xi}}_{f-1}$, the inaccurate prediction matrix $\breve{\boldsymbol{\Pi}}_f$ can be formed because $\boldsymbol{\Pi}_f = \boldsymbol{\Xi}_{f-1}\boldsymbol{\Xi}_f^{-1}$ as modeled in equation (5.16). Let $\boldsymbol{\Omega}$ denote the estimation error covariance matrix. Let $\hat{\boldsymbol{w}}_f$ be the optimal linear mean square *predicted* estimate of $\boldsymbol{w}_f$ with the knowledge of $\breve{\boldsymbol{\Pi}}_0, \cdots, \breve{\boldsymbol{\Pi}}_{f-1}$ and $\breve{\boldsymbol{\Xi}}_0, \cdots, \breve{\boldsymbol{\Xi}}_{f-1}$. Also, let $\hat{\boldsymbol{w}}_{f|f}$ be the optimal linear means square *filtered* estimate of $\boldsymbol{w}_f$ given $\breve{\boldsymbol{\Pi}}_0, \cdots, \breve{\boldsymbol{\Pi}}_f$ and $\breve{\boldsymbol{\Xi}}_0, \cdots, \breve{\boldsymbol{\Xi}}_f$. The same notation is applied to other matrices involved in estimation.

The pseudocode of the proposed robust and constrained Kalman filtering (RCKF) power allocation scheme is presented in Algorithm 2. The Algorithm generates the source and relay power allocation for given inputs which are the imperfect CSI, range of estimation error and target SNRs. In The subscriber index i is dropped in the pseudocode for notational brevity. After initialization, the covariance matrices and the prediction equation matrices are corrected to account for the estimation error (lines 4 to 12). The vector of correction parameters, $\hat{\boldsymbol{\lambda}}$, is fine tuned by varying ϱ. The $\hat{\boldsymbol{w}}_{f-1|f-1}$ and $\boldsymbol{\Omega}_{f-1|f-1}$ update phase corresponds to a constrained Kalman filter in which the output $\boldsymbol{\Upsilon}_f$ of the output equation is the target SNRs (line 15). The target SNRs, $\boldsymbol{\Upsilon}_f$, changes if any of the cooperating subscribers changes its required BEP or the ratio of the average channel gains on the broadcast channels is changed, otherwise, it is fixed. Once the

Algorithm 2 RCKF Power Allocation Scheme

1. *Initialization*
2. Initialize $\hat{\boldsymbol{w}}_{0|0}$
3. Initialize $\hat{\boldsymbol{\Omega}}_{0|0}$
4. *Correction argument evaluation*
5. $\hat{\boldsymbol{\lambda}} = (1+\varrho)||\mathbf{M}^T\boldsymbol{V}^{-1}\mathbf{M}||$
6. **while** frames available **do**
7. *Parameters correction to account for estimation error*
8. $\hat{\boldsymbol{Z}}_{f-1}^{-1} = \boldsymbol{Z}_{f-1}^{-1} + \hat{\boldsymbol{\lambda}}\boldsymbol{\xi}^{\Lambda^T}\left[\mathbf{O} + \hat{\boldsymbol{\lambda}}\,\boldsymbol{\xi}^{\Xi}\,\boldsymbol{\Omega}_{f-1|f-1}\,\boldsymbol{\xi}^{\Pi^T}\right]^{-1}\boldsymbol{\xi}^{\Lambda}$
9. $\hat{\boldsymbol{V}}_f = \boldsymbol{V}_f - \hat{\boldsymbol{\lambda}}^{-1}\mathbf{M}\mathbf{M}^T$
10. $\hat{\boldsymbol{\Omega}}_{f-1|f-1} = \left[\boldsymbol{\Omega}_{f-1|f-1}^{-1} + \hat{\boldsymbol{\lambda}}^{-1}\boldsymbol{\xi}^{\Pi^T}\boldsymbol{\xi}^{\Pi}\right]^{-1}$
11. $\hat{\boldsymbol{\Lambda}}_{f-1} = \boldsymbol{\Lambda}_{f-1} - \hat{\boldsymbol{\lambda}}\breve{\boldsymbol{\Pi}}_{f-1}\hat{\boldsymbol{\Omega}}_{f-1|f-1}\boldsymbol{\xi}^{\Pi^T}\boldsymbol{\xi}^{\Xi}$
12. $\hat{\boldsymbol{\Pi}}_{f-1} = \left(\breve{\boldsymbol{\Pi}}_{f-1} - \hat{\boldsymbol{\lambda}}\hat{\boldsymbol{\Lambda}}_{f-1}\hat{\boldsymbol{Z}}_{f-1}\boldsymbol{\xi}^{\Xi^T}\boldsymbol{\xi}^{\Pi}\right) \times \left(\mathbf{O} - \hat{\boldsymbol{\lambda}}\,\hat{\boldsymbol{\Omega}}_{f-1|f-1}\,\boldsymbol{\xi}^{\Pi^T}\boldsymbol{\xi}^{\Pi}\right)$
13. *Update $\hat{\boldsymbol{w}}_{f-1|f-1}$ and $\boldsymbol{\Omega}_{f-1|f-1}$*
14. $\hat{\boldsymbol{w}}_f = \hat{\boldsymbol{\Pi}}_{f-1}\hat{\boldsymbol{w}}_{f-1|f-1}$
15. $\boldsymbol{\Theta}_f = \boldsymbol{\Upsilon}_f - \breve{\boldsymbol{\Xi}}_f\hat{\boldsymbol{w}}_f$
16. $\boldsymbol{\Omega}_f = \breve{\boldsymbol{\Pi}}_{f-1}\hat{\boldsymbol{\Omega}}_{f-1|f-1}\breve{\boldsymbol{\Pi}}_{f-1}^T + \hat{\boldsymbol{\Lambda}}_{f-1}\hat{\boldsymbol{Z}}_{f-1}\hat{\boldsymbol{\Lambda}}_{f-1}^T$
17. $\boldsymbol{\Psi}_f^{-1} = \hat{\boldsymbol{V}}_f + \breve{\boldsymbol{\Xi}}_f\boldsymbol{\Omega}_f\breve{\boldsymbol{\Xi}}_f^T$
18. $\boldsymbol{\Omega}_{f|f} = \boldsymbol{\Omega}_f - \boldsymbol{\Omega}_f\breve{\boldsymbol{\Xi}}_f^T\boldsymbol{\Psi}_f^{-1}\breve{\boldsymbol{\Xi}}_f\boldsymbol{\Omega}_f$
19. $\hat{\boldsymbol{w}}_{f|f} = \hat{\boldsymbol{w}}_f + \boldsymbol{\Omega}_{f|f}\breve{\boldsymbol{\Xi}}_f^T\hat{\boldsymbol{V}}_f^{-1}\boldsymbol{\Theta}_f$
20. *Next frame power allocation*
21. $\boldsymbol{E}_{b_{f+1}} = \text{diag}\left(\boldsymbol{E}_{b_f}\right)\hat{\boldsymbol{w}}_{f|f}$
22. **end while**

estimate of the weights vector (i.e., $\hat{\boldsymbol{w}}_{f|f}$) is evaluated in line 19, the bit energy for the $(f+1)$th frame is allocated in line 21 following equation (5.13). Whereas the above presentation is focused on power allocation for subscriber-1, power is also allocated at subscriber-2 using the same approach.

5.2.1 Summary of the Proposed Scheme

Figure 5.3 is a flow chart representation of the proposed scheme. Operations with solid, dashed, dotted border are carried out at the BS subscriber-2 and subscriber-1, respectively. Rec. and CE stand for receive and channel estimator, respectively. The proposed scheme is semi-distributed in the sense that operations are carried out at both cooperating subscribers and the BS. At the beginning of the communication session, the BS receives the required BEP of both subscribers. Channel estimation for subscriber-i-to-BS $i \in \{1,2\}$ and subscriber-1-to-subscriber-2 channels is performed in every frame, respectively at the BS, and subscriber-2; the latter reports the estimates to the BS. The BS updates the ratio $\overline{h}^{(i)}/\overline{h}^{(1,2)}$ $i \in \{1,2\}$ and search the lookup tables for the target SNRs only if the average channel gain ratio is changed or the BEP requirements are changed. Each of the subscribers receives the target SNRs and channel estimate. The allocated bit energy is stored to be used to form the transition matrices for the next frame. Based on the received parameters, the proposed RCKF power allocation scheme allocates the bit energy of the next frame as shown in Figure 5.2. The execution of these operations continues until the communication session is terminated.

5.3 Simulation Results

In this section, simulation results are provided to demonstrate the performance of the proposed scheme in terms of achieving the optimal power allocation, robustness to channel estimation error and adaptive responsiveness to changes in the BEP requirements.

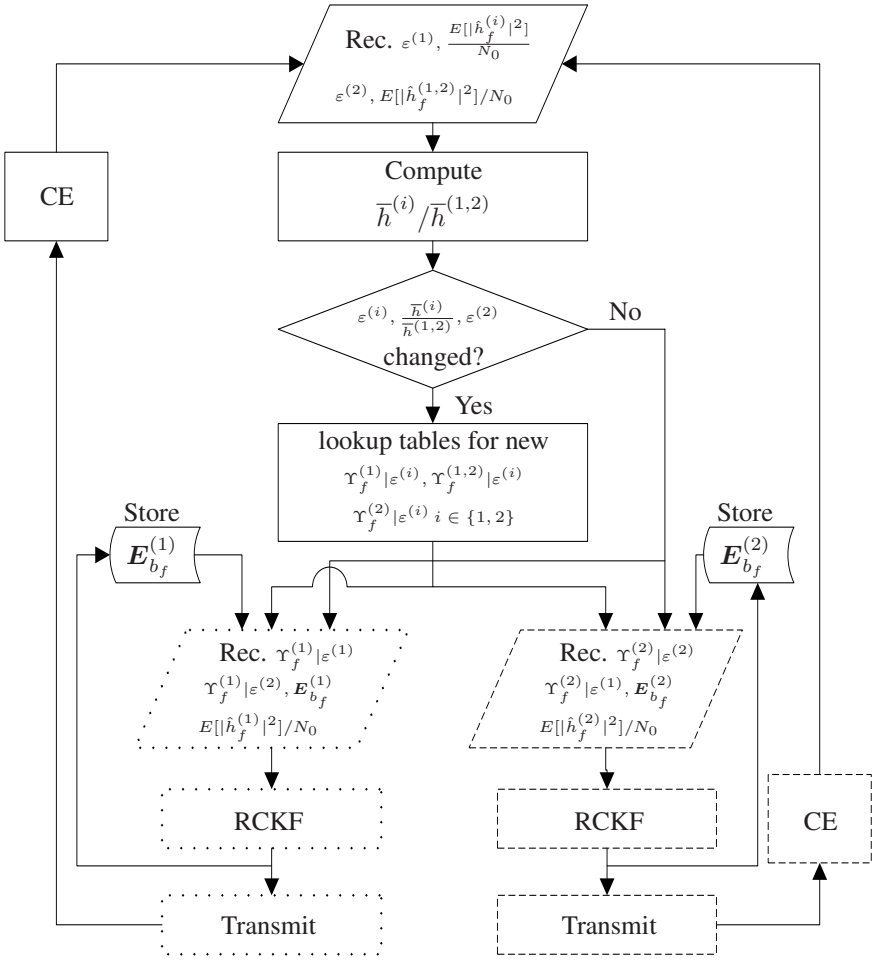

Figure 5.3: General flow chart of the proposed scheme. Operations with solid, dashed, dotted border are carried out at the BS subscriber-2 and subscriber-1, respectively. Rec. and CE stand for receive and channel estimator, respectively.

Consider a network consisting of a base station and two subscribers forming a cooperating pair. The transmission from both subscribers are experiencing frequency flat fading. The subscribers receive their channels CSI and the target SNRs to be satisfied from the BS. Note that the CSI reporting frequency and, hence, the frequency of power allocation depend on how fast is the channel varying. We consider the worst case scenario where a CSI is required for power allocation in each frame. Therefore, the prediction

matrix $\mathbf{\Pi}_f$ and output matrix $\mathbf{\Xi}_f$ vary from one frame to the other for both subscribers. Because channel estimation is carried out at the same base station for subscriber-i-to-BS, $i \in \{1, 2\}$ channels, the SNR perturbation models for these channels are considered to have equal parameters that are given by

$$\mathbf{M} = \begin{bmatrix} 0.06 & 0 \\ 0 & 0.06 \end{bmatrix}, \quad \boldsymbol{\xi}^{\Pi} = \boldsymbol{\xi}^{\Lambda} = \begin{bmatrix} 0.5 & 0 \\ 0 & 0.5 \end{bmatrix}, \tag{5.21}$$

and random contractions $\Delta^{(i)}$ for $i \in \{1, 2\}$ generated uniformly in the interval [-1,1] in each frame. This perturbation model corresponds to a perturbation error equivalent to $\delta\bar{\gamma}_f^{I^{(i)}} = 0.03\Delta^{(i)}$ for $i \in \{1, 2\}$ and $\delta\bar{\gamma}_f^{Q^{(i)}} = 0.03\Delta^{(i)}$ for $i \in \{1, 2\}$. In the following we focus on power allocation related to subscriber-1. In other words, we study the performance of the proposed scheme on all channels assigned to subscriber-1 (i.e., $I^{(1)}$, $I^{(2)}$ and $I^{(1,2)}$) that contribute to the evaluation of subscriber-1's BEP. Power allocation on $I^{(1)}$ and $I^{(1,2)}$ is performed by subscriber-1 and on $I^{(2)}$ by subscriber-2 (Figure 5.1).

Subscriber-1 is considered to have an average BEP requirement of $\varepsilon^{(1)} = 10^{-3}$ and average channel gain ratio of $\frac{\overline{h}^{(1)}}{\overline{h}^{(1,2)}} = 0.5428$. The target SNRs in dB that correspond to the required BEP and average channel gain ratio are $\Upsilon_f^{(1)}|\varepsilon^{(1)} = 13.57$, $\Upsilon_f^{(1,2)}|\varepsilon^{(1)} = 25$, $\Upsilon_f^{(2)}|\varepsilon^{(1)} = 16.53$. The evaluated target SNRs satisfy the condition given in equation (5.12) and satisfy the target BEP$= 10^{-3}$.

Figure 5.4 compares the average SNRs on channels allocated to subscriber-1 that are maintained by the RCKF and constrained Kalman filter (CKF) power allocation schemes. The major difference between RCKF and CKF is that the latter considers the received CSI estimated to be accurate and skips lines 4 to 12 in Algorithm 2. It can be seen from Figure 5.4 that the proposed RCKF power allocation scheme converges to the target SNRs (i.e., the allocated power converges to the optimum). Average SNRs on $I^{(1)}$ and $I^{(2)}$ converges faster than that on $I^{(1,2)}$ because power on the former is allocated based on the received estimate of the subscriber-i-BS, $i \in \{1, 2\}$ channels while on the latter, the allocated power is set equal to that allocated on $I^{(1)}$ since $I^{(1)}$ and $I^{(1,2)}$ are the broadcast channels. This supports our theocratical claim in Appendix B that power allocations that maintain an average SNR of $\Upsilon_f^{(1)}|\varepsilon^{(1)}$ on $I^{(1)}$ also maintains an average SNR of $\Upsilon_f^{(1,2)}|\varepsilon^{(1)}$

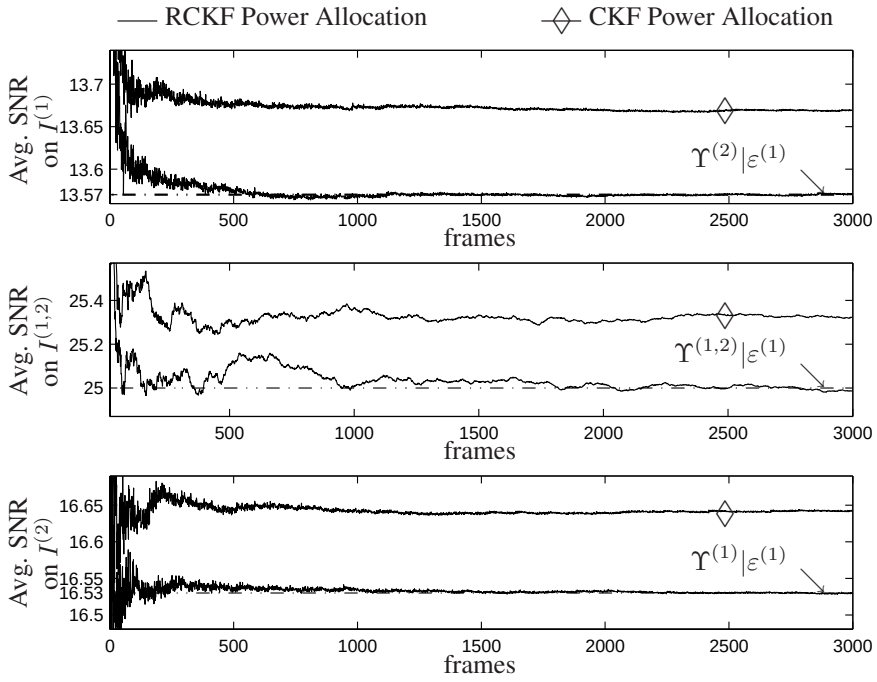

Figure 5.4: Average SNR on channels $I^{(1)}$, $I^{(1,2)}$ and $I^{(2)}$ that are allocated to subscriber-1

on $I^{(1,2)}$ if and only if $\frac{\Upsilon^{(1)}|_{\varepsilon^{(1)}}}{\Upsilon^{(1,2)}|_{\varepsilon^{(1)}}}$ equals $\frac{\overline{h}^{(1)}}{\overline{h}^{(1,2)}}$. The rapid fluctuations around the target SNRs results from the high variation of a channel with a Doppler frequency of 30 Hz. Maintaining the target SNRs achieves the optimum average BEP ($\varepsilon^{(1)} = 10^{-3}$) as can be seen from Figure 5.5. It is also shown in Figure 5.4 that ignoring CSI inaccuracy as in CKF results in supporting higher SNRs than the optimum ones (i.e., target SNRs) and hence supporting a BEP that is less than the optimum as shown in Figure 5.5. Schemes that ignore CSI inaccuracy waste battery power of both subscribers. Starting with an initial SNR that is higher than the target SNR at subscriber-1 results in an initializing BEP that is lower than the required BEP (Figure 5.5).

Figures 5.6 and 5.7 shows performance of the proposed scheme over 300 experiments in comparison with CKF. Each point in Figure 5.6 is an average of the achieved BEP deviation from the required BEP (i.e., $\varepsilon^{(1)} = 10^{-3}$) at the f-th frame over 300 experiments.

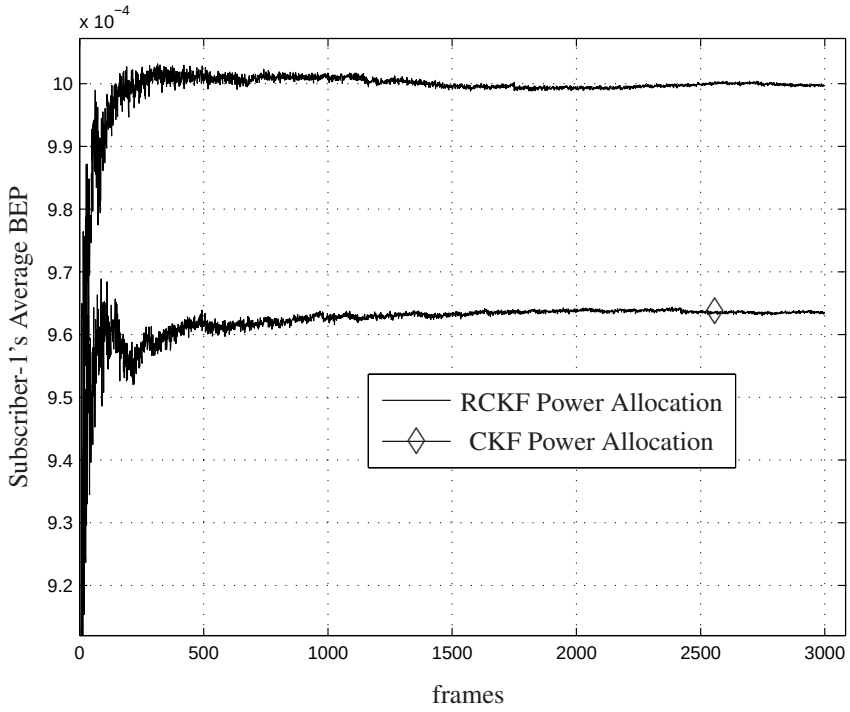

Figure 5.5: Average BEP of subscriber-1.

It is shown that after 200 frames, the proposed scheme shows an average error less than 0.5×10^{-5} which approaches zero after 1500 frames. On the other hand, CKF power allocation shows an error average that is about 3.6×10^{-5}. The proposed scheme not only outperform CKF in achieving the optimum BEP with zero error average but also with the minimum error variance as shown in Figure 5.7.

Whereas previous simulations results focused on demonstrating robustness of the proposed scheme to CSI inaccuracy, Figure 5.8 shows adaptive responsiveness of the proposed scheme to a change in the required BEP. Consider a change of subscriber-1's required BEP from $\varepsilon^{(1)} = 10^{-3}$ to $\varepsilon^{(1)} = 10^{-4}$ in the last 250 frames. In the 2750th frame, the base station computes the new target SNRs and reports them to the subscribers. Both subscribers adjust power weights to support the new BEP requirements only in 2 frames, as shown in Figure 5.8. Lower fluctuations are observed for frames beyond the 2750th frame; this is explained as follows: the BEP curves has higher slope at high SNR than at

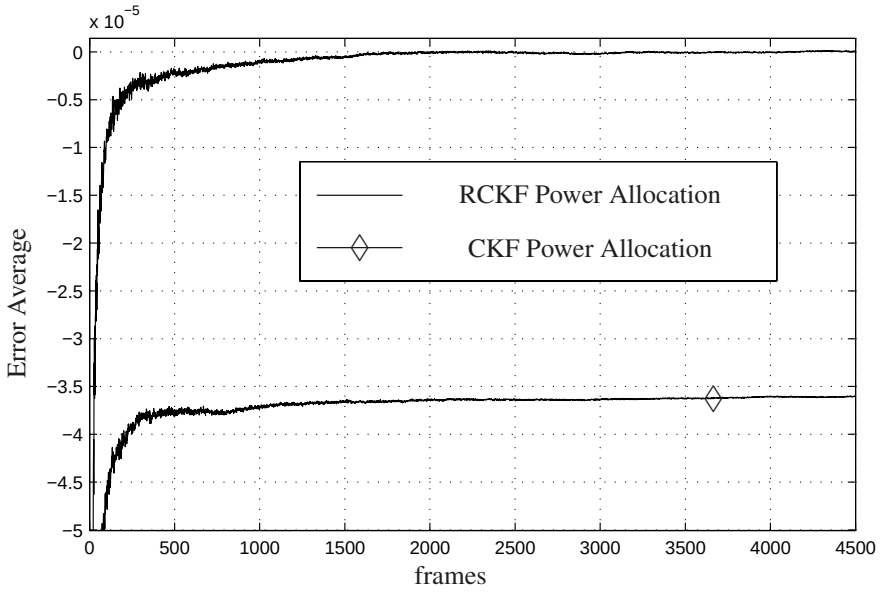

Figure 5.6: RCKF and CKF power allocation error average over 300 experiments.

low SNR; thus, the fluctuation at high SNR required for $\varepsilon^{(1)} = 10^{-4}$ results in low BEP fluctuation and the opposite is true for low SNR which is required for $\varepsilon^{(1)} = 10^{-3}$.

The simulation results demonstrate that the algorithm converges closely to the target SNRs in frames transmitted after the 1500-th frame for a Doppler frequency of 30 Hz, faster convergence can be shown for lower Doppler frequencies. The proposed scheme achieves the optimum while transmitting and adapting to channel variation because of its recursive nature which distinguishes it from other schemes. Schemes that allocate power only after convergence is reached at which the actual SNR is changed due to channel variation and the obtained solution is obsolete. On the other hand, the proposed RCKF allocates power for each frame (i.e., lines 7 to 21) and improves the solution over frames. Operations in lines 7 to 21 are all arithmetic and simple to perform for 2 by 2 matrices. Although, matrix inversion is considered to be computationally expensive [119], in the proposed scheme it is very efficient because inverted matrices are diagonal and their inverses are the reciprocals of the diagonal elements; thus, a matrix inversion is replaced by two element by element divisions. Similarly, matrices multiplication is replaces by

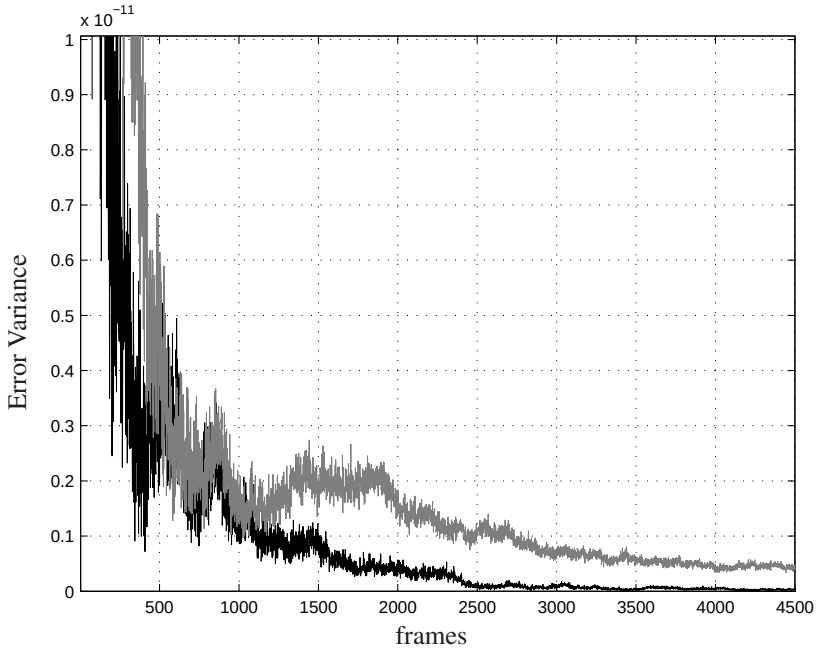

Figure 5.7: RCKF (black) and CKF (gray) power allocation error variance over 300 experiments.

two element by element multiplications because the matrices are diagonal of size 2 by 2.

In summary, simulation results and discussions suggest that the proposed scheme maintains the target SNRs despite of the CSI inaccuracy and allocates power for each frame with low computational complexity in addition to its fast responsiveness to changes in BEP requirements.

5.4 Summary

We have developed a robust and constrained Kalman filtering power allocation scheme for CD networks. The scheme is channel adaptive, minimizes allocated power that maintains target SNRs and satisfies subscribers' BEP requirements. It is robust to channel estimation error and is of low complexity and fast responsiveness; thus, the scheme is

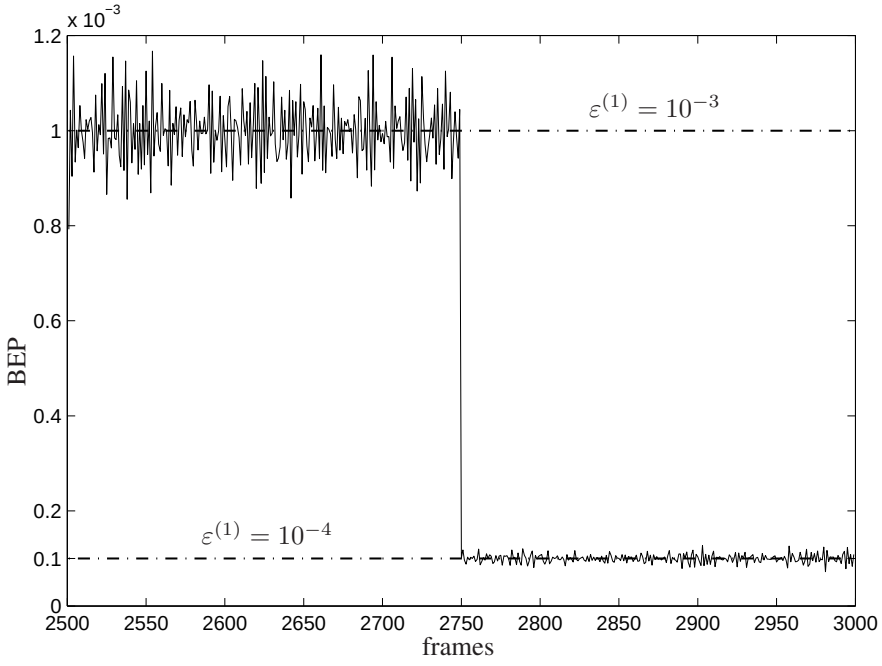

Figure 5.8: BEP of subscriber-1 over 2500 to 3000 frames where the BEP requirement is reduced from $\varepsilon^{(1)} = 10^{-3}$ to $\varepsilon^{(1)} = 10^{-4}$

practical for real networks implementations. Simulations results support our theoretical claim that the proposed scheme maintains the target SNRs on the subscribers-to-BS and inter-subscriber channels simultaneously. The proposed scheme performance has been compared with that of CKF power allocation schemes that ignore CSI inaccuracy. In particular, it has been shown that the proposed scheme, RCKF, out performs CKF in allocating the minimum power and satisfying BEP requirements with zero error average and error variance relative to the optimum. Our future research is to consider satisfying more QoS requirements besides average BEP. In addition, in our future work, we plan to implement the proposed scheme in embedded systems evaluation software to obtain insights on its performance in embedded systems.

Chapter 6

Conclusions and Further Works

6.1 Conclusions

Fast and cost effective deployment in addition to reliability in supporting multiple services are features that make service provides favour BWA networks. Last mile wireless access networks provide the last link connectivity between a wired point of presence and wireless subscribers who may reside in areas with different terrain profiles (i.e., urban, suburban, rural) and hence experience different channel impairments. The major challenges include these wireless channel impairments, scarce resources, multiple services with diverse QoS requirements, limited computational power, and inaccuracy of CSI, all of which motivate the development of practical resource allocation schemes to best utilize network resources while satisfying the network constraints.

In this thesis, we have investigated the effect of CSI inaccuracy on the performance of BWA networks and presented practical resource allocation schemes for different possible implementation scenarios of these networks. Our major objective is to develop practical resource allocation schemes for various transmission technologies employed by BWA networks, taking into consideration practical implementation challenges. The developed

schemes are practical in the sense that they consider CSI inaccuracy and require low computational power in addition to satisfying multiple services' QoS requirements and employed technologies' constraints.

One of the major practical issues we address is the inaccuracy of CSI estimates. It is intuitive that CSI inaccuracy affects the performance of BWA networks; however, a quantitative measure of this effect is required for the development of resource allocation schemes. We first develop an approach to the evaluation of ergodic mutual information. The considered system model captures the characteristics of OFDMA and SDF; thus, results can be applied to single carrier and direct transmission since they are special cases of OFDMA and SDF, respectively. The CSI inaccuracy was modeled as an additive circularly symmetric complex Gaussian random variable, which makes the deterministic CSI received by the RAU a random variable. Based on the statistical properties of the CSI on the source-to-relay, relay-to-destination and source-to-destination, the ergodic mutual information of the SDF scheme was evaluated. Numerical evaluations show that a substantial gain can be achieved by considering CSI inaccuracy. In addition, simulations show that with the knowledge of CSI inaccuracy statistics, channel adaptive schemes can achieve an ergodic mutual information, if the developed approach is adopted, close to the one attained if the perfect CSI is available .

The above-mentioned approach was used in power allocation for PMP OFDMA-based networks. Then, the resource allocation problem for PMP OFDMA-based networks was modeled as a NUM one and was shown to be $\mathcal{NP}$-complete. Multiple services were assumed to be supported which requires capacity portioning by the CAC. The aggregate rate allocated to each service was constrained by its capacity partition specified by the CAC. The developed resource allocation scheme was based on the dual decomposition approach; the problem was decomposed into a hierarchy of subproblems that are easier to solve. The complexity of the algorithm was shown to be low via complexity analysis. Numerical evaluations demonstrating the developed scheme performance in satisfying network constraints and accounting for CSI inaccuracy were presented.

Finally, another implementation scenario of BWA networks was considered: the

single carrier cooperative implementation scenario of BWA networks. The developed scheme allocates power for sources and relays that are employing a quadrature signaling cooperative scheme. The power allocation process was represented by an uncertain system in which uncertainty models the CSI inaccuracy. In addition, the proposed scheme maintains the target SNR on both broadcast channels (i.e., source-to-relay and relay-to-destination) which provides stronger guarantees on the maintained BEP. The uncertainty in the system and constraints imposed on the output equation to maintain target SNRs require the adoption of a robust and constrained Kalman filter to estimate the power allocation weights. Because it is designed based on a Kalman filter, the proposed scheme enjoys the low complexity and fast responsiveness of Kalman filter. Numerical evaluations demonstrate the proposed scheme's robustness to CSI estimation inaccuracy, responsiveness to changes in required BEP, and optimality in allocating power.

6.2 Further Works

The developed resource allocation schemes address a number of practical implementation issues of BWA access networks. There are still other implementation issues that are needed to be considered. The following are potential future research directions:

- The proposed schemes are based on the assumption that subscribers' channels are independent which is a common assumption in the literature [21, 24, 35, 38–57]. However, in relay scenarios, relay stations cover smaller areas than the base station; thus, subscribers supported by the same relay station may be closely located and may have correlated channels. Under such conditions, optimizing for resource allocation is meaningless because allocating a subcarrier to any subscribers with highly correlated channels performs the same. Hence, for subscriber with highly correlated channels, multiuser diversity cannot be exploited, and resource allocation gain over random assignment is negligible. This observation rises the following questions: Is the resource allocation gain worth the required computational

complexity ? For what value of correlation is the resource allocation gain over random assignment significant? These questions form an interesting direction for future research.

- The research presented in this thesis focuses on common implementation scenarios of BWA networks, specifically, a multicarrier (i.e., OFDMA) and direct (i.e., PMP) scenario in Chapter 4, and single carrier and cooperative in Chapter 5. A scenario not considered in this thesis is the OFDMA-based cooperative BWA, which should be of interest to service providers because it combats both large scale and small scale fading. Our work reported in [7] considers this implementation scenario, but it was not included in this thesis because it was developed based on the assumption that the CSI estimation is accurately known. Extending this work to consider CSI inaccuracy is one of our future projects.

- Research reported in Chapter 4 focuses on fairness among supported services and overlooks the importance of maintaining fairness among subscribers. We propose an opportunistic fair scheduling scheme in [15] for PMP scenarios that maintains fairness among subscribers. Our future plan is to extend this work to consider cooperative communication.

- The scheme proposed in Chapter 4 considers concave utility functions. However, subscribers may also have non-concave utility functions, say a step utility function that is not differentiable. In the future, the proposed scheme can be extended to cover other possible utility functions.

- The power allocation scheme presented in Chapter 5 is developed based Kalman filter that is widely accepted to be practical and implementable in embedded systems. It is our intention to investigate the performance of this scheme in embedded systems evaluation software like Labview[1] to obtain insights on its performance in real networks. Metrics such as running time in real time can be evaluated.

[1] http://www.ni.com/

Appendices

Appendix A

Mapping to d-MKP problem and $\mathcal{NP}$-completeness

Mapping our resource allocation problem to multi-dimension multi-choice Knapsack problem (d-MKP) which is a variation of a well known Knapsack problem (KP) proves that our problem is $\mathcal{NP}$-complete, because d-MKP is $\mathcal{NP}$-complete [135]. Similar general approaches can be found in [136] and [137].

The d-MKP problem is the problem of selecting one item from each group of items to pack in a knapsack (i.e., bag) such that the total value of packed items is maximized without exceeding the *dimensions* of the knapsack. Each group of items contains *variants* of the same type of items. For example, give a group of cellphones and group of laptops, each of the items has a dollar value, size and weight. The problem is to select one item form reach group, such that the dollar value of items in the bag is maximized and the *dimensions* (i.e., weight and size) of the bag are not exceeded. Note that Multi-choice refers to the cellphones and laptops groups. *Variants* refer to the different cellphones within a group (e.g. Motorola, Blackberry etc). The multi-*dimensions* refer to weight and size. In the following, the resource allocation problem of OFDMA-based networks modeled by (4.19) to (4.23) is mapped to the d-MKP problem.

The utility of subscriber, s, was denoted by $U^s(\overline{r}^s)$, where $\overline{r}^s$ is its the expected rate given by

$$\overline{r}^s = \sum_{n \in \mathcal{N}_s} E\left[r_n^s\right]. \tag{A.1}$$

Equation A.1 can be written as:

$$\overline{r}^s = \overrightarrow{E\left[r_n^s\right]} \left(\mathbf{w}^s\right)^T \ \ \forall s, \tag{A.2}$$

where $\overrightarrow{E\left[r_n^s\right]}$ is a vector of expected rates on subcarriers allocated to sTh subscriber. The subcarriers assignment is expressed by the N_{sc}- *dimensional* vector $\mathbf{w}^s$ that its elements:

$$\left[\mathbf{w}^s\right]_n = \left\{ \begin{array}{ll} 1 & \text{The } n\text{th subcarrier assigned to the } s \text{ subscriber} \\ 0 & \text{otherwise} \end{array} \right\} \ \forall n. \tag{A.3}$$

There are $2^{N_{sc}}$ possible subcarrier allocations for each subscriber and each allocation results in a specific expected rate. These different possible allocation are considered variants of the sth subscriber; thus, each subscriber is represented of a group of variants with expected rate $\overline{r}^{sv}$ and allocation vector for each variant $\mathbf{w}^{sv}$. Denote the group of variants of the sth subscriber by $\mathcal{G}^s$.

In OFDMA-based networks, each subcarrier of the total N_{sc} subcarriers is exclusively allocated to one subscriber which is modeled by the constraint in (4.21). In s-MKP, this constraint is represented by N_{sc} *dimensions* of the knapsack and each *dimensions* has maximum length of 1.

To summarize;

- Subscribers are represented by non-overlapping groups $\mathcal{G}^s \ \ \forall s = 1, \cdots, S$.
- Each group contains variants s^v of subscriber s. The vth variant has the *value* $U^s(\overline{r}^s)$ (i.e., expected rate) and the N- *dimensional* vector $\mathbf{w}^{sv}$ (i.e. subcarrier assignment). Note that $\left[\mathbf{w}^{av}\right]_n \in \{0, 1\}$.
- The maximum length on each *dimension* (i.e. subcarrier) is $\left[\mathbf{m}\right]_n = 1$.

Therefore, the resource allocation problem is to select one variant of each group $\mathcal{G}^s$ to maximize the *value* (i.e., sum of utilities) without exceeding the *dimensions* (i.e., subcarriers) of the knapsack (i.e., network). Thus, the resource allocation problem for OFDMA-based networks is d-MKP.

Appendix B

Proof of Maintaining Target Average SNR on the Broadcast Channels

Following the general steady-state analysis approach in [123] and the assumption of constant transition matrices [123, 125] over a window of frames [123, 125], we show that under the condition (5.12) power allocations that maintains $\Upsilon_f^{(1)}|\varepsilon^{(1)}$ on $I^{(1)}$ also maintains $\Upsilon_f^{(1,2)}|\varepsilon^{(1)}$ on $I^{(1,2)}$ at convergence. Let the average SNRs be defined as

$$\tilde{\boldsymbol{\Xi}}_f = \begin{bmatrix} E_{b_f}^{I^{(1)}} \overline{h}^{(1)} & 0 \\ 0 & E_{b_f}^{Q^{(1)}} \overline{h}^{(1)} \end{bmatrix}, \tag{B.1}$$

with the assumption that the average channel gains $\overline{h}^{(1)}$ and $\overline{h}^{(1,2)}$ are fixed over a window of frames. Starting with the substitution of line 15 in line 19 of Algorithm 2 and substituting $\tilde{\boldsymbol{\Xi}}_f$ for $\breve{\boldsymbol{\Xi}}_f$, we get

$$\hat{\boldsymbol{w}}_{f|f} = \hat{\boldsymbol{w}}_f + \boldsymbol{\Omega}_{f|f} \tilde{\boldsymbol{\Xi}}_f^T \hat{\boldsymbol{V}}_f^{-1} \left[\boldsymbol{\Upsilon} - \tilde{\boldsymbol{\Xi}}_f \hat{\boldsymbol{w}}_f \right].$$

At steady state where weights are equal, we can write

$$\hat{\boldsymbol{w}}_{ss} = \hat{\boldsymbol{w}}_{ss} + \boldsymbol{\Omega}_{ss} \tilde{\boldsymbol{\Xi}}_{ss}^T \hat{\boldsymbol{V}}_{ss}^{-1} \boldsymbol{\Upsilon} - \boldsymbol{\Omega}_{ss} \tilde{\boldsymbol{\Xi}}_{ss}^T \hat{\boldsymbol{V}}_{ss}^{-1} \tilde{\boldsymbol{\Xi}}_{ss} \hat{\boldsymbol{w}}_{ss}.$$

After terms rearrangement and cancellation, the above equation reduces to

$$\hat{\boldsymbol{w}}_{ss} = \boldsymbol{\Upsilon}\tilde{\boldsymbol{\Xi}}_{ss}^{-1}.$$

The $[\hat{\boldsymbol{w}}_{ss}]_{1,1}$ element that is related to the broacdcast phase transmission is

$$w_{ss}^{I^{(1)}} = \frac{\Upsilon_f^{(1)}|_{\mathcal{E}^{(1)}}}{E_{b_{ss}}^{I^{(1)}}\overline{h}^{(1)}}. \tag{B.2}$$

By repeating the above inductions but with the parameters related to the inter-subscribers channels, we arrive at

$$w_{ss}^{I^{(1,2)}} = \frac{\Upsilon_f^{(1,2)}|_{\mathcal{E}^{(1)}}}{E_{b_{ss}}^{I^{(1,2)}}\overline{h}^{(1,2)}}. \tag{B.3}$$

Dividing equation (B.2) by (B.3) results in

$$w_{ss}^{I^{(1)}} E_{b_{ss}}^{I^{(1)}} = w_{ss}^{I^{(1,2)}} E_{b_{ss}}^{I^{(1,2)}},$$

because $\frac{\Upsilon^{(1)}|_{\mathcal{E}^{(1)}}}{\Upsilon^{(1,2)}|_{\mathcal{E}^{(1)}}} = \frac{\overline{h}^{(1)}}{\overline{h}^{(1,2)}}$. Hence, power allocation that achieves a target SNR of $\Upsilon^{(1)}|_{\mathcal{E}^{(1)}}$ on $I^{(1)}$, also achieves a target SNR of $\Upsilon^{(1)}|_{\mathcal{E}^{(1)}}$ on $I^{(1,2)}$ at convergence, if and only if $\frac{\Upsilon^{(1)}|_{\mathcal{E}^{(1)}}}{\Upsilon^{(1,2)}|_{\mathcal{E}^{(1)}}} = \frac{\overline{h}^{(1)}}{\overline{h}^{(1,2)}}$. The same applies for subscriber-2 power allocation on its broadcast channels.

References

[1] C. M$\ddot{u}$ller, A. Klein, and F. Wegner, "Coverage extension of WiMAX using multi-hop in a low user density environment," *Frequenz journal of RF-Engineering and Telecommunications*, vol. 61, no. 1, pp. 3–6, 2007.

[2] Z. Abichar, Y. Peng, and J. Chang, "WiMAX: The emergence of wireless broadband," *IEEE IT Professional*, vol. 8, no. 4, pp. 44–48, 2005.

[3] "3rd generation partnership project (3GPP) specifications home page," [Online]. Available: http://www.3gpp.org/specs/specs.htm, 2008.

[4] T. Otsu, I. Okajima, N. Umeda, and Y. Yamao, "Network architecture for mobile communications systems beyond IMT-2000," *IEEE Personal Communications*, vol. 8, no. 5, pp. 31–37, Oct 2001.

[5] M. K. Awad, K. T. Wong, and Z. Li, "An integrated overview of the open literatures empirical data on the indoor radiowave channels delay properties," *IEEE Transactions on Antennas and Propagation*, vol. 56, no. 5, pp. 1451 – 1468, 2008.

[6] J. Laneman, D. Tse, and G. Wornell, "Cooperative diversity in wireless networks: Efficient protocols and outage behavior," *IEEE Transactions on Information Theory*, vol. 50, no. 12, pp. 3062–3080, 2004.

[7] M. K. Awad and X. Shen, "OFDMA based two-hop cooperative relay network resources allocation," in *Proc. IEEE International Conference on Communications (ICC' 08)*, Beijing, China, May 2008.

[8] M. Mehrjoo, M. K. Awad, and X. Shen, *WiMAX Network Planning and Optimization*, ser. Wireless Networks and Mobile Communications Series. CRC Press -Taylor & Francis Group, 2009, ch. Resource Allocation in OFDM-based WiMAX, pp. 113–131.

[9] M. K. Awad, V. Mahinthan, M. Mehrjoo, X. Shen, and J. W. Mark, "Downlink resource allocation for OFDMA-based multiservice networks with imperfect CSI," in *Proc. IEEE International Conference on Communications (ICC' 09)*, Dresden, Germany, May 2009.

[10] M. K. Awad, X. Shen, and B. Zogheib, "Uplink ergodic mutual information of OFDMA two-hop cooperative relay networks based on imperfect CSI," in *Proc. IEEE Global Telecommunications Conference (GLOBECOM' 08)*, New Orleans, LA, Dec. 2008.

[11] M. K. Awad, V. Mahinthan, M. Mehrjoo, X. Shen, and J. W. Mark, "A dual decomposition-based resource allocation for OFDMA networks with imperfect CSI," *IEEE Transactions on Vehicular Technology*, submitted.

[12] M. K. Awad, X. Shen, and B. Zogheib, "Ergodic mutual information of OFDMA-based selection-decode-and-forward cooperative relay networks with imperfect CSI," *Physical Communication*, in press.

[13] M. K. Awad, V. Mahinthan, X. Shen, and J. W. Mark, "Power allocation for cooperative networks with inaccurate CSI: A robust and constrained kalman filter approach," *IEEE Transactions on Wireless Communications*, submitted.

[14] M. Mehrjoo, M. K. Awad, M. Dianati, and X. Shen, "Maintaining fairness using weighting factors in wireless networks," in *Proc. IEEE Global Telecommunications Conference (GLOBECOM' 09)*, Honolulu, Hawaii, Dec. 2009, p. submitted.

[15] ——, "Design of fair weights for heterogeneous traffic scheduling in multichannel wireless networks," *IEEE/ACM Transactions on Networking*, submitted.

[16] M. K. Awad, V. Mahinthan, X. Shen, and J. W. Mark, "Power allocation for M-QAM cooperative diversity networks with inaccurate CSI: A robust and constrained kalman filtering approach," in *Proc. IEEE Global Telecommunications Conference (GLOBECOM' 09)*, 2009.

[17] K. Fazel and S. Kaiser, *Multi-Carrier and Spread Spectrum Systems*. J. Wiley, 2003.

[18] P. Vandenameele, L. Perre, and M. Engels, *Space Division Multiple Access for Wireless Local Area Networks*. Kluwer Academic Publishers, 2002.

[19] J. W. Mark and W. Zhuang, *Wireless Communications and Networking*. Prentice Hall, 2003.

[20] S. Haykin and M. Moher, *Modern Wireless Communications*. Pearson/Prentice Hall, 2005.

[21] H. Liu and G. Li, *OFDM-Based Broadband Wireless Networks: Design and Optimization*. Hobken, New Jersey: Wiley-Interscience, 2005.

[22] W. Tranter *et al.*, *Principles of communication systems simulation with wireless applications*. Prentice Hall Upper Saddle River, NJ, 2004.

[23] S. Hara and R. Prasad, *Multicarrier Techniques for 4G Mobile Communications*. Artech House, 2003.

[24] J. Cai, J. Mark, and X. Shen, "ICI cancellation in OFDM wireless communication systems," *Proc. IEEE Global Telecommunications Conference (GLOBECOM'02)*, 2002.

[25] C. Langton, "Orthogonal Frequency Division multiplex (OFDM) Tutorial," Oct 2007. [Online]. Available: http://www.complextoreal.com/chapters/ofdm2.pdf

[26] A. Carlson *et al.*, *Communication systems*. McGraw-Hill New York, 1986.

[27] R. Pabst, B. Walke, D. Schultz, P. Herhold, H. Yanikomeroglu, S. Mukherjee, H. Viswanathan, M. Lott, W. Zirwas, M. Dohler, H. Aghvami, D. Falconer, and G. Fettweis, "Relay-based deployment concepts for wireless and mobile broadband radio," *IEEE Communications Magazine*, vol. 42, no. 9, pp. 80–89, Sep. 2004.

[28] J. Burbank and W. Kash, "IEEE 802.16 broadband wireless technology and its application to the military problem space," in *Proc. IEEE Military Communications Conference (MILCOM '05)*, 2005.

[29] N. Esseling, B. Walke, and R. Pabst, "Performance evaluation of a fixed relay concept for next generation wireless systems," in *Proc. IEEE International Symposium on Personal, Indoor and Mobile Radio Communications. (PIMRC '04)*, vol. 2, 2004, pp. 744–751.

[30] H. Hu, H. Yanikomeroglu, D. Falconer, and S. Periyalwar, "Range extension without capacity penalty in cellular networks with digital fixed relays," in *Proc. IEEE Global Telecommunications Conference (GLOBECOM'04)*, 2004.

[31] R. Coud*é*, "Radio mobile software," April 2007. [Online]. Available: http://www.cplus.org/rmw/english1.html

[32] Siemens Mobile Communications, "WiMAX technical data," SIEMENS, Tech. Rep. [Online]. Available: http://gigaset.com/shc/0,1935,hq_en_1_123478_rArNrNrNrN,00.html

[33] SIEMENS, "Gigaset SE461 WiMAX modem or router technical data," SIEMENS, Tech. Rep.

[34] T. S. Rappaport, *Wireless Communications Principles and Practice*. Upper Saddle River, New Jersey, USA: Pearson Education International, 2002.

[35] D. Niyato and E. Hossain, "Adaptive fair subcarrier/rate allocation in multirate OFDMA networks: Radio link level queuing performance analysis," *IEEE Transactions on Vehicular Technology*, vol. 55, no. 6, pp. 1897–1907, 2006, 0018-9545.

[36] M. Kaneko and P. Popovski, "Adaptive resource allocation in cellular OFDMA system with multiple relay stations," in *Proc. IEEE Vehicular Technology Conference (VTC' 07-S)*, 2007.

[37] L. Huang, M. Rong, L. Wang, Y. Xue, and E. Schulz, "Resource allocation for OFDMA based relay enhanced cellular networks," in *Proc. IEEE Vehicular Technology Conference (VTC '07-S)*, 2007.

[38] J. Cai, X. Shen, J. W. Mark, and A. S. Alfa, "Resource allocation in wireless relay networks," in *Proc. IEEE Global Telecommunications Conference (GLOBECOM '06)*, 2006.

[39] G. Li and H. Liu, "Resource allocation for OFDMA relay networks," in *Proc. IEEE Asilomar Conference on Signals, Systems and Computers*, 2004.

[40] ——, "Resource allocation for OFDMA relay networks with fairness constraints," *IEEE Journal on Selected Areas in Communications*, vol. 24, no. 11, pp. 2061–2069, 2006.

[41] ——, "On the capacity of broadband relay networks," in *Proc. IEEE Asilomar Conference on Signals, Systems and Computers (ACSSC'04)*, 2004.

[42] T. Ng and W. Yu, "Joint optimization of relay strategies and resource allocations in cooperative cellular networks," *IEEE Journal on Selected Areas in Communications*, vol. 25, no. 2, pp. 328–339, 2007.

[43] S. Jing, Z. Zhao-yang, Q. Pei-liang, and Y. Guan-ding, "Subcarrier and power allocation for OFDMA-based regenerative multi-hop links," in *Proc. IEEE International Conference on Wireless Communications, Networking and Mobile Computing (ICWCNM'05)*, 2005.

[44] J. Boyer, D. Falconer, and H. Yanikomeroglu, "A theoretical characterization of the multihop wireless communications channel with diversity," in *Proc. IEEE Global Telecommunications Conference (GLOBECOM'01)*, 2001.

[45] H. Yanikomeroglu, D. D. Falconer, and V. M. Sreng, "Coverage enhancement through two-hop peer-to-peer relaying in cellular radio networks," *World Wireless Research Forum (WWRF) meeting*, vol. 7, 2002.

[46] M. Dohler, A. Gkelias, and H. Aghvami, "2-hop distributed MIMO communication system," *IEEE Electronics Letters*, vol. 39, no. 18, pp. 1350–1351, 2003.

[47] C. Feng-Seng and C. Kwang-Cheng, "Fair adaptive radio resource allocation of mobile OFDMA," in *Proc. IEEE International Symposium on Personal, Indoor and Mobile Radio Communications (ISPIMRC'06)*, 2006.

[48] J. Yun and M. Kacehrad, "PHY/MAC cross-layer issues in mobile WiMAX," Bechtel Corporation, Tech. Rep. 1, 2006.

[49] D. Galda, H. Rohling, and E. Costa, "On the effects of user mobility on the uplink an OFDMA system," *Proc. IEEE Vehicular Technology Conference (VTC'03-S)*, vol. 2, 2003.

[50] W.-I. Lee, B. G. Lee, K. B. Lee, and S. Bahk, "An OFDMA-based next generation wireless downlink system design with hybrid multiple access and frequency grouping techniques," *Journal of Communications and Networks*, vol. 7, no. 2, pp. 115–125, 2005.

[51] Z. Yuping and S. G. Haggman, "Intercarrier interference self-cancellation scheme for OFDM mobile communication systems," *IEEE Transactions on Communications*, vol. 49, pp. 1185–1191, 2001.

[52] J. Cai, X. Shen, and J. Mark, "Robust channel estimation for OFDM wireless communication systems - an H_∞ approach," *IEEE Transactions on Wireless Communications*, vol. 3, no. 6, pp. 2060–2071, 2004.

[53] ——, "Robust channel estimation for OFDM wireless communication systems - an H_∞ approach," in *Proc. IEEE Vehicular Technology Conference (VTC '02-F)*, 2002.

[54] D. Niyato and E. Hossain, "A novel analytical framework for integrated cross-layer study of call-level and packet-level QoS in wireless mobile multimedia networks," *IEEE Transactions on Mobile Computing*, vol. 6, pp. 322–335, 2007.

[55] ——, "A cooperative game framework for bandwidth allocation in 4G heterogeneous wireless networks," in *Proc. IEEE International Conference on Communications (ICC'06)*, 2006.

[56] ——, "A radio resource management framework for IEEE 802.16-based OFDM/TDD wireless mesh networks," in *Proc. IEEE International Conference on Communications (ICC'06)*, 2006.

[57] C. Wong, R. Cheng, K. Lataief, and R. Murch, "Multiuser OFDM with adaptive subcarrier, bit, and power allocation," *IEEE Journal on Selected Areas in Communications*, vol. 17, no. 10, pp. 1747–1758, 1999.

[58] Y. Yao and G. Giannakis, "Rate-maximizing power allocation in OFDM based on partial channel knowledge," *IEEE Transactions on Wireless Communications*, vol. 4, no. 3, pp. 1073–1083, 2005.

[59] A. Aresti, B. Ninan, and M. Devetsikiotis, "Resource allocation games in connection-oriented networks under imperfect information," *Proc. IEEE International Conference on Communications (ICC'04)*, 2004.

[60] I. Wong and B. Evans, "Optimal OFDMA Subcarrier, Rate, and Power Allocation for Ergodic Rates Maximization with Imperfect Channel Knowledge," in *Proc. IEEE International Conference on Acoustics, Speech and Signal Processing (ICASSP'07)*, 2007.

[61] M. Ergen, S. Coleri, and P. Varaiya, "QoS aware adaptive resource allocation techniques for fair scheduling in OFDMA based broadband wireless access systems," *IEEE Transactions on Broadcasting*, vol. 49, pp. 362–370, 2003.

[62] H. Yaghoobi, "scalable OFDMA physical layer in ieee 802.16 wireless MAN," *Intel Technology Journal*, vol. 8, no. 3, pp. 201–212, 2004.

[63] J. Chen and W. K. Tan, "A novel predictive dynamic channel allocation scheme for improving power saving and mobility in broadband wireless access networks," in *Proc. IEEE Mobile Computing*, vol. 28, Taoyuan, Taiwan, 2005, pp. 160–169.

[64] F.-S. Chu and K.-C. Chen, "Fair adaptive radio resource allocation of mobile OFDMA," in *Proc. IEEE International Symposium on Personal, Indoor and Mobile Radio Communications (ISPIMRC'06)*, 2006.

[65] J. M. Ku, P. K. Kim, S. J. Lee, S. Shin, and C. G. Kang, "On the performance of broadband mobile internet access system," in *Proc. IEEE International Symposium on Wireless Pervasive Computing (ISWPC'06)*, 2006, pp. 1–6.

[66] A. Leke and J. Cioffi, "Impact of imperfect channel knowledge on the performance of multicarrier systems," in *Proc. IEEE Global Telecommunications Conference (GLOBECOM' 98)*, Sydney, NSW, Australia, Aug. 1998.

[67] H. Lichte, S. Valentin, F. Eitzen, M. Stege, C. Unger, and H. Karl, "Integrating multiuser dynamic OFDMA into IEEE 802.11 a and prototyping it on a real-time software-defined radio testbed," in *Proc. Intl. Conf. on Testbeds and Research Infrastructures for the Development of Networks and Communities (TridentCom' 07)*, Orlando, Florida, May 2007.

[68] J. Gross, H. Karl, and A. Wolisz, "On the effect of inband signaling and realistic channel knowledge on dynamic OFDM-FDMA systems," in *Proc. of European Wireless*, Barcelona, Spain, Feb. 2004.

[69] Z. Yi and I. Kim, "Joint optimization of relay-precoders and decoders with partial channel side information in cooperative networks," *IEEE Journal on Selected Areas in Communications*, vol. 25, no. 2, p. 447, 2007.

[70] C. P. Sukumar, R. Merched, and A. Eltawil, "Joint power loading of data and pilots in OFDM using imperfect channel state information at the transmitter," in *Proc. IEEE Global Telecommunications Conference (GLOBECOM' 08)*, New Orleans, LA, Dec. 2008.

[71] F. Brah, L. Vandendorpe, and J. Louveaux, "Constrained resource allocation in OFDMA downlink systems with partial CSIT," in *Proc. IEEE International Conference on Communications (ICC'08)*, Beijing, China, May 2008.

[72] A. Alsawah and I. Fijalkow, "Fair service provision in OFDMA with partial channel-state information," in *IEEE 9th Workshop on Signal Processing Advances in Wireless Communications (SPAWC' 08)*, Recife, Brazil, 2008.

[73] W. Noh, "A distributed resource control for fairness in OFDM systems: english-auction game with imperfect information," in *Proc. IEEE Global Telecommunications Conference (GLOBECOM' 08)*, New Orleans, LA, Dec. 2008.

[74] G. Atia and A. F. Molisch, "Cooperative relaying with imperfect channel state information," in *Proc. IEEE Global Telecommunications Conference (GLOBECOM' 08)*, New Orleans, LA, Dec. 2008.

[75] J. Giese and M. Skoglund, "Space-time constellation design for partial CSI at the receiver," in *Proc. IEEE International Symposium on Information Theory (ISIT' 05)*, Adelaide, SA, 2005, pp. 2213–2217.

[76] D. Love, R. Heath, V. Lau, D. Gesbert, B. Rao, and M. Andrews, "An overview of limited feedback in wireless communication systems," *IEEE Journal on Selected Areas in Communications*, vol. 26, no. 8, pp. 1341–1365, Oct. 2008.

[77] S. Zhou and G. Giannakis, "Optimal transmitter eigen-beamforming and space-time block coding based on channel mean feedback," *IEEE Transactions on Signal Processing*, vol. 50, no. 10, pp. 2599–2613, 2002.

[78] S. Omar, A. Ancora, and D. Slock, "Performance analysis of general pilot-aided linear channel estimation in LTE OFDMA systems with application to simplified MMSE schemes," in *Proc. IEEE 19th International Symposium on Personal, Indoor and Mobile Radio Communications (PIMRC' 2008)*, 2008.

[79] I. C. Wong and B. L. Evans, "OFDMA downlink resource allocation for ergodic capacity maximization with imperfect channel knowledge," in *Proc. IEEE Global Telecommunications Conference (GLOBECOM' 07)*, Washington, DC, Nov. 2007.

[80] P. Xia, S. Zhou, and G. Giannakis, "Adaptive MIMO-OFDM based on partial channel state information," *IEEE Transactions on Signal Processing*, vol. 52, no. 1, pp. 202–213, 2004.

[81] S. Ohno and G. Giannakis, "Capacity maximizing MMSE-optimal pilots for wireless OFDM over frequency-selective block Rayleigh-fading channels," *IEEE Transactions on Information Theory*, vol. 50, no. 9, pp. 2138–2145, 2004.

[82] T. Yoo and A. Goldsmith, "Capacity and power allocation for fading MIMO channels with channel estimation error," *IEEE Transactions on Information Theory*, vol. 52, no. 5, pp. 2203–2214, 2006.

[83] A. Vakili, M. Sharif, and B. Hassibi, "The effect of channel estimation error on the throughput of broadcast channels," in *IEEE International Conference on Acoustics, Speech and Signal Processing (ICASSP06)*, 2006.

[84] L. Musavian, M. Nakhai, M. Dohler, and A. Aghvami, "Effect of channel uncertainty on the mutual information of MIMO fading channels," *IEEE Vehicular Technology Magazine*, vol. 56, no. 5 Part 1, pp. 2798–2806, 2007.

[85] J. Proakis *et al.*, *Digital Communication*. Osborne-McGraw-Hill, 2001.

[86] I. Gradshteĭn, I. Ryzhik, D. Zwillinger, and A. Jeffrey, *Table of Integrals, Series, and Products*. Academic Press, 2007.

[87] G. Arfken, *Mathematical Methods for Physicists*. Academic Press, 1966.

[88] M. Simon, *Probability Distributions Involving Gaussian Random Variables: A Handbook for Engineers and Scientists*. Kluwer Academic Publishers, 2002.

[89] M. Springer, *The Algebra of Random Variables*. J. Wiley & Sons, 1979.

[90] R. G. Laha, "On some properties of the Bessel function distributions," *Bulletin of the Calcutta Mathematical Society*, vol. 46, pp. 59 – 71, 1954.

[91] D. Niyato and E. Hossain, "A Queuing-Theoretic and Optimization-Based Model for Radio Resource Management in IEEE 802.16 Broadband Wireless Networks," *IEEE Transactions on Computers*, vol. 55, no. 11, pp. 1473–1488, 2006.

[92] G. Song, Y. Li, and M. Inc, "Utility-based resource allocation and scheduling in OFDM-based wireless broadband networks," *IEEE Communications Magazine*, vol. 43, no. 12, pp. 127–134, 2005.

[93] B. Rong, Y. Qian, and K. Lu, "Integrated Downlink Resource Management for Multiservice WiMAX Networks," *IEEE Transactions on Mobile Computing*, vol. 6, no. 6, pp. 621–632, Jun. 2007.

[94] C. Y. Ng and C. W. Sung, "Low complexity subcarrier and power allocation for utility maximization in uplink OFDMA systems," *IEEE Transactions on Wireless Communications*, vol. 7, no. 5 Part 1, pp. 1667–1675, 2008.

[95] Y. Xiao, C. Chen, and Y. Wang, "Fair bandwidth allocation for multi-class of adaptive multimediaservices in wireless/mobile networks," in *Proc. IEEE Vehicular Technology (VTC'01-S)*, Rhodes, Greece, May 2001.

[96] S. P. Boyd and L. Vandenberghe, *Convex optimization*. Cambridge University Press, 2004.

[97] D. Palomar and M. Chiang, "A tutorial on decomposition methods for network utility maximization," *IEEE Journal on Selected Areas in Communications*, vol. 24, no. 8, pp. 1439–1451, 2006.

[98] W. Yu and R. Lui, "Dual methods for nonconvex spectrum optimization of multicarrier systems," *IEEE Transactions on Communications*, vol. 54, no. 7, pp. 1310–1322, 2006.

[99] Z. Zhou and B. Vucetic, "Design of adaptive modulation using imperfect CSI in MIMO systems," *Electronics Letters*, vol. 40, no. 17, pp. 1073–1075, 2004.

[100] G. Song and Y. Li, "Adaptive resource allocation based on utility optimization in OFDM," *Proc. IEEE Global Telecommunications Conference (GLOBECOM'03)*, 2003.

[101] X. Zhang, E. Zhou, R. Zhu, S. Liu, and W. Wang, "Adaptive multiuser radio resource allocation for OFDMA systems," in *Proc. IEEE Global Telecommunications Conference (GLOBECOM'05)*, 2005.

[102] A. Goldsmith, *Wireless Communications*. Cambridge University Press, 2005.

[103] A. Lapidoth and S. Moser, "Capacity bounds via duality with applications to multiple-antenna systems on flat-fading channels," *IEEE Transactions on Information Theory*, vol. 49, no. 10, pp. 2426–2467, 2003.

[104] K. Suresh, I. S. Misra, and K. Saha (Roy), "Bandwidth and delay guaranteed call admission control scheme for QOS provisioning in IEEE 802.16e mobile WiMAX," in *Proc. IEEE Global Telecommunications Conference (GLOBECOM' 08)*, 2008.

[105] N. Z. Shor, *Minimization Methods for Non-Differentiable Functions*. Springer-Verlag New York, Inc. New York, NY, USA, 1985.

[106] A. Nosratinia, T. Hunter, and A. Hedayat, "Cooperative communication in wireless networks," *IEEE Wireless Communications Magazine*, vol. 42, no. 10, pp. 74–80, 2004.

[107] P. Liu, Z. Tao, Z. Lin, E. Erkip, and S. Panwar, "Cooperative wireless communications: A cross-layer approach," *IEEE Wireless Communications Magazine*, vol. 13, no. 4, pp. 84–92, 2006.

[108] Q. Zhang, J. Jia, and J. Zhang, "Cooperative relay to improve diversity in cognitive radio networks," *IEEE Wireless Communications Magazine*, vol. 47, no. 2, pp. 111–117, Feb. 2009.

[109] V. Mahinthan, J. W. Mark, and X. Shen, "Performance analysis and power allocation for M-QAM cooperative diversity systems," *IEEE Transactions on Wireless Communications*, to appear.

[110] I. Brown, D.R., "Resource allocation for cooperative transmission in wireless networks with orthogonal users," in *Proc. IEEE Conference Record of the Thirty-Eighth Asilomar Conference on Signals, Systems and Computers (ACSSC'06)*, 2004.

[111] L. Zhao and Z. Liao, "On the power allocation for decode-and-forward cooperative transmission over rayleigh-fading channels," in *Proc. IEEE Vehicular Technology Conference (VTC'07)*, Baltimore, MD, Sep. 2007.

[112] M. Chen, S. Serbetli, and A. Yener, "Distributed power allocation for parallel relay networks," in *Proc. IEEE Global Telecommunications Conference (GLOBECOM '05)*, University Park, PA, Nov. 2005.

[113] Y. Li, B. Vucetic, Z. Zhou, and M. Dohler, "Distributed adaptive power allocation for wireless relay networks," *IEEE Transactions on Wireless Communications*, vol. 6, no. 3, pp. 948–958, 2007.

[114] I. Maric and R. Yates, "Bandwidth and power allocation for cooperative strategies in Gaussian relay networks," in *Proc. IEEE Conference Record of the Thirty-Eighth Asilomar Conference on Signals, Systems and Computers (ACSSC'04)*, 2004.

[115] L. Musavian and S. Äıssa, "Distributed space-time block coded transmission with imperfect channel estimation: Achievable rate and power allocation," *Hindawi Publishing Corporation, EURASIP Journal on Advances in Signal Processing*, vol. 2008, pp. 1–9, 2008.

[116] T. Quek, H. Shin, and M. Win, "Robust wireless relay networks: Slow power allocation with guaranteed QoS," *IEEE Journal of Selected Topics in Signal Processing*, vol. 1, no. 4, pp. 700–713, Dec. 2007.

[117] A. Høst-Madsen and J. Zhang, "Capacity bounds and power allocation for wireless relay channels," *IEEE Transactions on Information Theory*, vol. 51, no. 6, pp. 2020–2040, 2005.

[118] Z. Qi, Z. Jingmei, S. Chunju, W. Ying, Z. Ping, and H. Rong, "Power allocation for regenerative relay channel with Rayleigh fading," in *IEEE Vehicular Technology Conference, 2004. (VTC'04)*, 2004.

[119] D. Simon, "Kalman filtering," *Embedded Systems Programming*, vol. 14, no. 6, pp. 72–79, 2001.

[120] K. Kim, J. Yue, R. Iltis, J. Gibson, N. Center, and T. Irving, "A QRD-M/Kalman filter-based detection and channel estimation algorithm for MIMO-OFDM systems," *IEEE Transactions on Wireless Communications*, vol. 4, no. 2, pp. 710–721, 2005.

[121] Z. Zaidi and B. Mark, "Mobility estimation for wireless networks based on an autoregressive model," in *Proc. IEEE Global Telecommunications Conference (GLOBECOM '04)*, Fairfax, VA, USA, Nov. 2004.

[122] K. Shoarinejad, J. Speyer, and G. Pottie, "A distributed scheme for integrated predictive dynamic channel and power allocation in cellular radio networks," in *Proc. IEEE Global Telecommunications Conference (GLOBECOM' 01)*, Los Angeles, CA, 2001.

[123] M. Elmusrati and H. Koivo, "Kalman filters applications in radio resource scheduling of wireless communication," in *Proc. IEEE 5th Workshop on Signal Processing Advances in Wireless Communications (WSPAWC' 08)*, 2004.

[124] Y. Chen and C. Chiang, "Adaptive beamforming using the constrained Kalman filter," *IEEE Transactions on Antennas and Propagation*, vol. 41, no. 11, pp. 1576–1580, Nov. 1993.

[125] A. Sayed, "A framework for state-space estimation with uncertain models," *IEEE Transactions on Automatic Control*, vol. 46, no. 7, pp. 998–1013, 2001.

[126] D. Simon and T. Chia, "Kalman filtering with state equality constraints," *IEEE Transactions on Aerospace and Electronic Systems*, vol. 38, no. 1, pp. 128–136, 2002.

[127] J. Porrill, "Optimal combination and constraints for geometrical sensor data," *The International Journal of Robotics Research*, vol. 7, no. 6, p. 66, 1988.

[128] A. Sampath, P. Kumar, and J. Holtzman, "Power control and resource management for a multimedia CDMA wireless system," in *Proc. IEEE International Symposium on Personal, Indoor and Mobile Radio Communications (PIMRC'95)*, 1995.

[129] L. Yun and D. Messerschmitt, "Power control for variable QoS on a CDMA channel," in *proc. IEEE Military Communications (MILCOM'94)*, Berkeley, CA, Feb. 1994.

[130] D. Simon, *Optimal State Estimation: Kalman, H_∞, and Nonlinear Approaches*. Hoboken, New Jersey: Wiley-Interscience, 2006.

[131] H. Bogucka, "Game Theoretic Model for the OFDM Water-Filling Algorithm with Imperfect Channel State Information," in *Proc. IEEE International Conference on Communications (ICC' 08)*, Beijing, China, May 2008.

[132] S. Sorooshyari and Z. Gajic, "A robust Kalman filtering approach to stochastic power control for time varying wireless networks," in *Proc. IEEE International Conference on Communications (ICC'05)*, Piscataway, NJ, May 2005.

[133] Q. Xia, M. Rao, Y. Ying, and X. Shen, "Adaptive fading Kalman filter with an application," *IFAC Automatica*, vol. 30, no. 8, pp. 1333–1338, 1994.

[134] L. Xie, Y. Soh, and C. De Souza, "Robust Kalman filtering for uncertain discrete-time systems," *IEEE Transactions on Automatic Control*, vol. 39, no. 6, pp. 1310–1314, 1994.

[135] S. Martello and P. Toth, *Knapsack problems: Algorithms and Computer Implementations*. John Wiley & Sons, Inc. New York, NY, USA, 1990.

[136] M. Akbar, E. Manning, G. Shoja, and S. Khan, "Heuristic solutions for the multiple-choice multi-dimension knapsack problem," *Proceedings of the International Conference on Computational Science-Part II*, pp. 659–668, 2001.

[137] M. Shabany and E. Sousa, "Joint rate allocation and routing scheme in multihop cellular CDMA networks," in *Proc. IEEE International Symposium on Computers and Communications (ISCC'04)*, 2004.